ASSESSING AND IMPROVING THE SIMULATION OF RUNOFF AND DESIGN FLOOD ESTIMATION IN URBAN AREAS USING THE *ACRU* AND SCS-SA MODELS

ZS Ndlovu

Submitted in partial fulfilment of the

requirements for the degree of MSc degree

Centre for Water Resources Research

University of KwaZulu-Natal

Pietermaritzburg

22 November 2022

ABSTRACT

Urbanisation is increasing at a rapid rate. Pervious and vegetated land is increasingly being replaced by impermeable surfaces (roads, pavements, driveways, parking lots, etc.) resulting in large portions of total imperviousness in catchments. The expansion of urban areas alters the natural underlying surface condition affecting catchment characteristics. The most common impacts of urbanisation on the hydrology of a catchment are increased runoff volumes, reduced baseflows owing to less infiltration taking place and a decrease in catchment response time. These changes can result in increased flood risk and subsequent damage to urban infrastructure and affect livelihoods. Therefore, accurate modelling of runoff and estimation of design floods of highly urbanised areas is necessary, especially in the often neglected catchments with informal settlements and infrastructure and in peri-urban catchments. Peri urban areas are defined as those areas located adjacent to a city area and have a mix of both rural and urban characteristics. Two rainfall-runoff models, namely the *ACRU* and the Visual SCS-SA model, were selected for application on catchments with typical South African urban conditions. The models have been developed and tested in urban catchments, however not extensively. The study areas are located in the South African urbanised cities of Tshwane and Pietermaritzburg. *ACRU* is a daily time step conceptual and physically-based agro-hydrological model that is relatively more data intensive compared to the simpler SCS-SA model. Therefore, information systems such as Remote Sensing (RS) and Geographic Information System (GIS) have been explored to aid as data sources and tools for acquiring model input parameters, at a more accurate level. The *ACRU* default values by Tarboton and Schulze (1992) and impervious area estimations derived by Loots (2020) were initially used to estimate the *ACRU* impervious parameters. Additionally, the pixel-based land cover classification method using satellite images was carried out in detail for this study as an attempt to map impervious surfaces and obtain impervious *ACRU* parameters with improved accuracy. Impervious land use classes were also extracted from the 2018 South African National Land Cover Database (SANLC), 2018 Global Man-made Impervious Surface (GMIS) and the 2010 Global Artificial Impervious Areas (GAIA). In order to use the *ACRU* and SCS-SA models confidently, the simulated results need to be verified against reliable observed data for each impervious scenario, if observed data is available. QGIS was used to obtain and process data into information required for the selected models. Several model input data such as slope, elevation, and catchment rainfall were estimated through GIS. The models over simulated observed design floods for the urban

catchments. Obtaining reliable observed data (rainfall and runoff), and satellite images with good resolution proved to be a consistent challenge throughout the study and could have contributed to the poor performance of the models. Urban area data dating back to the1990s was extracted from the GAIA method for most of the simulation period and a trend in impervious area expansion linked to urbanisation was detected and analysed against simulated streamflow from the urban catchments.

PREFACE

I, Zama Sibahle Ndlovu declare that

a) The research reported in this thesis, except where otherwise indicated, is my original work.

b) This dissertation has not been submitted for any degree or examination at any other university.

c) This dissertation does not contain text, data, figures, pictures, graphs or tables from another document, unless it is specifically acknowledged as being sourced from the original document. Where other sources have been quoted, then:

   i) their words have been paraphrased/re-written, and the general information attributed to them has been referenced, and

   ii) where their exact words have been used, their writing has been placed inside quotation marks, and referenced.

d) Where I have reproduced a publication, of which I am an author, co-author or editor, I have indicated in detail which part of the publication was actually written by myself alone and have fully referenced such publications.

e) This document does not contain text, graphics or tables copied and pasted from the Internet, unless they are specifically acknowledged, and the source is detailed, both in the document and in the References section.

Signed:  Date: 25/11/2022

Supervisor: Date:

Co-supervisor:  Date: 7/11/2023

TABLE OF CONTENTS

LIST OF FIGURES

LIST OF TABLES

ACKNOWLEDGEMENTS

I extend my gratitude to the National Research Foundation (NRF) and Umgeni Water for providing me with financial assistance towards completing my degree. I highly appreciate the assistance.

I also extend my gratitude and sincere appreciation to the following persons and institutions:

i) Professor Jeff Smithers, my supervisor and mentor. I wholeheartedly appreciate your guidance and dedicated supervision, it is truly unmatched.

ii) Ms Ione Loots, my co-supervisor. I am thankful for your co-supervision and willingness to help with the project.

iii) Dr Serge Kiala, an exceptional GIS specialist. I am forever grateful for your assistance with the remote and GIS components of the project.

iv) Dr David Clarke, for his assistance and valuable input towards the *ACRU* modelling section of the project.

v) The University of KwaZulu-Natal for providing me with the opportunity of furthering my studies and access to everything I needed towards completing my studies.

vi) The South African Weather Service for providing me with station data.

vii) The South African National Space Agency for providing me with satellite images.

viii) The National Geo-Spatial Information for providing me with old satellite imagery.

ix) The Centre for Water Resources Research for the administrative support.

x) And lastly my Mother, for the endless support and encouragement to complete this degree.

LIST OF ACRONYMS

Acronym / *Variable*	**Description**
ACRU	Agricultural Catchments Research Unit
AIA	Adjacent Impervious Areas
AMS	Annual Maximum Series
ASTERR	Advanced Spaceborne Thermal Emission and Reflection Radiometer
CN	Curve Number
COFRU	Baseflow storage in the *ACRU* model
CWRR	Centre for Water Resources Research
DCIA	Directly Connected Impervious Areas
DEA	Department of Environmental Affairs
DEM	Digital Elevation Model
DEPAHO	A horizon soil depth (m) in the *ACRU* model
DFE	Design Flood Estimation
DIA	Disjunct Impervious Surfaces
DWS	Department of Water and Sanitation
ERDAS	Earth Resources Data Analysis System
GEE	Google Earth Engine
GHBASE	Global Human Built-up and Settlement Extent dataset
GIS	Geographical Information Systems
HyspIRI	Hyperspectral Infra-Red Imager
HRU	Hydrological Response Unit
HSG	Hydrological Soil Groups
HSM	Hydrological Simulation Model
HSPF	Hydrologic Simulation Programme FORTRAN
IRS-1C	Indian Remote Sensing satellite-1C

ISA	Impervious Surface Areas
LANDSAT	Land Remote-Sensing Satellite
MAP	Mean Annual Precipitation (mm)
MARE	Mean Absolute Relative Error
MODIS	Moderate Resolution Imaging Spectroradiometer
MRE	Mean Relative Error
MSE	Mean Square Error
NDISI	Normalized Difference Impervious Surface Index
NDVI	Normalized Difference Vegetation Index
NFSP	National Flood Studies Programme
NGI	National Geo-spatial Information
NSE	Nash-Sutcliffe Efficiency
QFRESP	Quickflow response parameter in the *ACRU* model
RS	Remote Sensing
SANSA	South African National Space Agency
SAWS	South African Weather Services
SCS-SA	South African adaptation of the SCS-CN model
SMA	Spectral Mixture Analysis
SMDDEP	Critical stormflow depth (m) in the *ACRU* model
STORMF	Stormflow generated on the day of a rainfall event
SPOT	Systeme Probatoire d'Observation de la Terre
SWMM	Storm Water Management Model
WASHMO	Watershed Storm Hydrograph Model

1. INTRODUCTION

According to the United Nations (2019) the global population is estimated to be 7.8 billion people, with 55% of this population residing in urban areas. The United Nations (2019) project an increase to 68% of global population living in urban areas by the year 2050, indicating large scales of urbanisation. The term urbanisation can be defined as a complex socio-economic process that converts rural areas into urban settlements (Delgado, 1969). The combination of urbanisation and the overall world population growth is expected to result in an additional 2.5 billion people living in urban areas by 2050, with the majority of the population increase taking place in Asia and Africa (Chen *et al.*, 2014). The United Nations (2019) report that the population numbers in urban areas have increased from 751 million people in 1950 to 4.2 billion in 2018. South Africa follows a unique urbanisation trend that has been strongly influenced by the Apartheid history (Maharaj and Narsiah, 2002). Urbanisation peaked in the years following the announcement of the country's democracy (Maharaj and Narsiah, 2002). People were able to commute from place to place without being forced to reside in the allocated areas and, as a result, many rural inhabitants were drawn to the urban areas. Thus, rural land is being rapidly transformed to residential, commercial and industrial developments. The increase in urban population has resulted in the growth and expansion of informal settlements and peri-urban areas. Peri-urban areas have characteristics of both rural and urban areas (Bickford-Smith, 1995).

The expansion of urban areas has resulted in the build-up of impervious surfaces that have serious negative impacts on urban hydrology (Hameed, 2017). There are a range of methods and hydrological models available for estimating design floods in urban areas and these function successfully in some countries, but may not perform well when applied under different conditions (Tikkanen, 2013). Design floods refer to the magnitude of a flood that is associated to a degree of risk, and return period (Smithers, 2012). Several hydrological simulation models used for the estimation of runoff and peak floods have been developed and applied globally in urban environments, and these include the Storm Water Management Model (SWMM), the Agricultural Research Unit (*ACRU*), and the Soil Conservation Services (Hydrology) model, to name a few (Terstriep and Stall, 1974; Schütte and Schulze, 2017; Rabori and Ghazavi, 2018). These hydrological models require large amounts of input data at an accurate level to produce good simulations of runoff. Remote sensing (RS) and Geographical Information System (GIS)

are often integrated with hydrological models, resulting in a mutually beneficial interaction as depicted Figure 1.1.

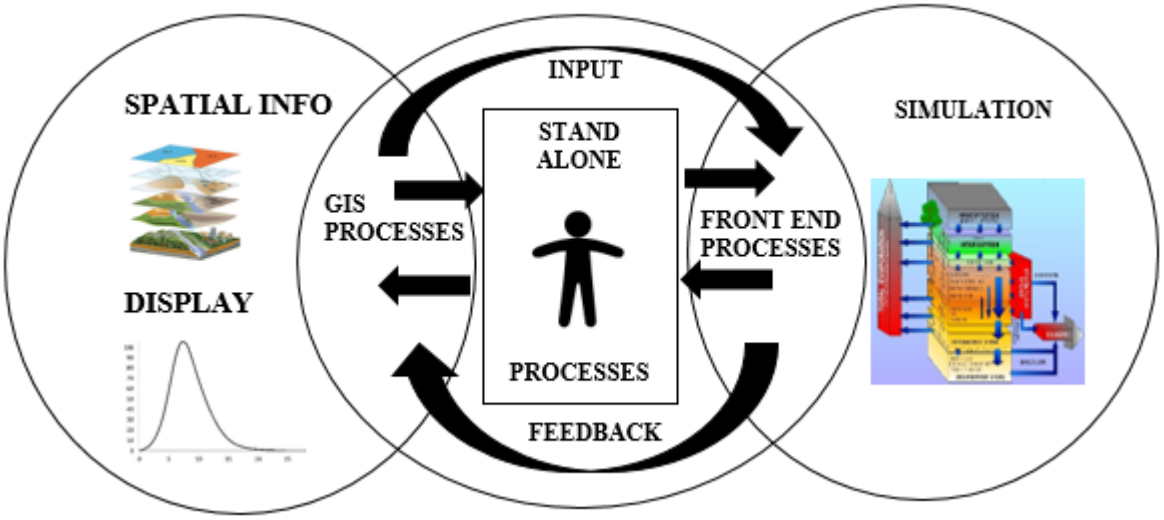

Figure 1.1 The GIS- Hydrological Modelling System (HMS) integration concept (Tarboton, 1992).

RS is a current method that is used to capture data from the surface of the earth (Lee *et al.*, 2011). RS is efficient in that reliable data of any resolution can be extracted for a particular region without the need for on-site data collection (Zhou and Wang, 2008). When estimating design floods from "complex" urban areas, several physical features that influence the hydrology of urban areas are required in order to obtain accuracy in hydrological modelling. Poor design flood estimation achieved by hydrological models is often as a result of inaccurate estimates of model input parameters, which can as a result affect the design of hydraulic structures.

The focus for this study is, therefore, to assess and improve the simulation of design flood estimation in urban areas using the rainfall-based *ACRU* and SCS-SA models. Rainfall-based methods have been selected for this study because they are more advantageous in simulating design flows with dynamic land uses compared to methods based on streamflow analysis. With longer rainfall records from multiple stations, more representative simulations can be achieved using these methods. Streamflow is directly affected by changing catchment conditions, and thus the non-stationarity of the streamflow records can produce unsatisfactory modelling results. Rainfall-runoff models are able to incorporate the physical features of a catchment and

more importantly model historical, present and future land uses from a catchment (Smithers, 2012). These models are user friendly, and the SCS-SA model is simple and relatively less data intensive.

The *ACRU* and SCS-SA models differ quite significantly in terms of their complexity in data processing, input data requirements, and overall practicality. Therefore, applying hydrological models that are technically different from each other on catchments with similar urban characteristics will highlight which model is suitable for application in which typical land uses. A few studies both locally and globally have investigated the application of the *ACRU* and SCS-SA models in urbanised catchments (Schulze, 1995b; Warburton *et al.*, 2010; Schütte, 2014). Both the models produced generally reasonable results as more work and research has, and is still being, incorporated into the modelling systems to enhance their applicability in diverse land uses. However, there are only a handful of studies that have assessed the performance of the *ACRU* and SCS-SA models in South African urban land uses. Therefore, owing to the necessity for further verification studies and additional improvements, the *ACRU* and SCS-SA models were selected for this study. The complex nature of the *ACRU* model requires accurate input data that influences the quality of simulations achieved. Therefore, one of the objectives of this study includes developing methods to parameterise the models using RS and GIS data extraction methods. The model performance will be assessed, and simulations and input parameters improved, if necessary. This will be done by gaining an understanding of the urban hydrological system with all of its complexities and finding better and simpler ways of representing them (through hydrological modelling) in order to minimise the adversity of derived impacts from the interaction of the urban and hydrological system.

Aim and Objectives

The aim of this study is to assess and evaluate the performance of runoff simulation and design flood estimation in urban areas using the *ACRU* and SCS-SA models. The following objectives were met in order to achieve the aim for this study:

a) Reviewing relevant literature based on international and local urbanisation trends and their effects on the hydrology of urban areas, application of the *ACRU* and SCS-SA models in urban areas and researching existing mapping methods of Impervious Surface Areas (ISA) that could be integrated with design flood estimation models.
b) Identify suitable study catchments and obtain reliable and consistent climate and land cover data to be used to derive model input data and parameters.
c) Use GIS and Remote Sensing to obtain more accurate input parameters and developing guidelines to estimate the impervious model parameters in urban areas.
d) Configure the *ACRU* and SCS-SA models using different impervious parameterisation methods and scenarios to detect the best configuration.
e) Assess and improve simulations from the models where necessary.
f) Study urban land cover change over time and the effect of impervious cover on streamflow

Urbanisation significantly influences the hydrology of a catchment. The effect of urbanisation on catchment hydrology is largely related to the catchment's increased impermeability and subsequent results of this increase. Additionally, several factors that affect the general hydrological cycle of a catchment are also influenced by urbanisation. The disturbance of the natural urban hydrology of a catchment due to urbanisation often leads to high streamflow volume and peak discharge, ultimately resulting in floods.

The following chapter contains a detailed literature review of factors affecting urban hydrology, design event and continuous design flood estimation methods as well as the developments and research that has been done on the *ACRU* and SCS-SA models.

2. REVIEW OF LITERATURE

The expansion of urban areas alters the hydrological cycle by the removal of pervious land and replacing it with impervious surfaces to accommodate the increase in population in urban areas (Wood, 2012). This results in a lower potential for infiltration to occur, leading to higher peak discharge. Arnold and Gibbons (1996) reported that the increased peak discharge is caused by the decrease in catchment lag time and the resulting lower groundwater recharge. The increase in peak discharge can affect downstream flood plains. The combination of garden irrigation and possible leaks in urban water supply networks could further distort the urban water balance (Schütte and Schulze, 2017). Falkenmark *et al.* (1999) noted an increase in streamflow due to urbanisation and the high volumes of streamflow were accompanied by an increase in groundwater flow as a consequence of leaking sewerage, water pipes and septic tanks and over-irrigation of gardens. Furthermore, the presence of water supply and sewage treatment infrastructure in urban areas assist in transferring large quantities of water and wastewater across urban catchments. Urban hydrology has sought to isolate artificial infrastructure flows from natural hydrological analysis. Nonetheless, an increasing awareness that inefficient and defective drainage networks can result in a surplus of water and contaminants to natural systems has led to a step toward integration of the hydrological cycle and the engineered water cycle (Bell *et al.*, 2016a). The impacts of urbanisation on the hydrological cycle can lead to an increase in the severity of flooding and subsequent potential impairment to property and urban infrastructure (Park and Lee, 2019). To reduce exposure to floods, some cities have reserved natural land by reducing the expansion of impervious surfaces and urbanisation. This natural land is referred to as a green belt, which describes an open area within a city, on which buildings and development are prohibited (Shaw *et al.*, 2012). Lennon *et al.* (2014) assessed the potential of using green infrastructure as an alternative approach to exploring evolutionary resilience in designing urban environments for improved drainage management.

Rainfall is the driving force of runoff in a rainfall-runoff relationship. In an urban area, with relatively little infiltration occurring, it takes a small amount of rainfall to contribute to runoff, indicating a low rainfall threshold to generated runoff (Choi *et al.*, 2016). Abustan *et al.* (2008) investigated the relationship between rainfall and runoff for the Sungai Catchment (48.3km^2) located in Wilayah Persekutuan Kuala Lumpur, which has an estimated impervious surface of 76.2%, and found a good correlation between the rainfall and runoff. Once the rainfall-runoff relationship has been established, a higher or lower peak discharge will depend on the amount

of runoff generated. Arnold and Gibbons (1996) noted that in informal urban areas, there are less impervious surfaces as opposed to formal urban areas indicating that formal urban areas could be more susceptible to floods, while taking into account the area's drainage and other related factors affecting floods. Rapid urbanisation has also often led to the deterioration and inefficiency of hydrological infrastructure in urban areas (Chen *et al.*, 2015). The increase in runoff in urban areas produces a hydrograph that is quicker to peak, quicker to recede and has a higher peak discharge (Packman, 1980).

Surface and sub-surface flows play a major role in urban hydrology, as the ultimate goal in the study of urban hydrology is to assess and compute the total runoff in urban areas (Grinfelde and Bakute, 2017). From the combination of both surface and sub-surface flow, a streamflow hydrograph is generated. In typical urban conditions, the hydrograph is expected to represent larger volumes of streamflow, a higher peak discharge and a decrease in the time of concentration compared to hydrological responses in rural catchments (Bell *et al.*, 2016b). A typical hydrograph showing the impact of an urban catchment is shown in Figure 2.1.

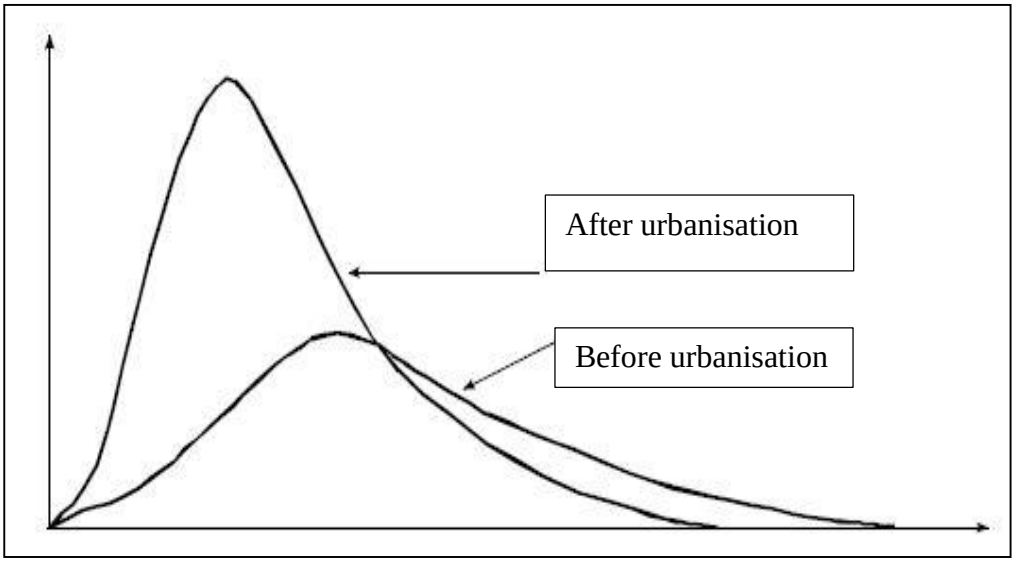

Figure 2.1 Changes in the flood hydrograph as a result of urbanisation (Bell *et al.*, 2016a)

2.1 Baseflow and Flow Peaks as a Result of Urbanisation

When precipitation falls on impervious areas, little of it is infiltrated and the majority contributes to surface runoff. Reduced infiltration decreases groundwater recharge, evapotranspiration and baseflow (Bell *et al.*, 2016a). The impacts of climate change such as

rainfall variability is more prevalent in urban areas due to the existing, identifiable and mostly human-induced climate change drivers. Typically erratic rainfall patterns occur in urban areas producing rainfall of high intensity and long duration (McGrane, 2016). Hence, such events can produce significant runoff with high flow peaks. Therefore, in these urban areas there is a higher risk of flooding.Factors Affecting Urban Hydrological Responses.

Factors that influence the hydrological responses of an urban catchment are discussed in the following sub-sections.

2.1.1 **Catchment permeability**

Catchment permeability refers to the areas in a catchment that allow for the infiltration of water (Pafka and Dovey, 2017). Although Total Impervious Areas (TIA) is a significant indicator of urban disturbance, a sub-category of impervious surfaces, Directly Connected Impervious Areas (DCIA), also known as Adjunct Impervious Areas (AIA), which refers to all impervious areas that are directly connected to a drainage system (Wang *et al.*, 2012) is the main indicator of urbanisation. Therefore, estimating DCIA from TIA can provide a picture of the extent of urbanisation in a catchment. A study by Alley and Veenhuis (1983) and later supported by Lee and Heaney (2003) suggested the use of an empirical relationship between DCIA and TIA. Lee and Heaney (2003) proposed a method of delineating DCIA for the derivation of the empirical relationship between DCIA and TIA while other studies showed independent calculations of DCIA from TIA (Wang and Dickinson, 2012). These methods involved superimposing storm water conveyances on maps of impervious areas to determine impervious areas connected to a storm water system (Brabec *et al.,* 2002; Walsh *et al.,* 2005). Lee and Heaney (2003) opposed this method of determining DCIA mostly because maps and geographic information system (GIS) data do not provide information about specific runoff routing from impervious surfaces based on drainage patterns. Therefore, for accurate determination of DCIA, reference to field investigations is recommended to detect and confirm where pipes are draining. A study done by Roy and Shuster (2009) evaluated the difference between TIA and DCIA in the Shepherd Creek suburban catchment (1.85 km^2) in Cincinnati, Ohio. Impervious surfaces estimated from GIS data and field investigations were compared to DCIA computed from published empirical relationships shown in Equation 2.1 and Equation 2.2 derived by Alley and Veenhuis (1983). TIA estimated from aerial photos was similar to TIA calculated from on-site evaluations, thus showing that imagery interpretation may be sufficient for TIA determinations for catchments

greater than 0.25 km^2. While these GIS data sources can be used to compute TIA, field assessments were required to accurately estimate DCIA within residential land use areas. Owing to the wide variation in per cent connectivity, the empirical relationships did not calculate an accurate percentage of TIA.

$$DCIA = (1.046 \times TIA) - 6.23\% \quad (2.1)$$

$$DCIA = 0.15 \times TIA^{1.41} \quad (2.2)$$

where

DCIA = Adjunct Impervious Areas (ha), and

TIA = Total Impervious Areas (ha).

Disconnected Impervious Areas (DIA) are another subcategory of TIA. DIA refers to all the impervious areas that drain into pervious areas such as onto permeable soil or vegetated land. Both the connected and disconnected impervious areas contribute to a catchment's impermeability (Alley and Veenhuis, 1983; Roy and Shuster, 2009).

2.1.2 **Drainage paths**

Rapid urbanisation has led to the unplanned and disorganised clustering of people into cities, resulting in the establishment of informal settlements. These informal settlements are often characterised by land uses with poor drainage making them prone to flooding, with the banks of the drainage channels and watercourses at risk of seepage and collapsing (Parkinson *et al.*, 2007). These regions lack proper drainage infrastructure, making them more susceptible to flooding because houses within these catchments are often located in low-lying areas are poorly served by urban infrastructure and services (Muthanna *et al.*, 2018).

An urban upgrading approach was developed in Indore, India called slum networking (Corburn and Sverdlik, 2017). This approach considered the interactions between slums and the natural drainage paths that affect urban infrastructure and the environment of the metropolitan area (Diacon, 1997; Parikh *et al.*, 2002). The goal for this approach was to alleviate flooding problems in the study area and in order to achieve this, information pertaining to the urban area's hydrology was required. Lucci *et al.* (2015) suggests that detailed information such as understanding the rainfall-runoff relationship of a catchment is critical prior to the construction

of the functional drainage pathways. For smaller catchments, a general relationship for rainfall intensity, duration and frequency and runoff was developed by Lumbroso *et al.* (2011), but for larger areas the relationship between rainfall and runoff cannot be estimated by simple relationships as it is very complex.

Kolsky (1998) reports that the assessment of drainage areas using catchment boundaries is imperative before the construction of a drainage infrastructure. This assessment can be deduced from computer design tools and sophisticated technologies. However, for achieving accurate results, field investigation are recommended by Parkinson *et al.* (2007). Most importantly, the acquisition of sufficient and reliable datasets is essential in design hydrology (Mejía and Moglen, 2010). Urbanisation has placed a great strain on urban drainage pathways resulting in inefficient and poor condition of drainage systems, particularly in informal developments. The growth of formal developments has, however, been accompanied by more efficient drainage paths.

2.1.3 **Catchment slopes**

The slope of a catchment influences many aspects of urban hydrology, but mostly surface generated runoff (Daniell *et al.*, 2015). Concreted, steep urban slopes produce large amounts of often turbulent surface runoff flowing at high velocities (Chen *et al.*, 2015). As a result, the flood peaks are higher, and in pervious parts of the catchment, soil erosion and sedimentation can occur. These processes affect the productivity of the surrounding soil as well as the storage capacity and general condition of dams (Bell *et al.*, 2016a). The combination of slope position and land use has a significant influence on surface runoff in urban hydrology. Measured runoff shows high variation across land-use type and slope position. In circular catchments with a homogeneous slope distribution, the runoff from various parts of the catchment reach the outlet more or less simultaneously provided the outlet is in the centre of the catchment, while an elliptical catchment equal in area with its outlet at one end of the major axis, would cause the runoff to be more distributed over time, thus resulting in smaller peak discharges compared to that of a circular catchment. Slopes, whether gentle or steep, influence the catchment response time and hence the duration of critical rainfall intensity and resulting peak discharges and volumes (Alexander, 2001).

2.2 Design Flood Estimation Methods

As mentioned in the previous sections, the typical condition of urban areas, i.e. a significantly larger proportion of impervious areas resulting in higher runoff and peak discharge, make urban areas more vulnerable to flooding (Arnold and Gibbons, 1996). Floods can be catastrophic and can result in the damage of urban infrastructure and property and in worse cases can lead to loss of life (Yang *et al.*, 2010). Design Flood Estimation (DFE) involves estimating the risk associated with a flood event of a particular magnitude or duration with a return period. DFE plays an important role in understanding urban hydrology through hydrological modelling simulation and aids in the planning and designing of hydrological infrastructure (Smithers, 2012). Smithers (2012) states that South Africa mostly relies on design flood estimation methods that were developed in the late 1960s and early 1970s and adds that these methods need to be updated as there is additional available data and new sets of methods that have been developed internationally. Alexander (2002) mentioned that there are large inefficiencies in design flood estimation procedures because of the lack of understanding of hydrological processes and flood magnitude –frequency relationships. There is thus an urgent need to modify and renew current design flood estimation methods as well as to create new approaches to accommodate unique hydrological urban characteristics of a region (Rangari *et al.*, 2015). There are a range of approaches to design flood estimation and the decision is based on data availability, catchment characteristics and whether the method is suitable and adapted for the study area (Smithers, 2012). These approaches are based on the analysis of flood/streamflow data and rainfall methods, as shown in Figure 2.2.

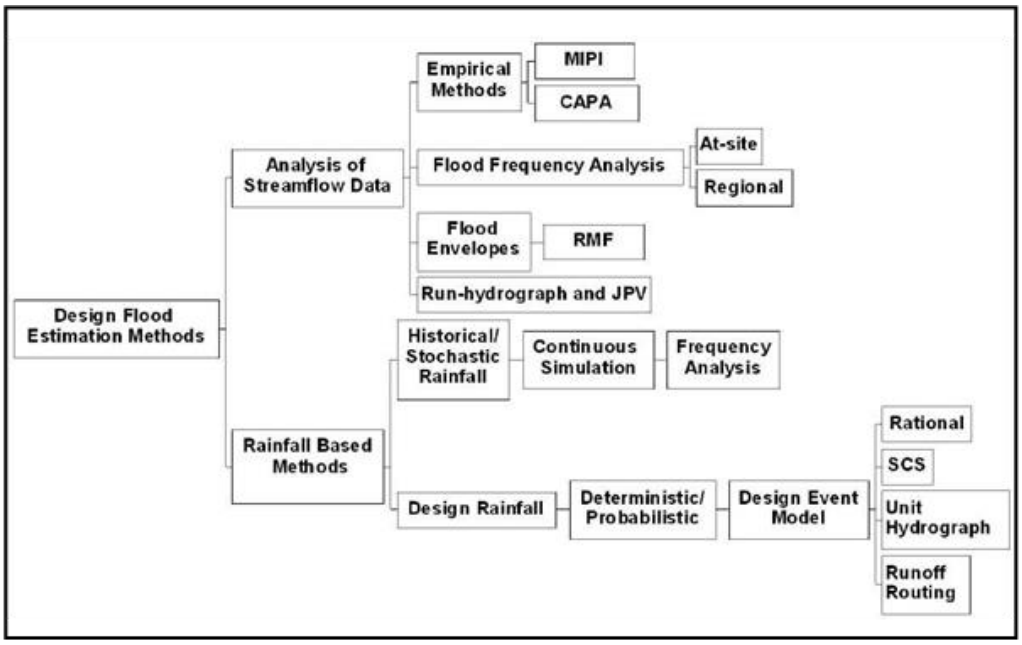

Figure 2.2 Approaches to design flood estimation (Smithers, 2012)

Rainfall based design flood estimation methods are divided into methods based on historical rainfall records (e.g. the *ACRU* model) and methods based on design event rainfall (e.g. the SCS-SA model).

2.2.1 **Approaches to design flood estimation**

Design event approach

Design event approaches are extensively used in all types of catchments. These approaches have the ability to combine complex, heterogeneous catchment processes into one process and do not require long periods of hydrological data (Smithers, 2011). During event-based modelling, the rainfall-runoff process is computer-generated for a single rainfall or streamflow event with the duration extending for hours to a few days (Hossain *et al.*, 2019). The event-based approach computes peak discharges and the level of water belonging to a combination of stochastic variables that influence the extent of floods. In order to account for losses, usually only the infiltration process is modelled. In this approach, the duration and return period of the design flood is important for the computation of peak discharge and other flood variables (Hoes and Nelen, 2005). There are several design event approaches such as the Rational Method, the Unit Hydrograph and the SCS method (Smithers, 2011).

Hoes and Nelen (2005) mentioned that the stochastic event-based approach is more credible than the single design event approach and has received less criticism. Lamb (1999) showed that event-based rainfall-runoff modelling produces distributions for flood frequency that vary more than results obtained from continuous rainfall-runoff simulations. Event-based models are subjective in the sense that the user assigns values for antecedent moisture conditions and then using an observed hydrograph, the values are calibrated (Hossain *et al.*, 2019). Calibration is often done using the automatic calibration method (Sun *et al.*, 2017).

Continuous simulation approach

Continuous Simulation Models (CSM) have been used and tested in several studies (Smithers *et al.*, 1997; Smithers *et al.*, 2001; Chetty and Smithers, 2005; Smithers *et al.*, 2007; Smithers *et al.*, 2013). CSM require a range of datasets which include rainfall data, maximum and minimum temperature, catchment characteristics, soil and land cover properties etc. Obtaining reliable and consistent data that is free of errors is one of the major challenges for DFE, especially in developing countries such as South Africa (Voigtländer *et al.*, 2008). CSM estimates design floods from a complete design hydrograph and, therefore, the calculated exceedance possibility of a flood event is not reliant on the exceedance possibility of the input rainfall (Goel *et al.*, 2000).

Schulze (1989) supports the continuous simulation modelling approach for design flood estimation mainly because: (a) of the precise estimation of design floods (b) long series of observed flood information usually not being available and is generally being inconsistent, non-homogenous and non-stationary, (c) there is sufficient reliable rainfall data in South Africa, and (d) the exceedance probability of floods has an inconsistent relation to the exceedance probability of rainfall depending on other variables. The drawbacks, however, include the challenges encountered in modelling soil moisture balances and obtaining input data, specific spatial and temporal scale, requirement of large input data and expert operation and lastly the overall complexity of the methods (Rahman *et al.*, 2002). However, because CSM have more advantages to the traditionally used design event models, the further development and evaluation of a CSM approach for DFE in South Africa has been included in the National Flood Studies Programme (NFSP).

Several international studies have conducted research on the application and development of CSM (Calver and Lamb, 1995; Calver and TATE, 1996; Cameron *et al.*, 1999; Lamb, 1999;

Kjeldsen, 2015; Cu and Ball, 2017). The following continuous simulation modelling applications have been referred to and used globally for design flood estimation:

a) In the United Kingdom, the Flood Estimation Handbook (FEH) and its proceeding updates is used for DFE.
b) Kjeldsen (2015) provided several statistical procedures that are dependent on the evaluation of observed streamflow data, where both at-site and regional methods were used in the study (Kjeldsen, 2015).
c) Ball *et al.* (2016) report the application of the Australian Rainfall and Runoff (ARR) approach as the national recommendation for DFE method in Australia.
d) In the USA, the Storm Water Management Model (SWMM) developed by the U.S. Environmental Protection Agency (USEPA is a dynamic rainfall-runoff simulation model, with CSM characteristics, used to simulate runoff quantity and quality. This model has been applied extensively in urban areas both in the U.S and internationally (Warsta *et al.*, 2017). SWMM is incorporated into urban drainage models that have been developed internationally, e.g. the Danish Hydraulic Institute (DHI) and MIKE URBAN software (DHI, 2017). SWMM has also been applied extensively for DFE in a range of land cover and land uses (Ahn *et al.*, 2014).

One of the drawbacks of using design event models is the assumption that the frequency of the estimated flood is equal to the frequency of the input rainfall for reliable inputs and model parameters (Pilgrim and Cordery, 1993; Rahman *et al.*, 2002). However, as stated by Smithers *et al.* (2013), numerous studies proved that this is not true and that analysing antecedent soil moisture conditions before a rainfall event is critical in determining the runoff response of the catchment (Schulze, 1979; Schulze, 1982; Schmidt and Schulze, 1984; Dunsmore *et al.*, 1986). Another limitation that affects the DFE application of design event models in estimating runoff is the inability to account for antecedent soil moisture conditions before a flood event, since this limitation affects estimations of flood frequency (Rahman *et al.*, 1998). Event based methods are usually applied using a deterministic approach and are most likely to be disadvantaged by the limitations associated with this method (Smithers *et al.*, 2013).

2.2.2 **Event-based approaches - SCS-SA Model**

The SCS method was developed by the Soil Conservation Services of the USA (SCS, 1972). The original SCS method was altered and developed to the SCS-SA model which is adapted for South African conditions and a range of refinement and developments were conducted to make it suitable for local applications (Schmidt *et al.*, 1987). The SCS-SA method is widely used

among practitioners because it is user-friendly and well-documented (Schulze *et al.*, 1992b). The SCS-SA model is a deterministic and simple model that computes the volumes of runoff for a given rainfall event (Schulze *et al.*, 1992b). The SCS-SA model is ideally applicable to catchments with an area less than 30 km^2.

Stormflow is defined by the SCS manual composed by Schulze *et al.* (2004b) as the direct runoff response to a known rainfall event and it includes surface and subsurface runoff flows, with baseflows not considered. Stormflow depth assumes a constant depth over the catchment and stormflow volumes can be calculated by introducing catchment area. The SCS-SA model computes runoff using the same equation (Equation 2.5) discussed in the *ACRU* section 2.3.3.

The SCS-SA method uses the catchment Curve Numbers (CN), which is an index of hydrological response for a given soil, land cover, and land management condition (Schulze *et al.*, 1992a). The curve number ranges between 0 and 100, with 100 assigned for an impermeable surface to near zero for highly permeable surfaces (Schulze *et al.*, 1992b). The CN is derived from available rainfall-runoff data and determined from catchment lag time and the Hydrological Soil Groups (HSG) (Schulze *et al.*, 2004a). The curve number is calculated in relation to the potential maximum retention, *S*, using Equation 2.3. The deficit of *S* in both the original SCS method and SCS-SA model is combined into a single variable represented as the catchment CN (Schulze *et al.*, 1992b).

$$S = \frac{25400}{CN} - 254 \tag{2.3}$$

where

S = Potential maximum retention (mm), and

CN = Curve Number

In the SCS-SA model, *S* is dependent on multiple catchment characteristics and is essentially referred to as the catchment response index. Derivation of CNs for South Africa was adapted from the original SCS method (SCS, 1972). The differences in CNs were usually attributed to variances in soil moisture (Schmidt *et al.*, 1987). A procedure was included in the original SCS method to modify average CNs (CN-II) for antecedent moisture conditions that fall within the wet (AMC-III) or dry (AMC-I) CN range. The curve number can be attuned to account for antecedent moisture conditions. The SCS-SA model accounts for typical antecedent moisture

conditions using the median condition and joint probability methods between rainfall and runoff (Schmidt *et al.*, 1987). Schulze and Pike (2004) produced curve numbers for a range of land use classes including urban classes for the SCS hydrological soil groups, shown in Table 2.1. This enabled the SCS-SA model to be applied in different catchments with a range of land uses It was deduced that the occurring total stormflow and the estimation of *S* are significantly dependent on the selected CN.

Table 2.1 CN for suburban and urban land use classes (After Schulze, 2004)

Land Cover Class	**Land Treatment/Practice/Description**	**Hydrological Soil Group**						
		A	**A/B**	**B**	**B/C**	**C**	**C/D**	**D**
Urban sub-urban Land Uses	1= Open spaces, parks, cemeteries 75% grass cover	39	51	61	68	74	78	80
	2= Open spaces, parks, cemeteries 75% grass cover	49	61	69	75	79	82	84
	3= Commercial/business areas 85% grass cover	89	91	92	93	94	95	95
	4= Industrial districts 72% impervious	81	85	88	90	91	92	93
	5= Residential: lot size 500m^2 65% impervious	77	81	85	88	90	91	92
	6 = " " 1000m^2 38% impervious	61	69	75	80	83	85	87
	7= " " 1350m^2 30% impervious	57	65	72	77	81	84	86
	8= " " 2000m^2 25% impervious	54	63	70	76	80	83	85
	9 = " " 4000m^2 20% impervious	51	61	68	75	78	82	84
	10= Paved parking lots, roofs, etc.	98	98	98	98	98	98	98
	11= Streets/roads: tarred, with storm sewers, curbs	98	98	98	98	98	98	98
	12= " gravel	76	81	85	88	89	90	91
	13= " dirt	72	77	82	85	87	88	89
	14= " dirt-hard surface	74	79	84	88	90	91	92

The calculation of peak discharge using the SCS-SA method is based on the triangular unit hydrograph concept shown in Figure 2.3. The peak discharge and storm hydrograph are computed by superimposing incremental triangular unit hydrographs corresponding to the distribution of stormflow depth over a period of time, as controlled by the distribution of the time of rainfall intensity and the lag time (Schulze *et al.*, 1992a). Surface runoff derived from effective rain (rain that produces stormflow) falling for a specific duration over a catchment is used to derive a unit hydrograph.

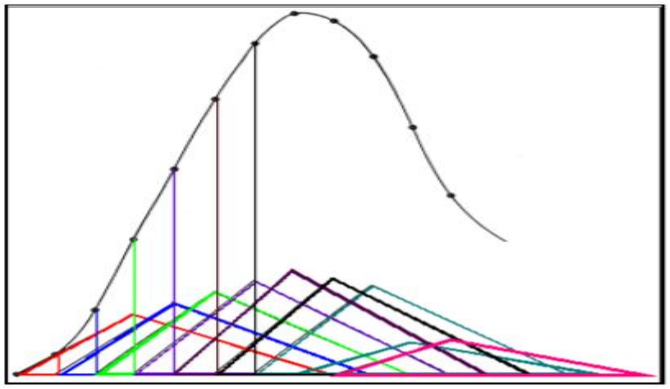

Figure 2.3 Superpositioning of incremental triangular unit hydrographs (Schulze, 1995a)

The unit hydrograph represents the temporal distribution of stormflow for a given incremental unit depth of rainfall with, ΔQ, taking place over a given time (Schulze *et al.*, 2004a). This is defined in Equation 2.4.

$$\Delta q_p = \frac{0.2083 A \Delta Q}{\Delta D/_2 + L} \quad (2.4)$$

where

Δq_p = peak discharge of incremental unit hydrograph ($m^3.s^{-1}$),

A = catchment area (km^2),

ΔQ = incremental stormflow depth (mm),

ΔD = unit duration of time (h), and

L = catchment lag.

Developments of the SCS-SA model and application in urban catchments

In order to enhance the estimation of design runoff volumes and peak discharges in small catchments in South Africa, the SCS-SA model underwent extensive modification and refining (Schmidt *et al.*, 1987; Schulze *et al.*, 2004b). The process has been improved owing to advancements and improvement in computer software and data accessibility. Modifications and

research have been done on some components of the SCS-CN such as the introduction of the three intermediate SCS soil groups for South African soil series, i.e. A/B, B/C, and C/D, compared with the original A, B, C and D soils. The soil water budgeting method has been included, four synthetic storm distributions have been regionalised and the Schmidt and Schulze lag equation underwent re-evaluation (Schmidt *et al.*, 1987). Further research in improvement of the SCS-SA model proved that for application in DFE, the SCS-SA model works better when the study catchment is divided into sub-catchments of similar characteristics as opposed to the catchment land uses being lumped into one catchment (Rowe and Smithers, 2018).

The SCS method was identified by Loots (2020) as a procedure that could be applied extensively in urban design flood estimation if the curve numbers were modified and assessed for different urban developments in South Africa. The SWMM model was selected as the DFE model for this study and since SWMM has the built-in option to incorporate an SCS infiltration process for urban areas, usable SCS curve numbers for urban land use classes could be estimated from the calibrated and verified catchment configurations. Calibrated parameters served as input data into the SWMM model and for the urban application of the SCS-SA deterministic design flood estimation method. The results from the CN calibration showed improved model response from the selected urban study catchment during significant rainfall events, where the simulation still overestimated the frequency of flow rates larger than 15 m^3/s, but the calibrated simulation mimicked the observed flow curve better for flow rates larger than 10 m^3/s. Applicable SCS CNs for the urban land use classes were then derived from the calibrated. The derived CNs from Loots (2020) were used in the configuration of the SCS-SA model for this study, as explained in the methodology Section 3.5.

Several studies using the SCS method in urban areas have been conducted both internationally and locally. Urbanization impacts were assessed by Rawls *et al.* (1981) using the SCS method where data from 175 urban catchments in different regions of the US were used to determine whether runoff curve numbers produced by measuring the fractions of land use and soils separately and integrating them using a weighted average method or by utilizing land use maps created by the USGS were comparable to curve numbers produced by the traditional SCS methods. The findings showed that for catchments between 0.1 and 472 km^2, estimations of runoff curve numbers were sensitive to the methodology of land use classification, but not particularly sensitive to the method of integrating soils and land cover data. Additionally, a set of curve numbers for the four hydrologic soil groups were developed from the data set. Aron

(1982) integrated the SCS runoff curve number into an urban rainfall-runoff model. Kao *et al.* (1973) used the SCS method to study the effects of urbanisation on peak discharge and runoff volume on small catchments. Kao *et al.* (1973) concluded in their study that: (a) The peak flow rate and total runoff volume from small urban catchments are linearly correlated, (b) the SCS method appears to be sufficiently sensitive to determine the effect of urbanization on the volume of runoff, and (c) urban catchments with the highest percentage of imperviousness do not necessarily produce the highest peak rates for a given volume of runoff. The last point is particularly interesting as most literature suggest an increase in runoff associated with an increase in imperviousness (Jacobson, 2011; Fan *et al.*, 2013; Xu *et al.*, 2016). This will depend on whether urban impervious areas are linked to a formal stormwater system or not.

2.2.3 **Continuous simulation - *ACRU* Model**

The *ACRU* model is a continuous simulation daily time step agro-hydrological model (Schulze, 1995a) which uses input data recorded daily. The model is characterised as a physically-based conceptual model that was initially developed for agricultural applications but has also been used successfully in urban areas (Tarboton and Schulze, 1991; Schmitz and De Villiers, 1997; Schütte and Schulze, 2017). The *ACRU* model can function in a lumped or distributed mode on catchments ideally not exceeding 30 km^2. The *ACRU* model input parameters can be directly calibrated however this is not recommended because the model is not characterised as a parameter fitting or optimising model (Schulze, 1994). Therefore, the parameters are assigned based on the physical characteristics of the catchment determined from field investigations and the model's performance is then tested against observed data, if available (Schulze, 1994). The important components of the hydrological cycle are represented in the *ACRU* model as depicted in Figure 2.4. A major advantage of the *ACRU* model, is that it is able to fully represent the contribution of baseflow to total streamflow (baseflow and stormflow), (Rowe, 2019).

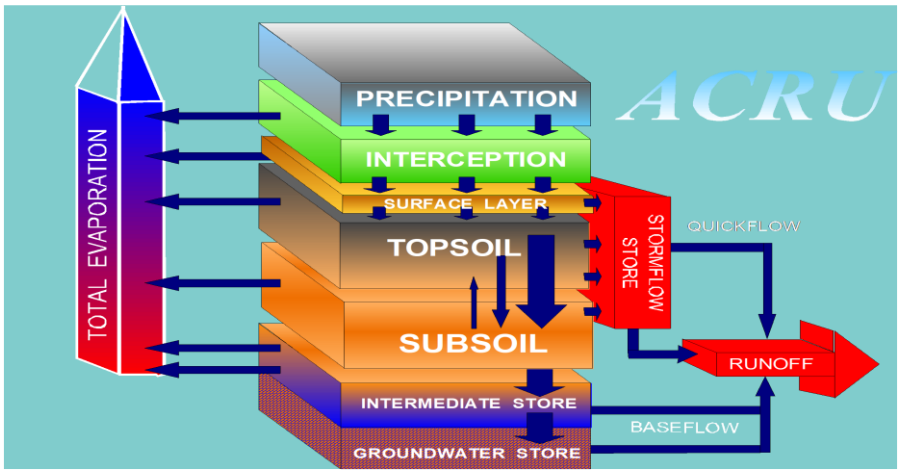

Figure 2.4 Components of the water balance in the *ACRU* system (Schulze, 1995)

The *ACRU* model continuously simulates daily flows and its input data includes daily rainfall, temperature, daily streamflow where available, land cover and soil characteristics, to name a few (Schulze, 1995a). During the estimation of urban design floods, particularly in this study, attention is paid to the simulation of observed streamflow and peak discharge by the *ACRU* model. Streamflow is defined by Schulze (1995a) in the *ACRU* manual as flow consisting of runoff from the catchments plus runoff from upstream catchments. Stormflow depth is another important concept in flow modelling in *ACRU*, and is defined as the water from a rainfall event generated on or near the surface of a catchment, contributing to the total flow in the streams within the catchment. The *ACRU* model uses a modification of the method developed by the SCS to estimate stormflow depth and volumes from small catchments. The SCS stormflow calculation equation is based on the concept that the runoff potential is an inverse function of the soil's relative wetness. Equation 2.5 shows how runoff is calculated in the *ACRU* model.

$$Q = \frac{(P-I_a)^2}{(P-I_a)+S} \tag{2.5}$$

where

Q = runoff (mm),

P = rainfall (mm),

S = potential maximum retention after runoff begins (mm), and

I_a = initial abstraction.

S, denoting the Soil Water Deficit, is calculated by the multi-layer soil water budgeting methods of *ACRU*, avoiding the need for the estimation of a final catchment CN. *S* is calculated as the difference between water retention at porosity and the actual soil water content before to a rainfall event, after the total evaporation for the day has been abstracted. Once the topsoil reaches field capacity, "surplus" water infiltrates into the subsoil (B horizon) as saturated drainage, *i.e.*, the soil structure within the *ACRU* model is divided into an A (topsoil) and B (subsoil) horizon, an intermediate zone and a groundwater store. This process adds water to the soil horizons and groundwater store and directly influence *S*. Another important hydrological process which also has a major influence on *S* is total evaporation. The soil moisture status is required to calculate the actual total evaporation as it regulates the evaporation rate from the soil and the transpiration rate of plants.

The calculation of peak discharge is also critical in the estimation of design floods and in the design of hydraulic structures. The *ACRU* model estimates peak discharge that is connected to the stormflow volume generated for a certain simulation period by presumably a single unit hydrograph. The model currently uses all the STORMF generated for the rainfall event on the day in the stormflow peak discharge equation (Equation 2.4). This represents the stormflow (surface runoff) contribution to total peak discharge (QPEAK). It is important to note that for small catchments particularly, the contribution of stormflow and baseflow/interflow to peak discharge can ultimately lead to over-estimations in peak discharge. Developing a methodology to account for rainfall intensity on a day-to-day basis to be incorporated within the *ACRU* model may be useful to adjust estimated lag times based on the rainfall intensity. This is important since there is a relationship between the two and they both influence the simulation of the stormflow contribution to peak discharge.

Verified estimations of peak discharge are seldom available at the specific location and estimations of design floods are usually based on the application of procedures which show the key processes influencing the runoff response of an area to rainfall. Peak discharge estimated from small catchments has some correlation to stormflow volume. The Annual Maximum Series (AMS) of daily peak discharge can be derived and an extreme value distribution fitted in order to analyse the probable magnitude of a flood (Schulze, 1979; Schmidt and Schulze, 1984; Schmidt *et al.*, 1987; Schulze, 1994). The SCS peak discharge equation shown in Equation 2.4 under the SCS-SA chapter is also used in the estimation of peak discharge in the *ACRU* model.

Land use is represented by the *ACRU* model in three processes *viz.* canopy interception, evaporation from vegetated and impervious surfaces and soil water extracted by plant roots (Schulze, 1995a). The *ACRU* model represents impervious areas of an urban catchment by dividing the impervious surface area into two classes of impervious areas, namely those that are directly connected to a stream or stormwater system, i.e. Adjunct Impervious Areas (AIA) and those areas that are not directly connected to drainage system, i.e. Disjunct Impervious Areas (DIA) as illustrated in Figure 2.5.

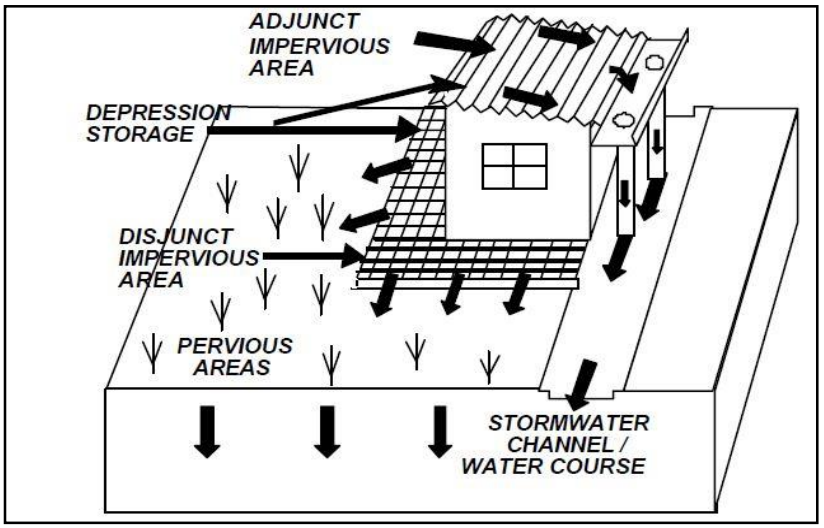

Figure 2.5 An *ACRU* representation of an urban catchment (Schulze, 1995a)

Tarboton and Schulze (1991) developed typical parameter values for different types of urbanisation as shown in . These values have also been used in recent land use studies in the uMgeni catchments (Warburton *et al.*, 2010; Schütte, 2014; Schütte and Schulze, 2017).

Table 2.2 Default impervious values for different types of urbanisation (Tarboton and Schulze, 1991)

Land Cover	**Average % impervious area**	**Fraction of ADJIMP**	**Fraction of DISJIMP**
CBD / commercial			
- Industrial	85	0.70	0.15
- high density	70	0.40	0.30
- medium density	50	0.30	0.20
- low density	30	0.15	0.15
Formal residential			
- high density	65	0.50	0.15
- medium density	40	0.25	0.15
- low density	20	0.05	0.15
Informal residential			
- urban in character	30	0.00	0.30
- rural in character	10	0.00	0.10
Open space parkland	05	0.00	0.05

Tarboton *et al.* (1992) used Geographical Information System (GIS) as a tool to form a complementary interface between GIS and the *ACRU* modelling system, where GIS was used to extract information to input into the *ACRU* model for efficient operation and accurate simulations. The mutual interaction between the *ACRU* model and GIS and its contribution to decision support systems is further described by (Kienzle, 1993; Schulze, 1995b; Kiker *et al.*, 2006).

Developments of the *ACRU* model and application in urban catchments

The *ACRU* model has been applied and verified on data from various countries including South Africa, Eswatini, Zimbabwe, Canada, New Zealand, Germany and the USA. Schulze (2021) reported on a number of verification studies conducted on various components of the *ACRU*

model. Smithers *et al.* (2013) looked at further verifying and developing the *ACRU* model as a daily-time step continuous simulation modelling approach. The amount of work done towards the improvement and verification of *ACRU'*s modelling system makes it a suitable hydrological model for application in a hydrologically complex urbanised catchments with a mix of different land uses. Mauck (2012) evaluated the hydrological responses to future predictions of urban growth in the uMgeni catchment, South Africa. An urban growth model was employed to produce scenarios of reasonable future urban expansions and these scenarios were modelled using a hydrological model to simulate the hydrological responses to urban growth. The Slope, Land use, Excluded areas (areas were urban growth is not expected to occur e.g. conservational areas), Urban Extent, Transport routes and Hill shade (SLEUTH) urban growth model by Silva and Clarke (2002) was used for predicting the scale and location of where urbanisation is expected to expand to and the *ACRU* model was used to assess the hydrological responses accompanied with the urban growth. The *ACRU* model provided good results, showing increases in streamflow from the predicted urban expansion scenarios.

Schmitz and De Villiers (1997) added an urban component to the *ACRU* model, which was originally created to replicate a catchment with less than 20% imperviousness. Tarboton *et al.* (1992) then changed the model to increase its adaptability to work in urban regions with greater than 20% imperviousness. This study worked on integrating urban models such as the Watershed Storm Hydrograph Model (WASHMO), the wash off and runoff equations adopted in the Storm Water Management Model (SWMM) and Hydrological Simulation Programme FORTRAN (HSPF) water quality models as sub-models for the *ACRU* model to allow the model to function on a completely urbanised catchment with regards to runoff, and hydrograph development. The results from the above study included accumulation equations from the rainfall-runoff model WASHMO. A version of the *ACRU* model was thus expanded to model design floods and non-point pollution from urban areas with a higher degree of reliability. Warburton *et al.* (2010) assessed the performance of the *ACRU* model in different land uses, and concluded that the *ACRU* model can be used with confidence to simulate the streamflows of the three selected catchments and was able to represent the hydrological responses from the range of climates and diversity of land uses present within the catchments. . Schütte and Schulze (2017) evaluated the projected impacts of urbanisation on flows within the uMngeni catchment. The study concluded that urbanisation drastically altered the total flow in the catchment by introducing increases in the total runoff (made up of an increase in baseflow and stormflow) for

both current urbanisation and future urbanisation projections. Myeza (2019) conducted research on improving the modelling of the hydrological impacts of urban land use in the Limpopo North water management area (32 094 km^2). Regardless of the issues related to a lack of hydrological data, verification of the *ACRU* model to simulate the water flows in the selected catchment by comparing the simulated versus the observed streamflow was performed. The *ACRU* model performed adequately, as it was able to be further used to assess the influences of land use on the water flows of Limpopo. Myeza (2019) estimated the percent impervious area for an urban land use class by determining the average percentage impervious areas through the representative samples chosen for each urban land use area estimation and examined water resources planning and modelling for application in land use change. The *ACRU* model simulated streamflow correlated well to the observed, and both the high and low flows were simulated well with a good mean and variance of the observed flows. Based on Myeza (2019), the *ACRU* model was deemed fit to simulate the partitioning of precipitation into green and blue water under different land use conditions, which was one of the objectives for the study.

Several research projects have added to the development and application of the *ACRU* model for DFE and results of these projects have been discussed by Smithers *et al.* (2007) and Smithers *et al.* (2013). Smithers *et al.* (2007) incorporated the developments and improvements into the *ACRU*'s modelling system and the Thukela Catchment (29 036 km^2) in South Africa was used as a case study to evaluate the methodology. The outcomes of the projects emphasised the challenge associated with using the model in a functioning catchment, i.e. where documentation of water abstractions and changes in land cover are non-existent. Unreliable and inconsistent observed data resulted in further challenges with verification (Smithers *et al.*, 2013). The results and discussion of the studies concluded that dividing catchments into smaller homogenous sub-catchments or HRUs is more feasible and instead of lumped information, land cover and area weighted soils produce better results. Conceptual and practical improvements have also been performed on the SCS runoff equation used by the *ACRU* model (Schulze, 1995a). Rowe (2015) conducted introductory research towards the development and refinement of a CSM method that can be used both internationally and locally for DFE. Rowe (2019) also looked at ways to develop the conceptual basis of representing hydrological condition classes and land management in the *ACRU* modelling system, with reference to the responses calibrated into the SCS-SA model through the CN approach. This included confirmation of the conceptual improvements using the limited observed rainfall and runoff data available.

2.3 The Use of Remote Sensing and GIS to Map Impervious Surface Areas

A catchment's physical characteristics must be assessed spatially and temporally to achieve realistic and representative hydrological results and simulations (Hameed, 2017). For many decades, engineers and hydrologist have used Geographical Information Systems (GIS) and satellite-based remote sensing technologies to measure land surface parameters (Verma *et al.*, 2009). With recent developments in computer technology, the integration between RS and hydrological models has become more efficient and preferred to field surveys with GPS, which can be expensive and time consuming (Vazquez *et al.*, 2018).

Several studies pertaining to the use of RS and satellite imagery for detecting land cover were done in the late 1970s and 1980s. During this period, new methods were still being invented and developed. Anderson (1976) developed a land use classification method that uses remotely sensed data. This method was a standard for land cover and land use mapping for two decades. When the first Landsat satellite image was launched in 1972, it included four spectral bands and a 79 m spatial resolution, hence facilitating mapping of land cover/land use (Slonecker *et al.*, 2001). During 1982, a new innovative period of multi-spectral remote sensing was developed, which was followed shortly thereafter by the launch of Landsat 4 satellite imagery. The Thematic Mapper sensor on Landsat 4 significantly improved the spatial resolution and was made up of seven spectral bands. Wheeler (1986) demonstrated the improved ability of the thematic mapping sensors to identify urban land cover using spectral bands. The developments around remotely sensed products brought about immense progress in the discriminatory competence of remote sensing analysis in urban environments.

The launch of the Systeme Probatoire d'Observation de la Terra (SPOT) by France in 1986 included 20 m multi-spectral and 10 m panchromatic data. Jadkowski *et al.* (1990) reported on the value of SPOT data for application in urban areas. According to Jadkowski *et al.* (1990), research and development of imaging data for identifying impervious areas can be categorized into broad classes that are contingent on the process of obtaining and converting imagery into usable information. These categories are based on the primary uses of remotely sensed data, and are grouped as follows; (a) interpretive applications, (b) spectral applications, and (c) modelling applications. Interpretive applications involve a human analyst interpreting data after manually extracting information from the images by analysing the texture, tone, shape etc. Spectral information involves computer processing of data from spectral sensors to enable land

cover classification or mapping impervious surfaces. Modelling applications refer to the process of transferring information from remotely sensed imagery as direct input data into a hydrological model.

2.3.1 Importance of impervious surface area mapping in urban hydrology

A detailed assessment and mapping of impervious surfaces in an urban area is essential for simulating the hydrological impacts of urbanisation and this is particularly studied in urban drainage and environmental sciences (Shu *et al.*, 2018). There is a general lack of data, whether it be hydrological or physical, in certain urban catchments, e.g. in under-developed informal urban areas. Therefore, RS can serve as a more accurate alternative tool for obtaining data for hydrological modelling in such areas and in ungauged regions (Pourali *et al.*, 2014).

The percentage of the catchment that is impervious and pervious is one of the essential variables necessary for accurately modelling runoff and varies significantly with land use categories and sub-categories (Cronshey, 1986; Warwick and Tadepalli, 1991). Remote sensing and GIS methods have been reported to produce relatively reliable estimates of impervious and pervious areas (Strahler *et al.*, 1986; Slonecker *et al.*, 2001; Yang *et al.*, 2003; Weng and Lu, 2009). In reviewing the approaches of impervious surface mapping, Brabec *et al.* (2002) discussed four different methods, i.e. using a planimeter to quantify impervious areas on aerial photography, totalling the number of intersections on superimposed grids on an aerial photograph, image classification, and estimating impervious surface coverage based on the percentage of urbanization in a catchment.

2.3.2 Remote sensing methods for impervious surface area mapping

Lu *et al.* (2014) summarised the general ISA mapping methods and main procedures and also examined the impacts of scale issues when choosing remote sensing data. In order to achieve reliable and representable ISA mapping and estimation, it is important to consider the selection of suitable remote sensing data, image pre-processing and choosing suitable variables, development of ISA estimation models, and assessment of the estimates (Sun *et al.*, 2017). It is essential to plan an optimal method that is suitable to a specific study site or purpose to avoid errors.

A study by Ruiz Hernandez and Shi (2018) conducted in Mexico, on the town of Ciudad Juarez, proposed a new method for mapping urban land uses by using an integration of spatial metrics

and texture assessment in an object-based image analysis classification. Spatial and texture metrics were extracted from a high resolution satellite image using the machine learning algorithm of Random Forests land cover classification. The satellite image classification method includes selecting meaningful spatial indices, mostly by visual evaluation and combining the image and texture values to produce the classification. The method proved to be reliable by producing an overall 92.3 % accuracy in the classification and a kappa coefficient (measure of how the land cover classification results match the values assigned by chance) of 0.896. This classification procedure excluded the use of census or primary data, therefore enabling its applicability in developing countries. In a recent study done by Bui and Mucsi (2021) in Binh Duong province, Vietnam, they investigated running a combination of the object-based and pixel-based classification methods on multi-temporal Landsat images using GIS analyses. By following this method, a connection between land cover and land use was identified and using the Random Forests classifier, land cover and land use functions were extracted and classified. The study revealed that the connection between land use and land cover was as a result of the spectral, spatial and temporal linkages between the two, therefore, the land cover map could be converted into a land use map and vice versa. The achieved accuracy for the classification was 93.86%.

The methods of applying and using remotely sensed data have evolved and developed over the years, but still follow the same concepts. In another study, Weng (2012) discussed the major methods and impacts of spectral, spatial, temporal and geometric features on ISA mapping and estimation performance. Table 2.3 provides a brief overview of the major ISA mapping approaches using satellite images, grouped into six classes based on the use of remote sensing variables and methods.

Table 2.3 Different methods for mapping and estimating ISA

Category	Major methods	Data-sets	References
Per-pixel-based classification methods	Maximum likelihood classifier; decision tree classifier; expert rules	IKONOS, QuickBird, Landsat	(Goetz *et al.*, 2003; Powell *et al.*, 2007; Lu *et al.*, 2011)
Object based methods	Segmentation-based classification	QuickBird, IKONOS	(Ji and Jensen, 1999; Hu and Weng, 2011; Lu *et al.*, 2011)
Sub-pixel based classification methods	ERDAS sub-pixel classifier; Artificial neural networks; ISA as one endmember	Landsat, ASTER, IRS-1C	(Ji and Jensen, 1999; Rashed *et al.*, 2001; Phinn *et al.*, 2002; Weng and Hu, 2008; Hu and Weng, 2009; Van de Voorde *et al.*, 2009)
SMA based methods	Addition of low- and high-albedo fractions; modified approach based on low-albedo, high-albedo, and land surface temperature; Spatially adaptive SMA.	Landsat,CHRIS/ Proba, HyspIRI, MODIS	(Rashed *et al.*, 2003; Wu and Murray, 2003; Wu, 2004; Lu and Weng, 2006; Powell *et al.*, 2007; Weng *et al.*, 2009)
Threshold -based methods	Threshold based on NDISI; hybrid method based on NDVI and cluster analysis	QuickBird Landsat	(Xu, 2010; Lu *et al.*, 2011)

2.4 Discussion and Summary of the Literature Review

Urbanisation is increasing at a rapid rate. One of the consequences of the unplanned and haphazard increase in urban areas is the increase in runoff volume, peak discharge and a change in catchment response time. The changes are a result of the continuous expansion of impervious surfaces. This results in a higher risk of flooding and damage to urban infrastructure and subsequent impact on the economic losses and potential loss of life. There are several factors that affect the hydrological processes of an urban catchment, i.e. the catchment's permeability, drainage paths and catchment slope. The growth of impervious surfaces directly influences the above-mentioned factors, subsequently aggravating the consequences that result from the interaction between the catchment's attributes and hydrological processes. Therefore, rainfall-runoff modelling is more necessary in urban areas for flood estimation and ensuring the construction of suitable drainage infrastructure. Application of rainfall-runoff models in urban areas assist not only in the planning and design of hydrological structures, but also in decision making related water management in urban areas.

Design flood estimation involves estimating the risk associated with a flood event of a particular magnitude, with risk frequently expressed as a return period. There are a range of design flood estimation methods available for application, but only a few of these methods are suitable for the unique urban conditions found in South Africa. Several studies mentioned in the literature review call for further development of existing design flood estimation methods as there is an abundance of available data to do so. Refining these methods and modelling software could expand their versatility and competence in catchments with a range of land uses and different characteristics. South Africa comprises of a large area percentage of informal areas settlements by area that have a range of urban land uses unique to South Africa. These settlements are characterised by poor infrastructure and a rather more complex hydrology due to their combination of both rural and urban features.

The continuous simulation *ACRU* and the design event SCS-SA models have been selected as the rainfall-based design flood estimation methods for application in this study. The selected models are able to estimate design floods for different types of developments as tested by some studies mentioned in the literature. The SCS-SA model makes use of a simplified technique based on the catchment's soil and land cover characteristics expressed as a single parameter i.e. the CN, while the daily time-step *ACRU* model explicitly represents the processes that affect

the soil moisture status by simulating the components of the soil water budget. Attention is drawn to the land cover properties of urban areas and their influence on runoff generation, therefore the SCS-SA model is suitable for this study as it incorporates land cover classification that accounts for a variety of land management practices and hydrological conditions. The SCS-SA model has proven to be an accepted and well-established method for estimating design floods because the CNs used in the model were generally derived from observations. An important characteristic of both the *ACRU* and SCS-SA models is that they are able to estimate peak discharge from a range of land uses and use the same stormflow volume peak discharge equations with different levels of sophistication of the variables used.

Continuous simulation models such the *ACRU* model require long records of historical data and verification against observed data. Modelling urban areas requires a detailed analysis of the percentage of impervious surfaces, drainage, land cover and condition and soils data in order to simulate runoff volumes. These datasets need to be reliable and accurate to produce good simulations. Obtaining reliable and accurate data is often a challenge in hydrological modelling, especially for informal urban settings. One of the most important and difficult pieces of information to extract are percentages of impervious surfaces covering an urban catchment. Multiple remote sensing and GIS methods to estimate urban impervious surfaces have been reviewed. Land cover classification using remotely sensed data has proven to provide reasonable estimates of land cover classifications in urban areas. RS applications with satellite images was initiated in the early 1970s and has developed and drastically improved over the years. The integration of RS and GIS with hydrological models has also become more common in recent publications.

As an addition, literature not only suggests that more research needs to be directed at applying and assessing the performance of hydrological models in diverse urban areas, but also towards updating and developing design flood estimation methods and integrating them with other software and data sources platforms such as GIS and RS to improve their performance.

3. METHODOLOGY

This chapter outlines the methodology adopted to accomplish the aims and specific objectives of the study. The detailed description of the selected study sites is included in the methodology. Data collection and assimilation processes are also detailed below. The remote sensing classification methods used for mapping imperviousness and configuration through QGIS (Sherman *et al.*, 2004) are included in the methodology. The structuring and configuration of the *ACRU* and SCS-SA models are also discussed below.

3.1 Selection and Description of Research Sites

Catchments that have urban characteristics were selected for the study. The study catchments are located in two urbanised areas in South Africa, in the Gauteng and the KwaZulu-Natal provinces. Two study catchments were selected from the City of Tshwane (Catchments A2H054 and A2H063) and one from Pietermaritzburg (Catchment U2H057). As shown in Figure 3.1, Catchments A2H054 and A2H063 are situated north-east of the City of Tshwane's central business district and Catchment U2H057 is located between Edendale and Ridgepark within the district of Umgungundlovu, as shown in Figure 3.2. In Catchment A2H054 the Hartebees Spruit drains onto an urban area in the East of Tshwane, consisting of suburban areas, agricultural land, and a mix of industrial and business areas. Catchment A2H063 is located between the Meintjieskop in the south and the Magaliesberg in the north and is known as the Moot. The catchment comprises of residential areas, with sports grounds, agricultural areas, woodlands and industrial and business land use.

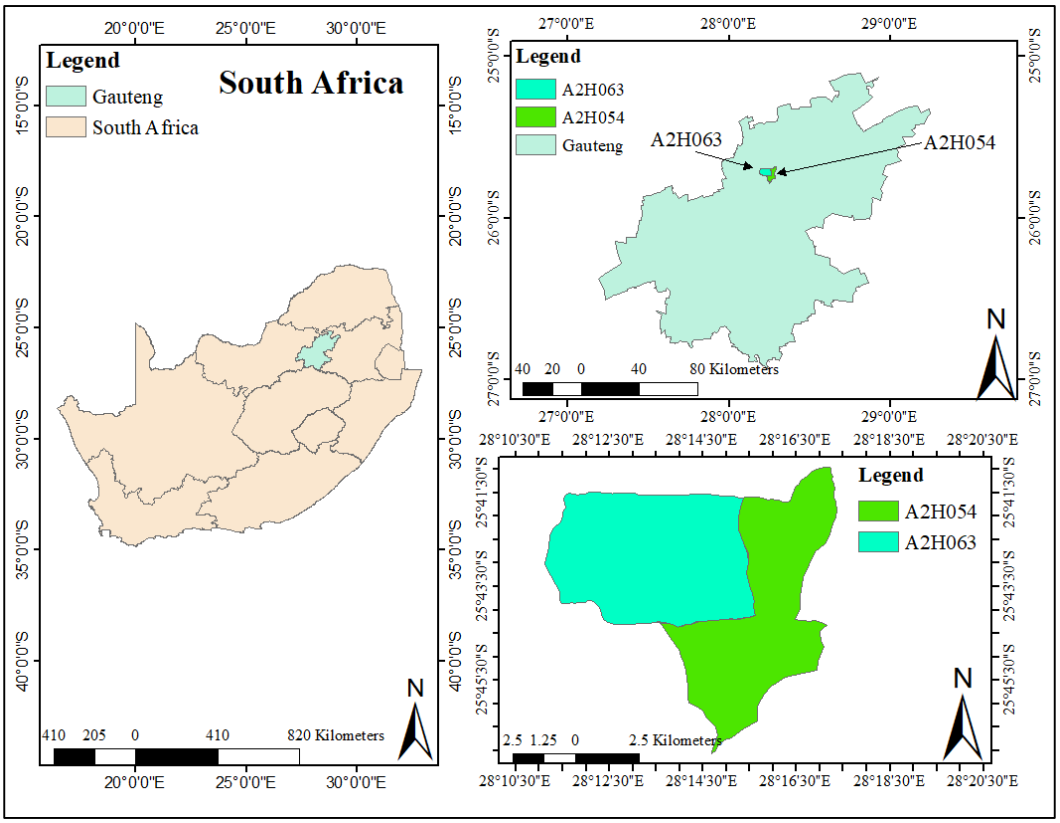

Figure 3.1 Location of the A2H054 and A2H063 Catchments in the Gauteng province

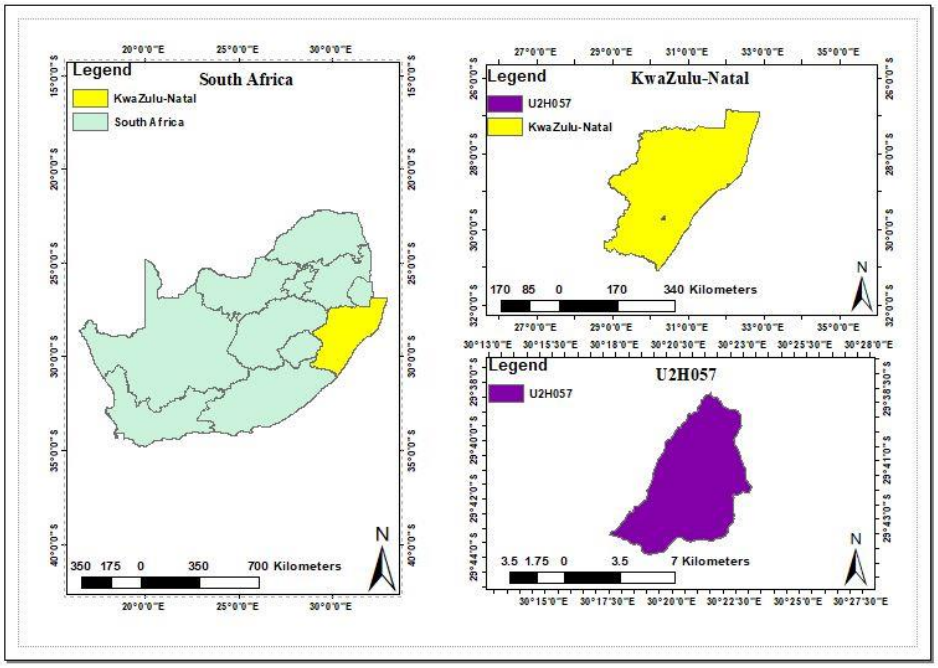

Figure 3.2 Map depicting the location of Catchment U2H057 in the KZN province

The green areas are covered with mostly grassland with some bushes and trees (Loots, 2020). Catchment U2H057 has a mix of different settlements and urban development types. There is contrast in land use types within the catchment. A large portion of the catchment comprises of underdeveloped, informal settlements with rural characteristics while on the other side of the catchment, there exist developed and urbanised residential areas with paved yards and roads.

The catchments were chosen due to their small sizes as seen in Table 3.1 and relative homogeneity in terms of urban development types in the catchments (Loots, 2020). Data availability and their location within densely urbanised provinces were also an attraction for their selection as the study catchments. The catchment Mean Annual Precipitation (MAP), slope and altitude are summarised in Table 3.1 and detailed explanations of how these catchment characteristics were derived are provided in the individual data collection sub-sections. The catchments in Tshwane experience a humid sub-tropical climate, with long, hot, and rainy summers, and short mild winters. The climate in Pietermaritzburg can be described as warm and temperate with significant rainfall occurring even during the summer months. The average annual temperature in Tshwane is 17.8 °C and in Pietermaritzburg is 27.4 °C.

Table 3.1 Study catchment characteristics

Catchments	**Area (km^2)**	**MAP (mm)**	**Slope (%)**	**Altitude (m)**
A2H054	33.23	730	4.51	1349
A2H063	29.65	730	4.32	1302
U2H057	48	966	8.48	845

Initially, a combination of the 2018 South African National Land Cover database (Thompson, 2019) and visual interpretation from fieldwork, based on either the availability or lack of basic urban water drainage systems such as culverts and kerb inlets, provided an overview of the kind and level of development. Subsequently, detailed land cover classifications were conducted using RS and GIS. Additional and thorough field investigations were then conducted for all the three catchments to verify the remote sensing and GIS classification. The field investigations for the catchments in Tshwane were carried out by Loots (2020). The areas in the catchment identified as informal were characterised with under-developed and inefficient stormwater

drainage systems with illegal dumping in the open channels and streams. The type of settlements and building materials used for the homes also indicated the level of development, with houses that were built with mud and stones, plastic sheeting, corrugated metal, wood and cardboard. Houses surrounded by less impervious features such as paved walkways, paved roads and proper water-proof roofs also fell under the informal category.

3.2 Derivation of Data and Information Required for Input to Models

Information required by the *ACRU* and SCS-SA models was collected for the study catchments and transformed into hydrological information and used to generate the modelling inputs. The data collected includes the following, with more details provided in the sections below:

a) Locational and catchment: Catchment names, geographical location and altitude.
b) Hydrological: Streamflow data from gauging weirs, a catchment response time.
c) Climate: Rainfall, monthly averages of temperature and evaporation.
d) Soils: Hydrological properties of soils including horizon depths and soil water retention properties and percentage of different soil types in the catchment.
e) Land use and land cover: Crop coefficients, leaf area indices, interception loss rates, root distribution, and impervious surface areas (adjunct and disjunct impervious areas).

3.2.1 Rainfall

Daily rainfall data from stations surrounding Catchments A2H054 and A2H063 and seven rainfall stations surrounding Catchment U2H057 were collected from SAWS. The stations' coordinates were plotted together with the catchments to compare the distance between the rainfall stations and the catchment boundary as shown in Figure 3.3 and Figure 3.4. For the Gauteng catchments, only one of the six stations was within the catchment boundary and for the catchment in KZN, none of the stations were within the catchment boundary.

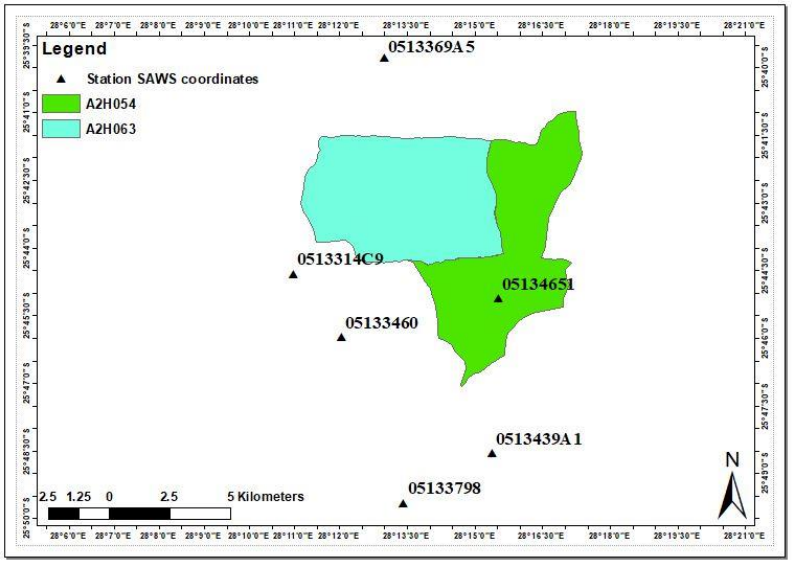

Figure 3.3 Rainfall stations surrounding land within Catchments A2H054 and A2H063

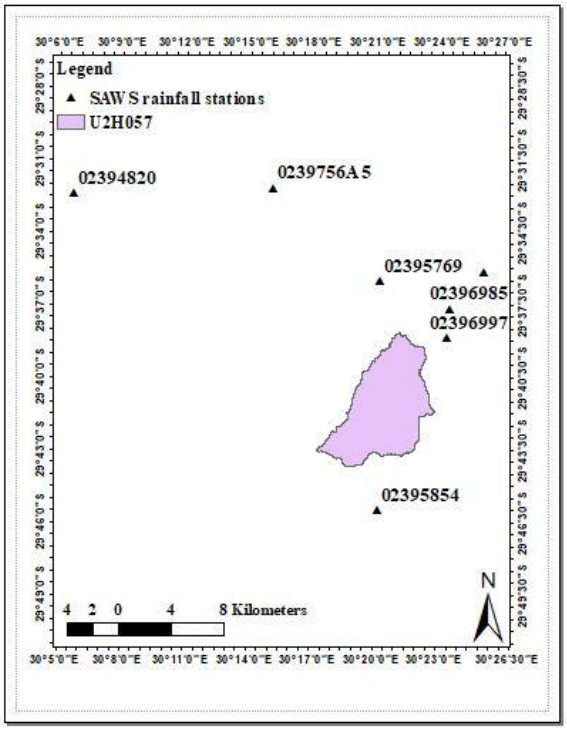

Figure 3.4 Rainfall stations surrounding Catchment U2H057

The following factors were considered for the selection of the rainfall station for each study catchment.

a) distance from catchment centroid,
b) record length,
c) reliability,
d) number of missing values, and
e) percentage of infilled data.

Rainfall data from Station no. 02396985 were obtained from the South African Weather Service (SAWS) for Catchment U2H057 for a record length of 23 years (1995-2018). Rainfall data were also extracted from the Daily rainfall utility tool by Lynch (2003) for years prior to 1995 for the study catchments. This was done to extend the period of data obtained from SAWS from 1985 to 2018 for Catchments A2H054 and A2H063. The DWS gauging station for Catchment U2H057 only has data starting from 1995. The simulation period that rainfall and streamflow data was collected for is summarised in Table 3.2 for all the study catchments. The daily rainfall utility provided reliable patched historical rainfall data. Some series of rainfall data obtained from SAWS had missing rainfall and were infilled using data from surrounding stations using a monthly regression analysis approach (Pegram, 1997). This was done to produce a consistent record length for the rainfall data to match the available flow data obtained from the Department of Water and Sanitation (DWS). Owing to the constraints in data availability, the model simulations were only undertaken from 33 and 23 years of data for the Tshwane Catchments and Catchment U2H057, respectively.

Table 3.2 Rainfall and runoff data sources snd simulation periods for the study catchments

Data sources	**A2H054**	**A2H063**	**U2H057**
SAWS	1994-2018	1994-2018	1995-2018
Rainfall Utility tool	1985-1993	1985-2018	-
Flow data (DWS)	1985-2018	1985-2018	1995-2018
Total simulation period (yrs)	33	33	23

Monthly adjustment factors were calculated for the newly selected rainfall station in order to ensure that the rainfall from the selected station (in or neighbouring to Catchment A2H063) is representative of the areal rainfall of the catchment. The adjustment was done so as to convert point rainfall to catchment rainfall. The adjustment factors were calculated by dividing the median catchment rainfall by the median of the gauge rainfall. The calculated adjustment factors for Catchment U2H057 are included in Table 3.3, and the highlighted cell indicates that the adjustment factor for July was out of the *ACRU* model range (0.7-1.3). This could be as a result of errors in both catchment and gauge rainfall, and therefore the highest default factor of 1.3 was recorded for July.

Table 3.3 Rainfall adjustment factors calculated for Catchment A2H063

Month	**Jan**	**Feb**	**Mar**	**Apr**	**May**	**Jun**	**Jul**	**Aug**	**Sep**	**Oct**	**Nov**	**Dec**
Catchment median (mm)	102	93	91	36	18	7	6	16	35	72	92	101
Gauge median (mm)	115	84	82	34	21	7	1	13	36	77	93	137
Adjustment factor (mm)	0.89	1.11	1.11	1.06	0.86	1.00	**6.00**	1.23	0.97	0.93	0.99	0.74

3.2.2 **Temperature**

The *ACRU* model requires daily rainfall and A-pan evaporation values. Multiple options to estimate A-pan values are available to use depending on the availability of data (Schulze, 1995a). Monthly averages of maximum and minimum temperatures were obtained from the weather stations, and these were used for the estimation of the monthly A-pan equivalent evaporation. The Hargreaves and Samani (1985) daily A-pan equivalent reference evaporation equation was used to calculate the daily evaporation values using maximum and minimum temperature. Bezuidenhout (2005) reported that the Hargreaves and Samani (1985) equation simulates reasonable daily reference evaporation values for South Africa. Daily minimum and maximum temperature were collected for each study catchment for record lengths shown in Table 3.4.

Table 3.4 Year of temperature data for the study catchments for the respective simulation periods

Temperature	A2H054	A2H063	U2H057
Daily min temp	1985-2018	1985-2018	1995-2018
Daily max temp	1985-2018	1985-2018	1995-2018

3.2.3 Soils information

The soils information was obtained from the SCS soil class map at terrain unit resolution (Schulze and Schütte, 2018) shown in Figure 3.5. The soils map coverage consisted of detailed information of the soils making up the individual terrain units, including physical characteristics for each Land Type. The SCS soils classes at terrain unit level correspond to the SCS soil groupings as shown in Table 3.5. The different variables such as the horizon depths, wilting points, field capacity and porosity, and horizon responses were identified by clipping the soils map to the extent of each HRU shapefile. In the case where the HRU land use is dispersed spatially in the catchment, then an average of the soil parameters was calculated for each HRU.

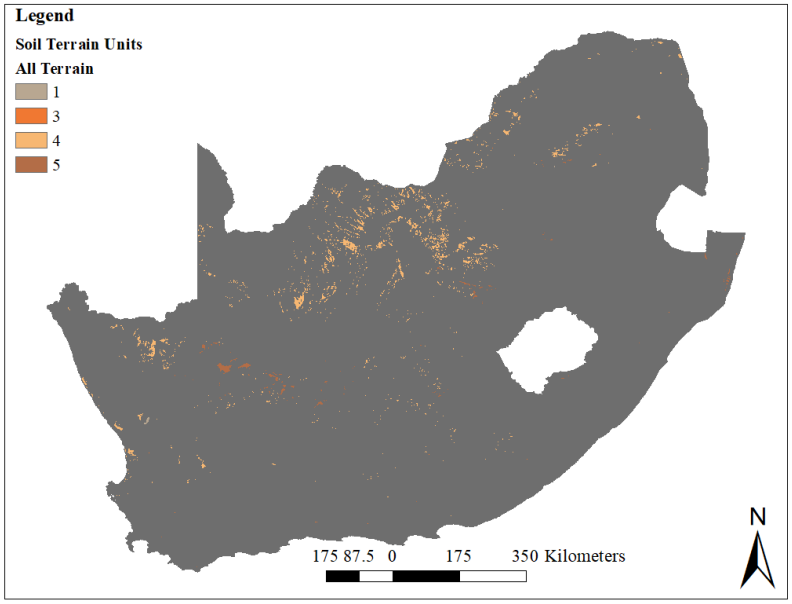

Figure 3.5 SCS-SA soil groups in South Africa mapped at terrain unit level (Schulze, 2018)

Table 3.5 Relating SCS terrain units to the SCS soil groups (Schulze *et al.*, 2004a)

SCS terrain unit	SCS soil grouping	Textural class (USDA, 1986)
1	A	Sand
2	A/B	Loamy sand
3	B	Sandy loam
4	B/C	Loam, silt loam
5	C	Sandy clay loam, clay loam
6	C/D	Silty clay loam, sandy clay, silty clay
7	D	Clay

The soils map provided different Land Type codes shown in Figure 3.6, Figure 3.7 and Figure 3.8 within each catchment and these were identified for each HRU within the catchment. Using the Land Type inventory by Schulze (1995a), the Land Type codes were matched to their corresponding soil form and series and SCS soil groups and these are provided in Table 3.6, Table 3.7 and Table 3.8 for each study catchment.

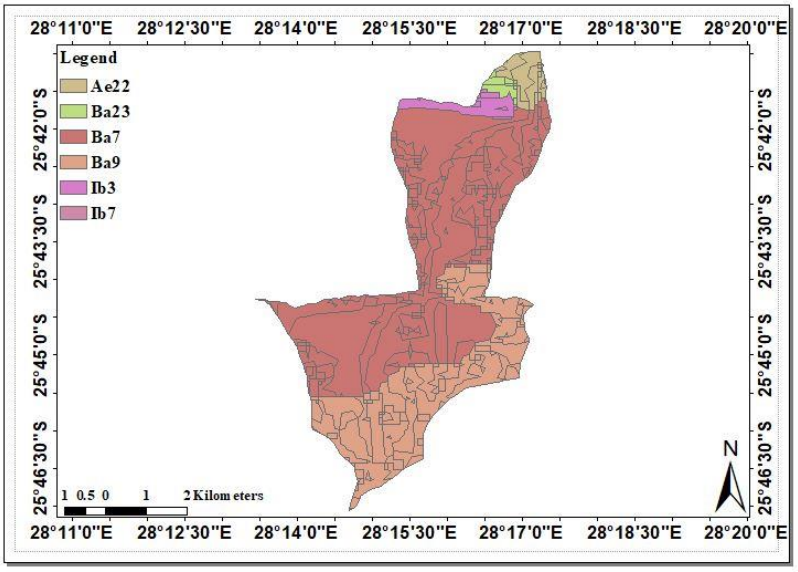

Figure 3.6 Land Types in Catchment A2H063

Table 3.6 Land Type code translation into series, SCS group and typical texture classes in A2H054

Land Type code	Soil form and series	SCS group	Typical texture class
Ba7	Hutton Makatini Hu 37	B/C	SaCl
Ba8	Shortlands Glendale Sd 21	B	SaCl
lb3	Rocks	C/D	LmSa/SaLm

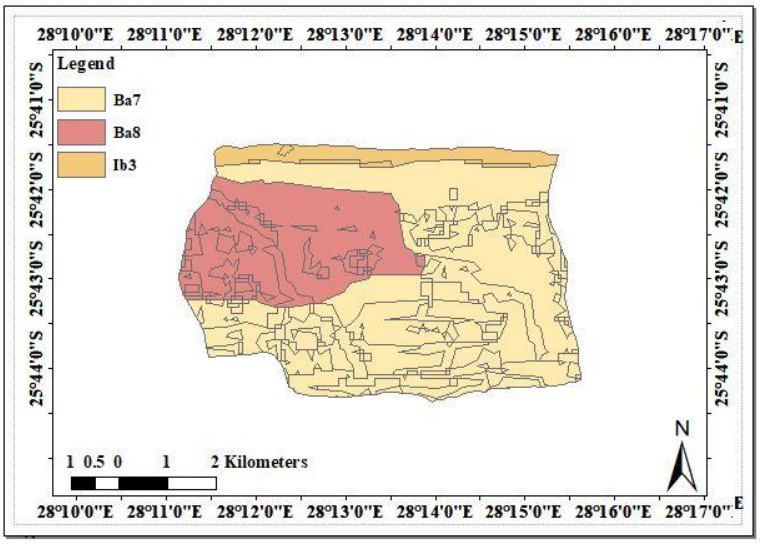

Figure 3.7 Land Types in Catchment A2H063

Table 3.7 Land Type code translation into soil form and series, the SCS group and typical texture classes in Catchment A2H063

Land Type code	Soil form and series	SCS group	Typical texture class
Ae22	Hutton Shorrocks Hu 36	A/B	SaClLm
Ba23	Hutton Msinga Hu 26	A	SaClLm
Ba7	Shortlands Glendale Sd 21	B/C	SaCl
Ba9	Rocks	C/D	LmSa/SaLm
lb3	Rocks	C/D	LmSa/SaLm
lb7	Rocks	C/D	LmSa/SaLm

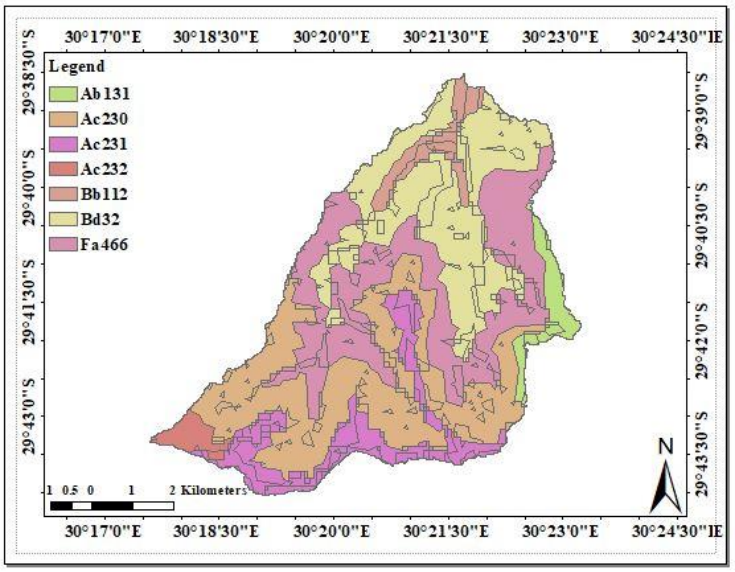

Figure 3.8 Land Types in Catchment U2H057

Table 3.8 Land Type code translation into soil form and series, SCS group and typical texture classes in Catchment U2H057

Land type code	Soil series	SCS group	Typical texture class
Ab131	Hutton Doveton Hu 27	A/B	SaCl
Ac230	Hutton Balmoral Hu 18	A/B	Cl
Ac231	Hutton Balmoral Hu 18	A/B	Cl
Ac232	Hutton Balmoral Hu 18	A/B	Cl
Bb112	Hutton Vimy Hu 28	A/B	Cl
Bd32	Saintfaiths	C	Cl
Fa466	Saintfaiths	C	Cl

3.2.4 **Streamflow data**

Daily average flow data were extracted from the three gauge stations, i.e. A2H063, A2H054 and U2H057 from the DWS website. The data were converted from cubic meters per second to millimetres per day to conform to the standard format required by the *ACRU* model. Equation 3.1 was used to convert the flow data to the required units. The observed Annual Maximum Series (AMS) of peak discharges was also downloaded from the DWS website for the available

years and these served as observed peaks which were compared to the modelled design peak discharges.

$$Q = \frac{(x * 60 * 60 * 24)}{(y * 10^6 * 1000)} \quad (3.1)$$

where

Q = daily streamflow (mm/day),

x = streamflow (m^3/s), and

y = catchment area (km^2)

3.3 Parameters for Impervious Urban Areas

The ADJIMP and DISJIMP components in the *ACRU* model represent impervious surfaces in an urban catchment and are therefore very important parameters when running the hydrological model in a catchment with impervious surfaces. A HRU is made up of the pervious fraction and the ADJIMP and DISJIMP fractions. Runoff and peak discharge are heavily influenced by these impervious components, especially the ADJIMP fraction. Extracting accurate and representable impervious surfaces in a catchment therefore plays a huge role in obtaining reliable estimates of the ADJIMP and DISJIMP area fractions. Impervious land cover can be extracted from remote sensing land cover classifications or from readily available national and global datasets. Previous studies (section 2.2.3) have made use of default values of ADJIMP and DISJIMP fractions from the *ACRU* manual. The remote sensing land cover classification method which was used for this study, the additional impervious datasets used and default values obtained from previous studies are discussed in this section.

3.3.1 Model default parameters

Tarboton *et al.* (1992) used False Colour Composite (FCC) SPOT satellite images, aerial photographs, orthophotos and field verification to classify land cover for the uMgeni catchment. From this classification, it was found that 10% of the uMgeni catchment was covered with urban land cover with varying proportions of imperviousness in each land cover. From this study, urban land cover default values shown in Table 3.9 were derived and have been used in

other more recent land use modelling studies such as (Warburton *et al.*, 2010; Warburton, 2012; Schütte, 2014; Aduah *et al.*, 2017; Kusangaya *et al.*, 2017).

Table 3.9 Default ADJIMP and DISJIMP values derived by Tarboton and Schulze (1992)

Built-up Class	**Pervious Fraction**	**Impervious Fraction**	**Adjunct Fraction**	**Disjunct Fraction**
Built-up - Urban - Residential - Formal	0.35	0.65	0.15	0.50
Built-up - Urban - Residential - Informal	0.35	0.65	0.15	0.50
Built-up - Urban - Smallholdings	0.95	0.05	0.00	0.05
Built-up - Urban - Recreational	0.95	0.05	0.05	0.00
Built-up - Urban - Commercial	0.15	0.85	0.70	0.15
Built-up - Urban - Industrial	0.30	0.70	0.40	0.30
Built-up - Urban - Transport	0.00	1.00	1.00	0.00
Built-up - Rural	0.90	0.10	0	0.10

3.3.2 **Extracting impervious data from the GMIS dataset**

The Global Man-made impervious Surface (GMIS) dataset documented by De Colstoun *et al.* (2017) from Landsat provides global estimates of fractional impervious cover derived from the Global Land Survey (GLS) Landsat datasets for 2010, shown in Figure 3.9. The GMIS dataset comprises of two components; global estimations of impervious cover and per-pixel associated uncertainty for the global impervious cover. Layers in both datasets are co-registered at a common spatial resolution of 30m. The global man-made impervious cover dataset for 2010 derived from GLS data, is one of the first 30m datasets to be produced and it is accompanied with the Global Human Built-up and Settlement Extent dataset (GHBASE). These datasets are widely used for a range of studies such as assessing the fine details of urban land cover at 30m resolution and the influence of impervious surfaces on the natural environment. This dataset was used in this study to compare impervious land cover data with the classification results obtain from following the pixel-based land cover classification method.

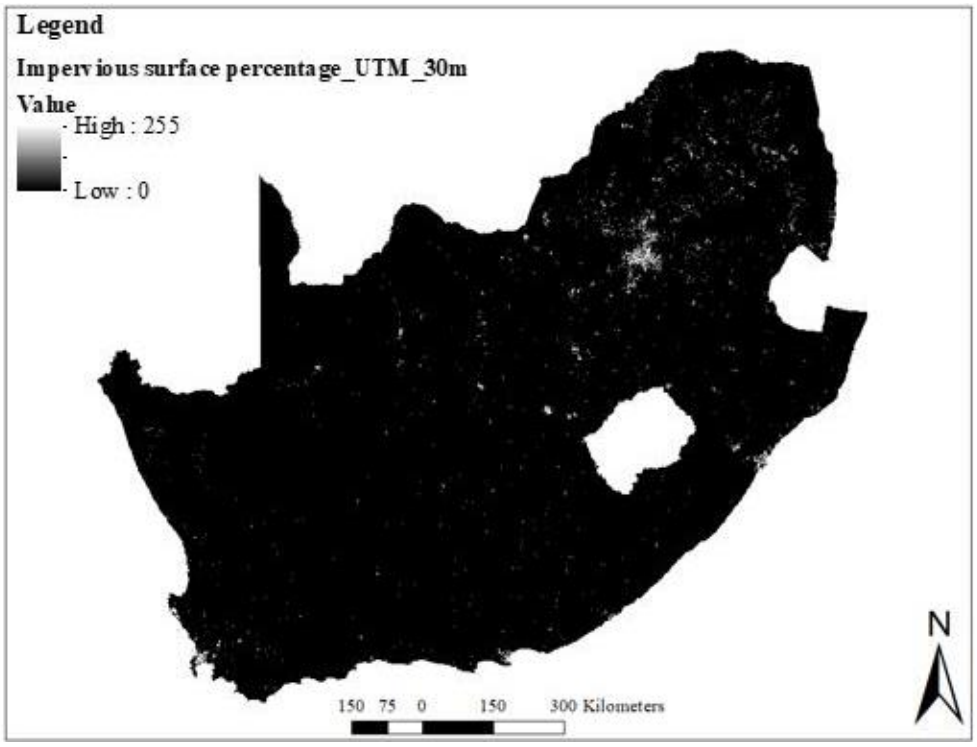

Figure 3.9 The Global Man-made Impervious Surface (GMIS) mapped for South Africa by De Colstoun *et al.* (2017)

3.3.3 **Extracting impervious data from the GAIA**

A second dataset, the Global Artificial Impervious Areas (GAIA), served as an additional dataset for verifying and comparing the impervious land cover computations derived from the two datasets described above. The dataset is shown in Figure 3.10. The dataset was downloaded for each region separately with reference to coordinates of the catchment. This dataset provides annual changes in global impervious surface area, also produced at a 30 m resolution for the period of 1985 to 2018. Supervised classification and temporal consistency checking was used to determine the change from pervious to impervious land cover. Pixels that are considered impervious are above 50% impervious. The year where pervious changed to impervious is identified from the pixel value which ranges from 34 (year 1985) to 1 (year 2018) (Gong *et al.*, 2020).

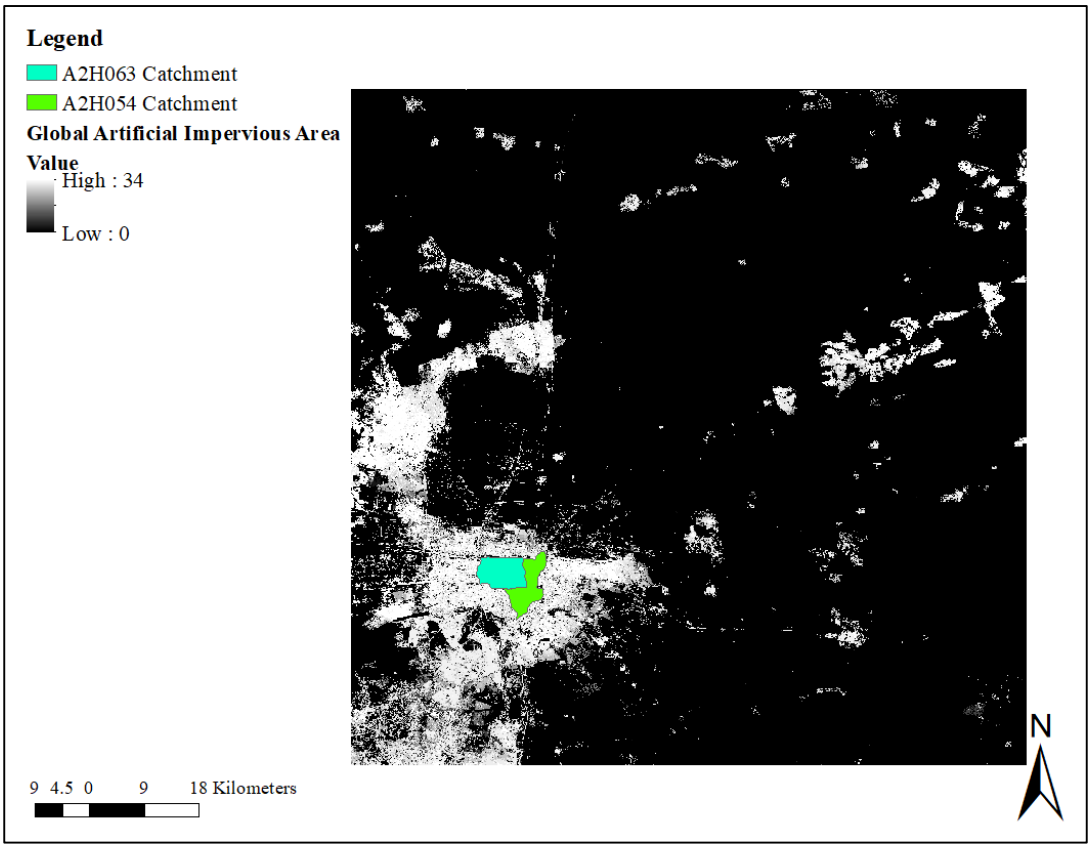

Figure 3.10 The Global Artificial Impervious Areas (GAIA) dataset by (Gong *et al.*, 2020), focused on the area around the two Gauteng study catchments.

3.3.4 **Mapping imperviousness using RS and GIS (the pixel-based land cover classification method)**

The process of classifying remote sensing imagery and its interpretation has provided an opportunity for extracting land use and land cover information. Remote sensing images cover large geographical spaces with high temporal frequency and spatial resolution for application in multiple disciplines, including the mapping of impervious surfaces.

A combination of the per-pixel based classification (supervised) and object-based (un-supervised) classification methods were used to classify Sentinel 2-level 2A, SPOT, and orthophoto aerial images to extract land cover information (Marceau *et al.*, 1990; Geneletti and Gorte, 2003; Phiri *et al.*, 2020). Sentinel images were downloaded from Google Earth engine and SPOT and aerial images were obtained from the SANSA (South African National Space Agency) and the NGI (National Geo-Spatial Information) respectively. Figure 3.11 shows an illustration of the different type of satellite images (Catchment U2H057) obtained from the

different image sources (for all three catchments). These satellite images were used to collect training samples and to run the land cover classification.

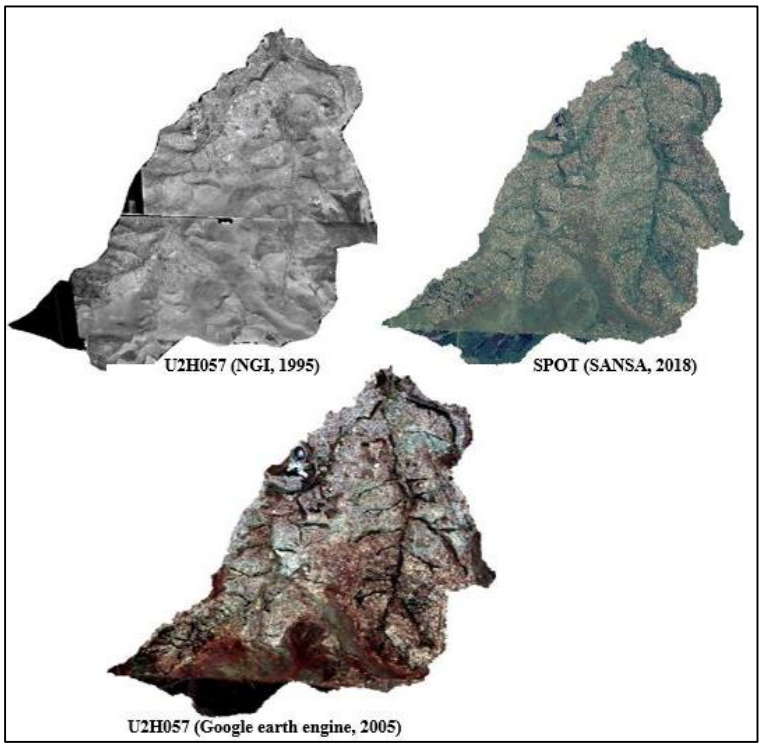

Figure 3.11 Satellite images used for the pixel-based land cover classification completed for this study

In pixel-based classification methods, each pixel represents a single land use type. In this method, the remote sensing imagery is seen as a collection of pixels consisting of spectral information, and therefore spectral variables and their transformations (e.g. principal components, vegetation indices, etc.) are input to per-pixel classifiers. These classification methods are divided into two groups: supervised and un-supervised classifiers. Un-supervised classifiers divide a satellite image into a number of different classes based on the natural arrangement of the image values and functions without the assistance of training data or prior knowledge of the study site.

Supervised classification involves a human analyst who manually collects representative training samples with a known class type from a standard land cover map. In this study, the 2018 SANLC map was used. The spectral properties of each pixel in the image are compared with those of the training samples. Vegetation and ISA have different spectral signatures especially regarding vegetation indices. The Normalised Difference Vegetation Index (NDVI)

can be used to distinguish between the non-vegetated and vegetated classes through the thresholding method, which was briefly referred to during the classification process. Bare soils, waterbodies and ISA are included under non-vegetated classes. The main step was to separate ISA from bare soils and waterbodies through a classification method often referred to as the cluster analysis method. The supervised per-pixel based, and the threshold classification methods were applied on Google Earth Engine (GEE) and on Python Colab platforms. Scripts consisting of functions, equations and models were developed and run for the remote sensing images, and the resulting images were downloaded and further processed and analysed in ArcMap and QGIS. ArcMAP and QGIS are geospatial processing programs that were used to create, view, edit, and analyse the geospatial data. These programs were used for various computations as they enable a user to create maps, explore datasets and assign symbols to features accordingly (Mitchell and Minami, 1999; Graser *et al.*, 2017).

Initially the land cover classifications were run on GEE using the per pixel classification method. A script was written on GEE and an image collection was imported and filtered by the study record, across the extent of the study area, and including a cloudy pixel percentage, reduced by applying the median function and then lastly clipping this out for the desired study area. The images were exported with their respective bands, except for Band 1, 10 and 9 because these bands have a very coarse resolution of 60 m and therefore are not suitable for the objective of this study. Images with a resolution of less than 10 m and consisting of multiple bands i.e. Red, Green, and Blue (RGB) were used for the classification to produce accurate results. The downloaded RGB composite image was used for visualisation to collect the land cover training samples from the study areas by identifying impervious, pervious, and bare land cover features. The goal for running the classification was to map out and distinguish the impervious from the pervious land cover. Once the training samples had been collected, a code was created in order to extract the reflectance values (e.g. a measure of visible and usable light reflected from a surface when illuminated by a light source) at each of the trained sample points. Once the classification had been conducted, it was noted that the threshold method did not work. The algorithm failed to distinguish between ISA and bare soil. Therefore the classifications were then conducted using a python script and the EnMAP-Box (Enhanced Map) plugin on QGIS. EnMAP Box is a python plugin for QGIS that is designed to process and visualise hyperspectral remote sensing data (Rabe *et al.*, 2018).

Python was selected because it can be fully optimised and can be used to undertake complex analysis. A script was written in Python, for creating a model based on the reflectance values that were exported from GEE. The reflectance values were split into training and test datasets. The training datasets made up the 70% of the data and the test was the remaining 30%. A model was created using the 'extra trees classifier.' This classifier was selected because it is powerful and robust (Patel and Suthar, 2020). The created model was optimised by tuning the parameters of the model such as the number of estimators (also known as number of trees), the criteria, and maximum depth. This was done by changing the parameter values and taking note of which value produced the best classification results, as the overall accuracy of the classification changes each time the parameters are altered. Illustrated in Table 4.5 is a confusion matrix that enables visualisation of the performance of a supervised algorithm (Haghighi *et al.*, 2018). Mean F1 accuracy is defined as the weighted average of Precision and Recall.

Table 3.10 A typical confusion matrix layout detailing the classification results for Catchment U2H057

Measure	**Estimate [%]**	**95 % Confidence Interval [%]**	
Overall Accuracy	76	70	82
Kappa Accuracy	78	72	79
Mean F1 Accuracy	74	-	-

The Random Trees classifier in the QGIS software was used to run the land cover classification for the study catchments to test and compare the results from the different classification methods applied through GEE and Python. A combination of the above classification procedures was applied and the most efficient method that produced reasonable results was used for the classification for the rest of the study catchments. The random trees classifier, through the EnMAP-Box plugin on QGIS, was chosen as it was user-friendly, fewer computational errors were encountered while using this method, and it produced better land cover classifications that provided a good idea of the imperviousness in the study catchments. The classification provided practical representations of the pervious and impervious area proportions within the catchments.

3.3.5 Procedure adopted to extract ADJIMP and DISJIMP from TIA estimated from the Pixel-based method

The machine learning classification procedure identified the areas that are pervious and impervious within the study catchments. However, from the total area of impervious surfaces in the catchment, adjunct (connected to drainage channels and streams) and disjunct impervious areas (disconnected from drainage channels and draining onto pervious areas) are required as critical inputs into the *ACRU* hydrological model when modelling an urban catchment. The adjunct impervious areas were calculated by adding the area of the impervious surfaces that are located next to streams and drainage systems, i.e. surface drains, slopes and gutters. The DISJIMP were then easily identified as they are equal to one minus the total ADJIMP.

Stormwater drainage information for the study catchments in Tshwane was obtained from the local municipality. A dense river network was derived from the NASA STRM 30 m DEM database using GEE. GIS tools were used to extract the longest watercourse and the respective tributaries of the main stream in each catchment using the DEM. The Strahler order shown by the DEM image on the right hand side of the arrow in Figure 3.12 was computed using QGIS tools. The stream order can also be reduced to match the purpose of the study. In this case, the Strahler order was calculated for order six. The stormwater drainage data and the natural stream network were then used to determine the adjunct impervious surfaces. Figure 3.13 is an illustration of the stream network computations that were carried out for Catchment U2H057. The same procedure was applied to all the study catchments.

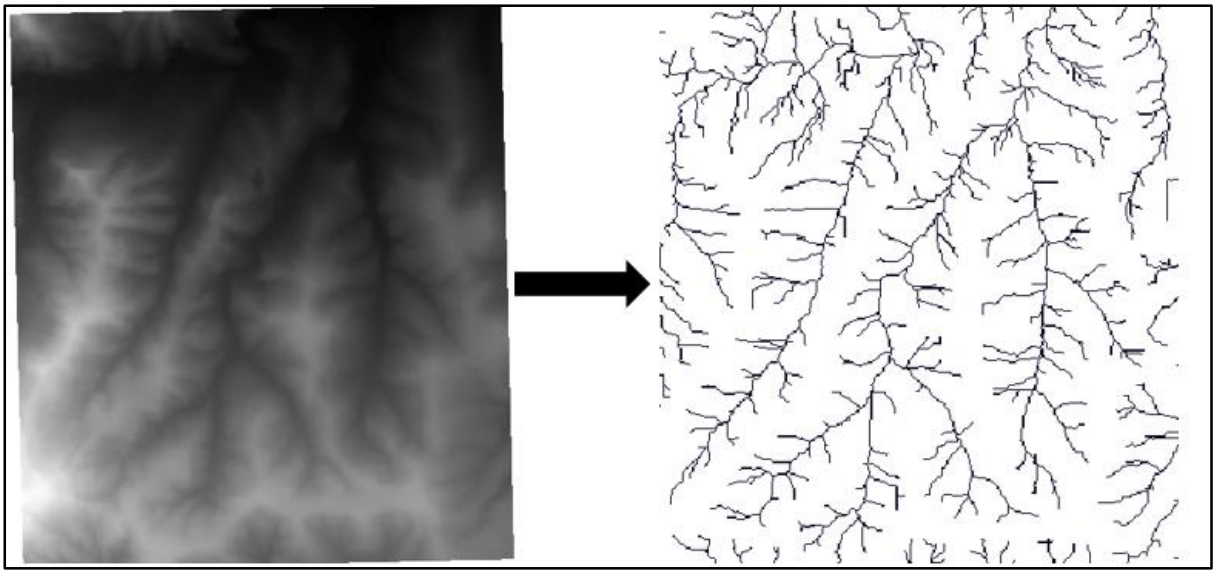

Figure 3.12 An example of the Digital Elevation Model used to extract the river network for Catchment U2H057

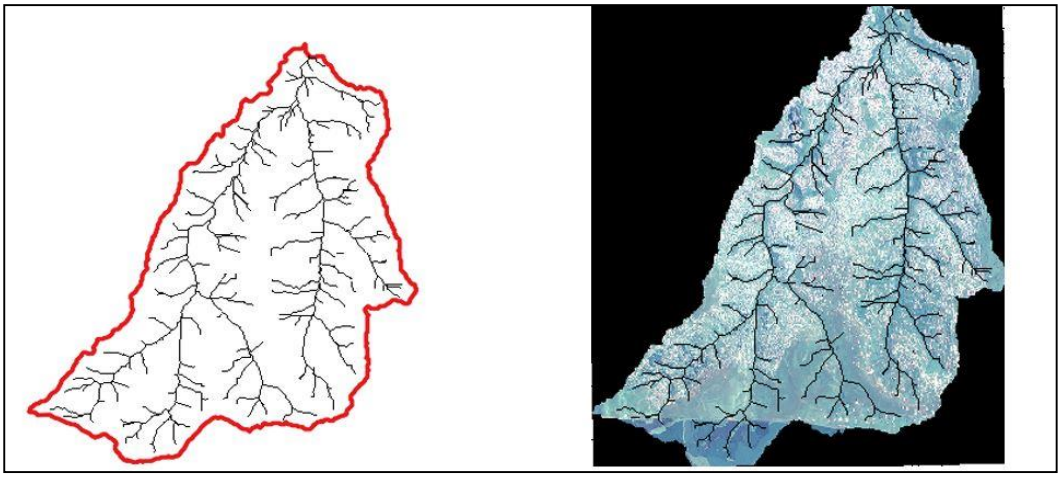

Figure 3.13 River network for Catchment U2H057

From Figure 3.13, it can be seen that the stream lines derived from the DEM follow the demarcated stream lines of the catchment to some extent, as seen from the multi-spectral image in the second image in Figure 3.13. The DEM is, however, not 100% accurate and required digitizing and elimination of the stream lines that flowed through buildings or followed an unrealistic pathway. The same procedures were followed for deriving the stream network for the catchments in Tshwane shown in Figure 3.14.

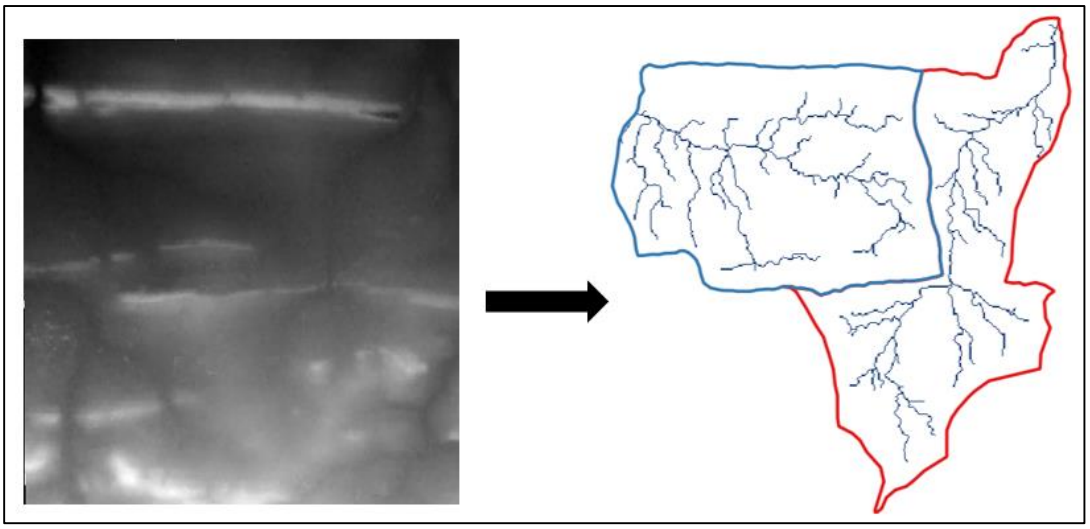

Figure 3.14 DEM used for river network extraction for the catchments in Tshwane

After calculating and identifying the stream order, the adjunct and disjunct impervious surface areas could be calculated for Catchments A2H054 and A2H063 due to the availability of stormwater drainage information. The stormwater drainage information was available in the form of an ESRI-shapefile. It consisted of the location of outlets, junction points, inlets, pipes, channels, and culverts within the study catchments in Tshwane. These structures are designed to drain surplus rain and ground water from impervious surfaces such as building roofs, roads, pavements etc. Figure 3.15 shows all the stormwater systems and stream network within Catchment A2H054. This completes the information required to compute the areas of adjunct impervious surfaces for the catchments in Tshwane.

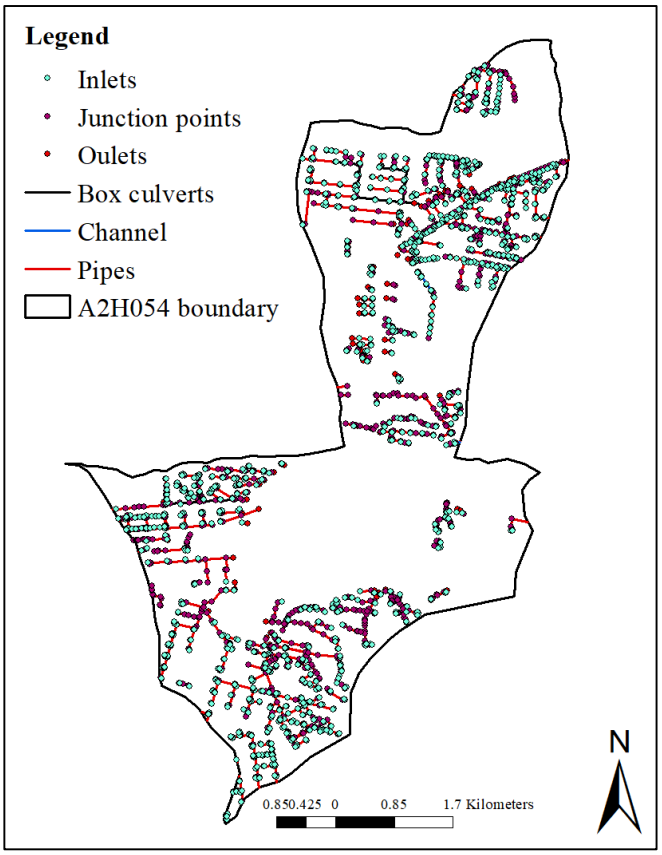

Figure 3.15 Location of the stormwater drainage systems within Catchment A2H054

To estimate the adjunct and disjunct impervious surfaces for Catchments A2H054 and A2H063, a buffer distance of 50 m from impervious features to the stormwater system and streams was used to estimate the area of adjunct impervious surfaces. Figure 3.16 illustrates the impervious surfaces from Catchment A2H054 that had to be extracted first to estimate the adjunct impervious areas. The computations to extract the impervious and pervious land covers were performed using ArcMap and QGIS tools. As alluded to above, it was essential to extract the total impervious area so as estimate the adjunct and disjunct impervious fractions. The maps in Figure 3.16 illustrate the extracted impervious and pervious surfaces achieved for Catchment A2H054, with the same method then being applied for Catchment A2H063.

Figure 3.16 Impervious surfaces extracted for Catchment A2H054

The above method used to derive the adjunct and disjunct impervious surfaces was followed for the catchments in Tshwane, owing to the availability of stormwater sytems information. Stormwater systems information was not available for Catchment U2H057; therefore, estimation of the adjunct and disjunct impervious areas was based on the calculated areas of impervious and pervious land cover from the classified land cover map, the DEA land cover maps and from the field visits conducted in the study catchments. The land cover classification maps indicated that Catchment U2H057 was dominated by pervious vegetated land and, therefore, disjunct impervious surfaces.

3.4 *ACRU* Model Configuration and Parameterisation

A climate file consisting of the station name, date, rainfall and streamflow data (with missing data flags by -99.9) was created by following the specific format required by the *ACRU* model. The rainfall data were collected from the closest rainfall station with relatively reliable data.

Pretoria University Rainfall Station 0513435A4 was used for Catchment A2H054 and Pretoria UNISA 0513314C9 was used for Catchment A2H063. The Pietermaritzburg Rainfall Station 02396985 was selected to be used for Catchment U2H057. As mentioned previously, rainfall data from the surrounding stations were used to patch the missing rainfall detected from the selected stations. The *ACRU* model was set up in a manner where each land use class or group was added as an individual hydrological response unit (HRU), and the streamflow relationship was set up as illustrated by Figure 3.17.

The catchment is represented as a sub-catchment in the *ACRU* structure, and within the sub-catchment there are vegetated and urban HRUs where the flows from the urban HRUs are directed to the ADJIMP and DISJIMP components. The streamflow from the ADJIMP component is directed to the sub-catchment node, then the catchment node and finally the exit node. The streamflow from the DISJIMP component is directed to the pervious portion of the urban HRU (where it drains and contributes to the soil water budget of the pervious component), then to the sub-catchment node, the catchment node and lastly the catchment exit node. The streamflow from the vegetated HRU flows directly to the sub-catchment node, then contributes to the catchment node and then exits the catchment.

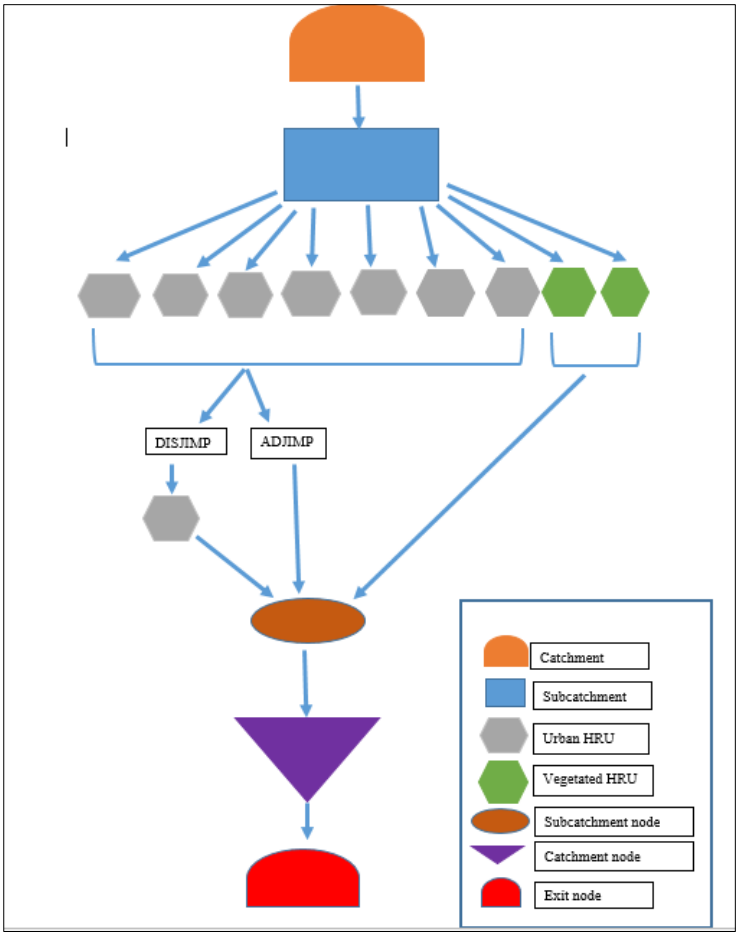

Figure 3.17 Streamflow relationship

3.4.1 **Land use re-classification and HRU configuration**

The land use classes identified from the 2018 SANLC map were grouped into 9 HRUs in order to reduce the number of HRUs added to the model structure, hence simplifying the modelling process, but simultaneously also ensuring that the actual catchment land cover was represented. The land use grouping method and *ACRU* parameterisation adopted from Schütte *et al.* (2020) was followed for this section of the methodology. However, because modelling urban land uses was one of the foci for this study, the urban land uses or built-up HRUs were further divided into 5 urban HRUs to accommodate a wider variety of urban land uses within the catchments. The basis for the grouping is that land cover/use classes with more or less similar hydrological responses are grouped under a single modal class. The land uses classes were divided into the following HRUs;

a) Natural vegetation and natural rocks
b) Bare surfaces and mining

c) Forest plantations
d) Urban residential
e) Urban recreational
f) Village and smallholdings
g) Commercial and transport (roads and rail)
h) Industrial
i) Agriculture.

Natural vegetation and rock (consisting of naturally vegetated areas that may include rocky areas) were modelled as HRU 1. The rock component was modelled as an impervious surface in the *ACRU* model due to its impervious characteristics. The land use classes modelled under HRU 1 are mapped in Figure 3.18 for Catchment A2H054. The *ACRU* configuration for HRU 1 is summarised in Table 3.11. STOIMP is an *ACRU* parameter referring to the surface storage capacity (i.e. depression storage, or initial abstraction) of impervious surface, which needs to be filled before stormflow begins. The storage fluctuates and is diminished as a result of evaporative demand. Schulze and Davis (2018) suggested that 80% of the impervious area is assumed to release flow directly to a stream and the 20% of the flow contributes to the surrounding pervious surfaces.

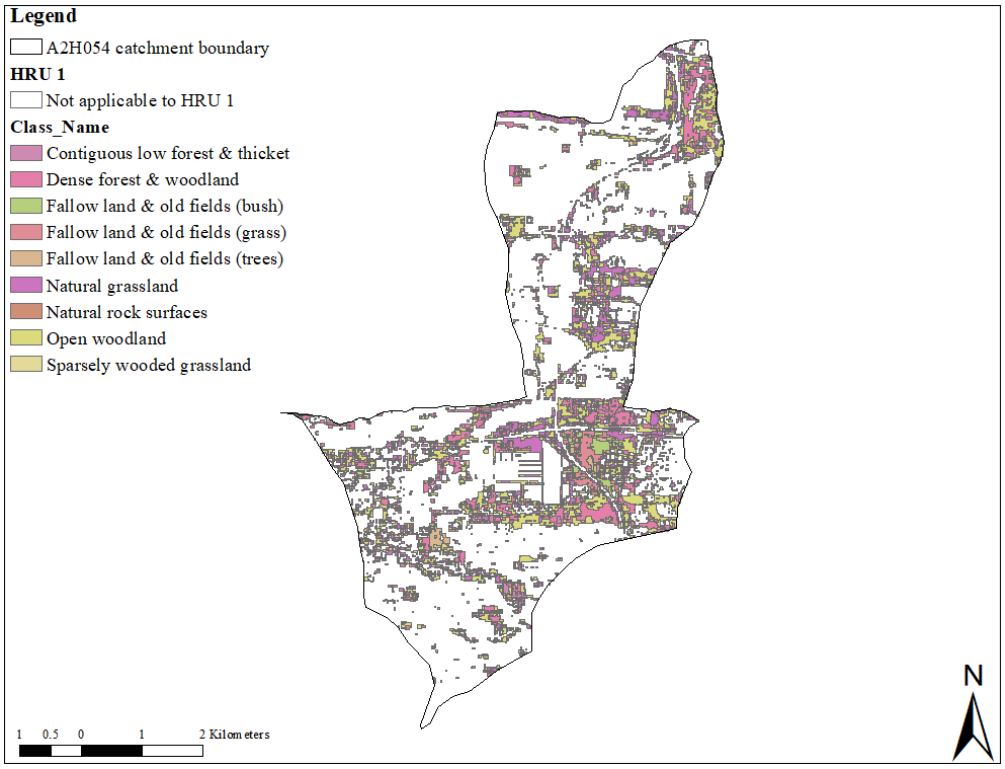

Figure 3.18 Land use classes modelled under HRU 1 for Catchment A2H054

Table 3.11 Summary of *ACRU* parameters for HRU 1 (Schulze and Davis, 2018)

HRU Components	**Description**
Adjunct impervious	*Natural - Rock (80%)*, STOIMP=5 mm
Disjunct impervious	*Natural - Rock (20%)*, STOIMP=5 mm

Bare land cover and mining are modelled in HRU 2. This land cover class includes non-vegetated pervious surfaces, areas that are naturally bare, eroded areas or excavated areas and tailing dumps. Landfill is also included since it is modelled in a similar manner to mining. Land use classes included under this HRU group are mapped out in Figure 3.19, thereby also illustrating the distribution of the land use class within the catchment. The *ACRU* configuration for HRU 2 is summarised in Table 3.12.

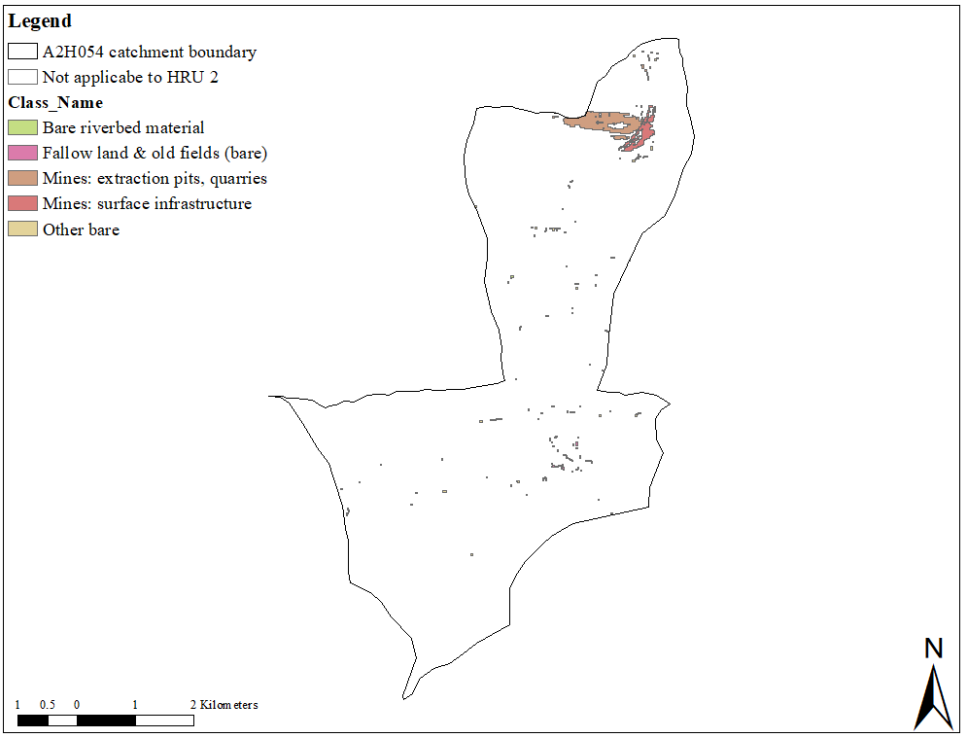

Figure 3.19 Land use classes modelled under HRU 2 for Catchment A2H054

Table 3.12 Configuration of HRU 2 components (Schütte *et al.*, 2020)

HRU Components	**Description**
Pervious portion	Model all bare (non-vegetated) pervious surface land cover parameters for all three classes
Adjunct impervious	Used to represent mining water using STOIMP=999
Disjunct impervious	None

HRU 3 consisted of forest plantations. This group is modelled separately from the natural vegetation and natural rock HRU because the *ACRU* model parameters for forest plantations are different from other vegetated land cover. Forest plantations are one of the leading streamflow reducing activities and they also have a long growth cycle when compared to other cultivated land cover. Each catchment is expected to consist of rows of forest plantations with a range of maturity levels, however only fully matured trees are considered in this HRU group as shown in Figure 3.20. Table 3.13 shows the forest plantation parameter values from Schulze and Davis (2018) that were used for the configuration of the *ACRU* model.

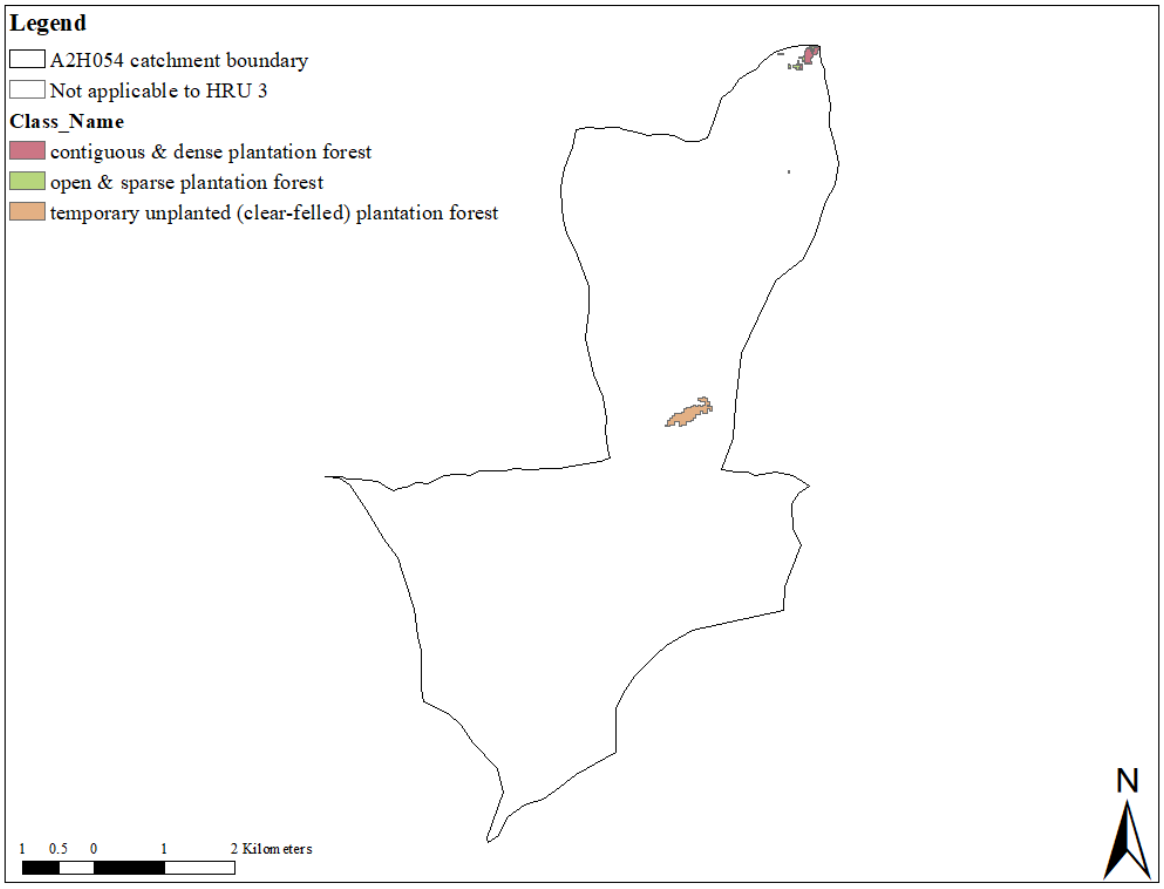

Figure 3.20 Land use classes modelled under HRU 3 for Catchment A2H054

Table 3.13 Summarised configuration of HRU 3 for the *ACRU* model (Schütte *et al.*, 2020)

HRU Components	**Description**
Pervious portion	Modal of: • *Pines* • *Eucalypts* • *Acacia (Wattle)* • *Other* Use modal forest plantation genus for parameterisation.
Adjunct impervious	None
Disjunct impervious	None

The urban land uses were grouped and modelled as shown in Figure 3.21, covering urban residential, recreational, village and smallholdings, commercial and transport and industrial land uses. These land uses make up the built-up land cover group and are considered, according to literature, as the main features that define an urban area. They are characterised by larger areas covered with imperviousness. The following vegetation types were modelled for the urbanised HRUs: a) unimproved grassland in poor condition, for formal residential areas and rural built up areas; and b) improved grassland in good condition in the remaining built-up area. The summarised *ACRU* configuration for the urban HRUs is shown in Table 3.14

Table 3.14 Summarised *ACRU* configuration of HRU 4 (Schütte *et al.*, 2020)

HRU Components	**Description**
Pervious portion	Area weighted fraction of the HRU based on pervious fraction for the different groupings present. Parameterisation, assumed: (i) informal and rural built-up groupings vegetated with degraded unimproved grassland, and (ii) other groupings vegetated with improved grassland. The modal grouping of these two was used in parameterisation.
Adjunct impervious	Area weighted fraction of the HRU based on adjunct impervious fraction for the different groupings present. Water bodies in built-up areas modelled as adjunct impervious areas.
Disjunct impervious	Area weighted fraction of the HRU based on disjunct impervious fraction for the different groupings present.

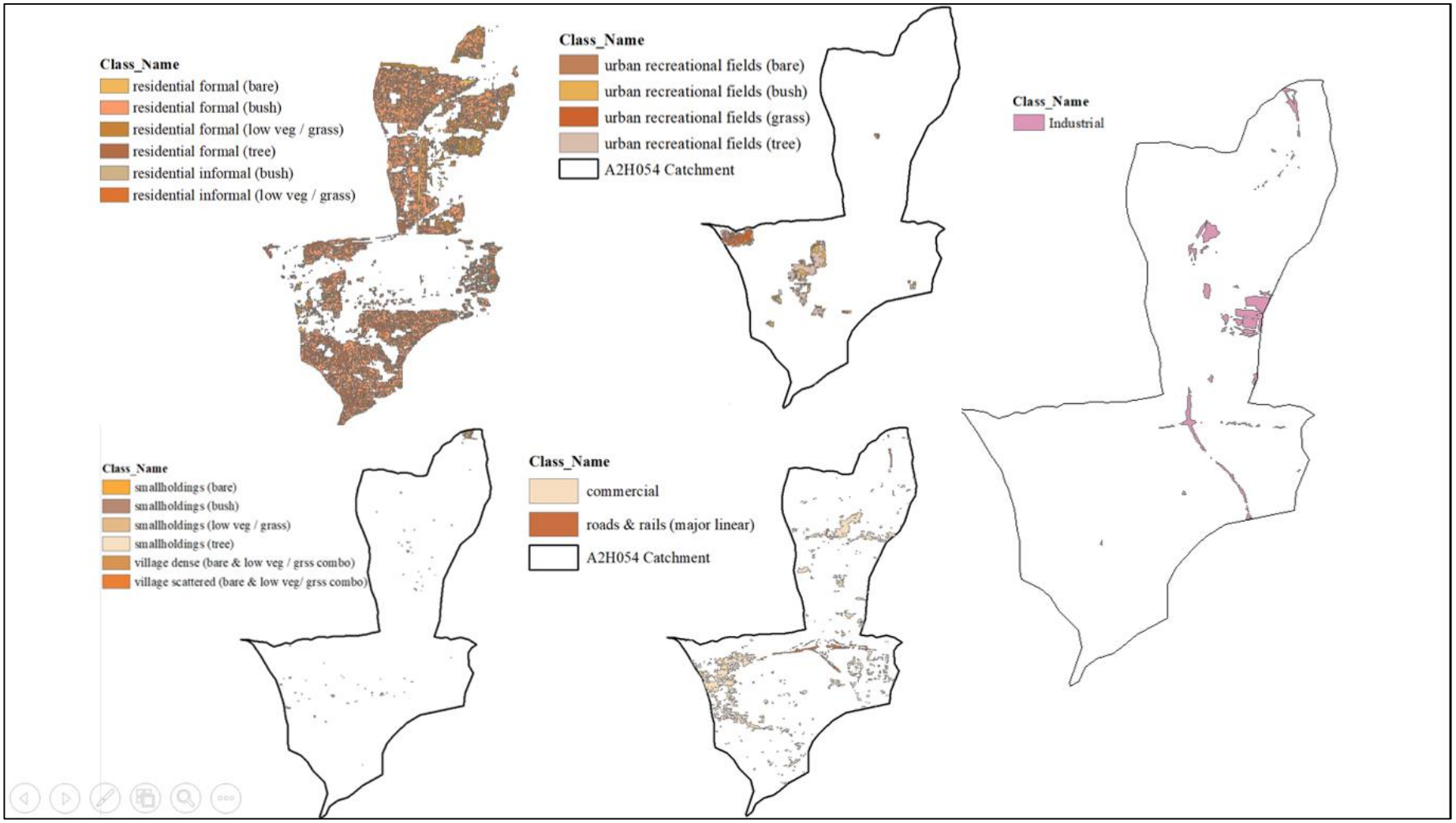

Figure 3.21 Urban land uses grouped into individual HRUs as configured in the *ACRU* model for Catchment A2H054

HRU 5 represents all the agricultural land use classes in Catchment A2H054 shown in Figure 3.22. Various annual and perennial crops and crop types are included in the 2018 SANLC datasets. When modelling the agriculture land cover class, the dryland and irrigated crops were modelled the same during the configuration of *ACRU* model. *ACRU* parameter values for a range of commercial and subsistence annual crops were used based on the dominant agricultural crop in the catchment. The *ACRU* COMPOVEG file was used to parameterise the vegetation variables. Table 3.15 shows the summarised configuration of the *ACRU* model for HRU 5.

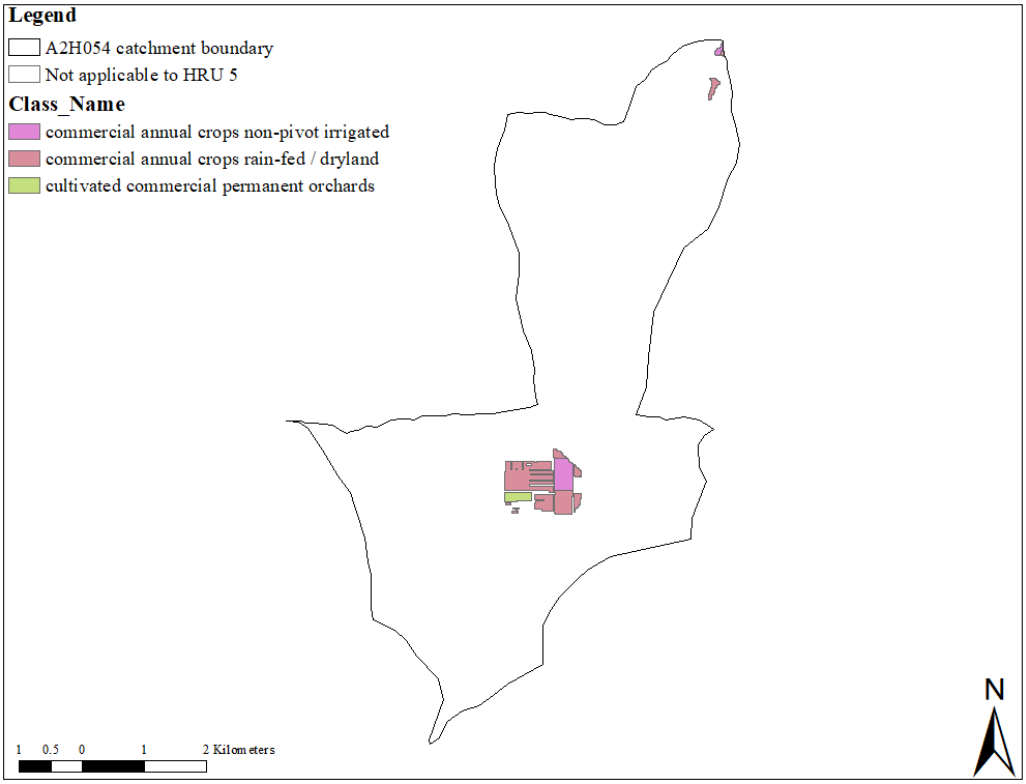

Figure 3.22 Land use classes modelled under HRU 5 for Catchment A2H054

Table 3.15 *ACRU* parameterisation of HRU 5 (Schütte *et al.*, 2020)

HRU Components	**Description**
Pervious portion	Modal agricultural crop. Parameterise according to modal class
Adjunct impervious	Lakes, Rivers, and Coastal Water modelled with STOIMP=0.
Disjunct impervious	None

Maps illustrating the land uses classes grouped into individual HRUs for Catchments A2H063 and U2H057 are included in Appendix A.

3.4.2 Calculating ADJIMP and DISJIMP areas from estimated TIA

The total adjunct and disjunct impervious areas were extracted from the catchments total impervious area as discussed in section 0. The urban catchments were divided into pervious and impervious areas and the impervious portion was further divided into adjunct and disjunct categories. The total pervious and impervious areas estimated for each catchment as well as their respective adjunct and disjunct impervious areas, are illustrated in the following Figures labelled as Figure 3.23, Figure 3.24 and Figure 3.25.

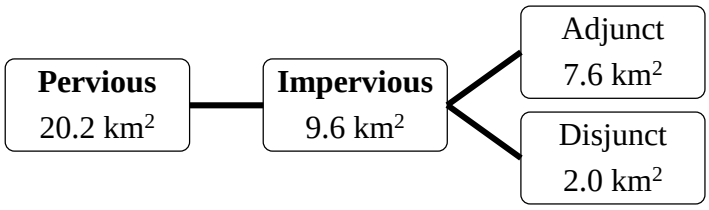

Figure 3.23 Land cover divisions in Catchment A2H054

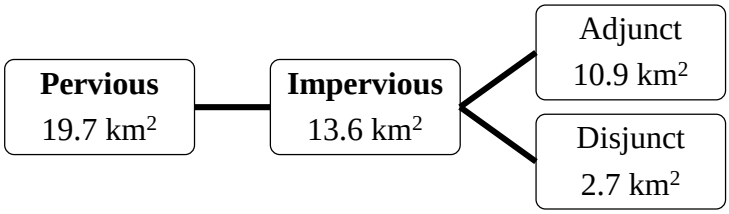

Figure 3.24 Land cover divisions in Catchment A2H063

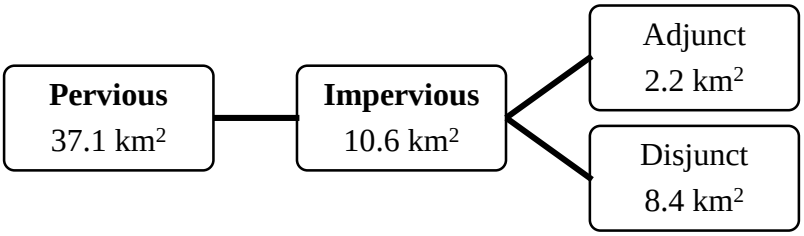

Figure 3.25 Land cover divisions in in at Catchment U2H057

These adjunct and disjunct impervious areas estimated from the Figures above were used to calculate the final impervious parameters to input into the *ACRU* model. The estimates of ADJIMP and DISJIMP percentages were derived by analysing the classified maps/shapefiles of each individual HRU against google images. This provided a good idea of the impervious areas that are adjunct and those that are disjunct in each HRU that has impervious surfaces. Therefore, the vegetated and fully pervious surfaces had zero ADJIMP and DISJIMP percentages. In Catchment A2H054, natural vegetation and natural rock was identified to have 20% of its impervious surfaces as adjunct and 80% as disjunct. The rock components of this HRU served as the impervious surfaces, and therefore, it is approximated that 20% of the surface flow from the natural rocks will contribute to streamflow via stormwater drainage systems that are distributed across the catchment. 80% of surface flow from the impervious rock component will drain onto the surrounding natural pervious vegetation. The total area of the natural vegetation and natural rock HRU was estimated to be 9.49 km^2. The HRU was then divided into 9.41 km^2 of pervious surfaces and 0.08 km^2 covered by impervious surfaces. From the 0.08 km^2 of impervious surfaces, 20% of the impervious area was calculated to be the ADJIMP and 80% of the impervious areas was calculated to be the DISJIMP area fraction for the HRU.

The same concept was applied to the other HRUs with impervious surfaces. Based on the sources used to identify, classify and group the agricultural land uses under the agriculture HRU, it was observed that the agricultural land uses also consisted of impervious land cover in the form of impervious compacted soils (as a result of pathways and probably dry conditions), tarred surfaces (driveways around the farms for tractors and other farm vehicles), and the farm house roofs. The combination of the aforementioned accounted for the small percentage of impervious land cover of which majority was identified as DISJIMP areas owing to the vast areas of surrounding vegetated land. The sum of the areas of each HRU equalled to the total area of the catchment. The individual areas of the HRUs were calculated by summing up the areas of each land use classes (2018 SANLC) that were grouped under the HRU.

3.5 SCS-SA Model Configuration and Parameterisation

The individual catchments were discretised for the SCS-SA model so as to explicitly represent the physical characteristics of the catchments. The catchment discretisation for the SCS-SA model included lumping the land cover classes extracted from the 2018 SANLC map into sub-catchments that corresponded to the SCS-SA land cover groupings as demonstrated by the

SCS-SA manual, and at the same time ensuring that the re-classified land cover groupings accommodated the catchment's different land cover/land use types accurately. Nine sub-catchments were modelled for each catchment to increase the representation accuracy of the actual land cover in the catchments, as demonstrated in the *ACRU* section. Land cover classes with similar hydrological responses were grouped together, i.e. land cover classes that receive, infiltrate and convey stormwater in a similar manner were grouped into the same sub-catchment. These land covers are also likely to have similar impervious areas, sizes and shapes, topography, vegetation, geological conditions, antecedent moisture conditions and groundwater conditions.

The runoff volume and peak discharge values were calculated for the catchments. The Schmidt-Schulze equation shown in Equation 3.2 was selected to calculate the catchment's response time, which was used in the calculation of peak discharge using the SCS peak discharge equation.

$$L = \frac{A^{0.35} MAP^{1.1}}{41.67 y^{0.3} {I_{30}}^{0.87}} \quad (3.2)$$

where

L = catchment lag time (h),

A = catchment area (km^2),

MAP = mean annual precipitation (mm),

y = average catchment slope (%), and

I_{30} = 2-year return period 30-minute rainfall intensity (mm/h).

Loots (2020) determined curve numbers from available soil and land cover information. The curve numbers were estimated for the applicable DEA land use types found in Catchments A2H054 and A2H063 based on the land use types and curve numbers used by Schulze *et al.* (2004b). A link between the 2018 SANLC classes and the re-classified SCS-SA sub-catchments can be seen in Table 3.16. The SCS soil groups were identified for each sub-catchment by clipping the old SCS map of Schulze and Horan (2008), since in this case, the older SCS soils map provided a better summary/average of the catchment SCS soil group with the sub-catchment shapefile and identifying the dominant soil group within the sub-catchment.

This was then used to derive the curve numbers for each sub-catchment. Curve numbers adapted from the SCS-SA manual for Catchment U2H057 are shown in Table 3.17.

Table 3.16 Estimated curve numbers for the sub-catchments of Catchments A2H054 and A2H063 (Loots, 2020)

SCS-SA sub-catchments	**Associated SCS land cover classes**	**Curve Number**						
		1	**2**	**3**	**4**	**5**	**6**	**7**
		A	**A/B**	**B**	**B/C**	**C**	**C/D**	**D**
Forested land	Forests and plantations – Humus at depth 100 mm; compactness: moderate	34	47	59	64	69	72	75
Grassland	Veld/pasture in fair condition	49	61	69	75	79	82	84
Barren land	Woods, high stormflow potential	45	56	66	75	77	80	83
Cultivated	Forests and plantations – Humus at depth 25 mm; compactness: loose/friable	37	49	60	66	71	74	77
Built-up residential	Residential: lot size 1350 m^2 (30% impervious)	57	65	72	77	81	84	86
Urban sports and golf (dense trees/bush)	Open spaces, parks, cemeteries (95% grass cover)	39	51	61	68	74	78	80
Urban commercial	Commercial/business areas	89	91	92	93	94	95	95
Urban industrial	Industrial districts (72% impervious)	81	85	88	90	91	92	93
Mines and Quarries; Roads and rail	Commercial/business areas	89	91	92	93	94	95	95
	Commercial/business areas	89	91	92	93	94	95	95

Table 3.17 Curve numbers for the sub-catchments in Catchment U2H057, estimated from Loots (2020)

SCS-SA sub-catchments	Associated SCS land cover classes	Curve Number						
		1	2	3	4	5	6	7
		A	A/B	B	B/C	C	C/D	D
Forested land	Forests and plantations – Humus depth 100 mm: compactness: moderate	34	47	59	64	69	72	75
Grassland	Veld/pasture in fair condition	49	61	69	75	79	82	84
Barren land	Woods, high stormflow potential	45	56	66	75	77	80	83
Cultivated	Forests and plantations – Humus depth 25 mm; compactness: loose/friable	37	49	60	66	71	74	77
Built-up residential	Residential: lot size 4 000 m^2 (20% impervious)	51	61	68	75	78	82	84
Urban recreational (sports and golf dense trees/bush)	Open spaces, parks, cemeteries (95% grass cover)	39	51	61	68	74	78	80
Urban commercial	Commercial/business areas	89	91	92	93	94	95	95
Urban industrial	Industrial districts (72%impervious)	81	85	88	90	91	92	93
Mines and Quarries	Commercial/business areas	89	91	92	93	94	95	95
Roads and rail	Gravel roads	76	81	85	88	89	90	91

4. RESULTS AND DISCUSSION

This chapter includes results from the land cover classifications obtained from the pixel-based classification method conducted for this study and the classification verification which was completed during site visits (Section 4.1). The verification of the land cover classification confirms the validity of the classification results obtained using the pixel-based remote sensing method. Total impervious area estimates computed from the pixel-based classified maps, and extracted from the GMIS and GAIA impervious datasets, are included and analysed. These are then used to parameterise the *ACRU* model and streamflow simulations are assessed and discussed in Section 4.3. The land cover classification maps completed for each catchment using the different methods are included, together with the impervious *ACRU* parameters in the Appendix Sections B and C respectively. The streamflow simulations obtained using the impervious data from the pixel-based classification method are further refined for Catchment U2H057 by investigating and improving *ACRU* input data.

The SCS-SA model's performance in urban catchments with a range of land uses is analysed and discussed in Section 4.4.1. Design runoff depths and peak discharge are compared against values computed from the observed runoff data. The SCS-SA model's performance is also assessed for different scenarios to investigate its optimum performance in an urban catchment. The performance of both models for the selected urban catchments is compared by assessing the design values and comparing them against the observed data. The *ACRU* and SCS-SA models' performances are evaluated by examining the simulated peak discharge against observed values.

MARE, MRE, and NSE statistical methods are used to further assess the performance of the models by comparing the observed with the simulated streamflow volumes and peak discharge. MARE refers to the measure of prediction accuracy, generally used in model evaluation because of its in-built interpretation of relative error. It ranges between 0 to ∞, with lower values being better. MRE assist in judging the goodness of fit between observed and simulated values (with ratios closer to zero indicating good performance). NSE is used to assess the predictive ability of a hydrological model and it ranges between -∞ to 1(with 1 being the optimal value), with values <0 indicate poor model performance. The statistical evaluations are included for the results section 4.3.3 under the discussions and conclusions sub-sections.

Historical trends in estimated urban areas for each study catchment are assessed and analysed with simulated streamflow to detect and understand trends and relationships between urbanisation and runoff generation.

4.1 Verification of the Pixel-based Land Classification Method

Loots (2020) conducted field surveys for Catchments A2H054 and A2H063 and this field-based information was used to verify the classification results produced by the pixel-based classification method. The total impervious and disjunct impervious surfaces for the residential, commercial and industrial 2018 SANLC classes in Catchments A2H063 and A2H054 are shown in Table 4.1, where L is the lower quartile (25%), M is the median (50%) and H is the upper quartile (75%). The images in Figure 4.1 show that these catchments comprised of mostly paved roads and most of the houses had paved yards and formal drainage, networks with a resultant higher adjunct portion than observed in Catchment U2H057. The images taken from the field surveys show a significant difference in the development and overall imperviousness in the land use between Catchments A2H054 and A2H063 and Catchment U2H057 near Pietermaritzburg.

Table 4.1 Total impervious and DISJIMP values calculated from field investigations by Loots (2020)

SANLC Classification	**TIA (%)**			**DISMP (%)**		
	L	M	H	L	M	H
Residential formal (trees)	11	17	23	0	0	0
Residential formal (bush)	39	44	50	0	0	21
Residential formal (low vegetation/grass)	51	58	63	0	17	34
Residential formal (bare)	54	61	68	0	18	76
Residential informal (trees)	7	14	21	0	0	7
Residential informal (bush)	24	30	37	0	0	0
Residential informal (low vegetation/grass)	38	43	51	0	0	0
Residential informal (bare)	35	40	45	0	0	0
Commercial	71	81	87	63	65	69
Industrial	85	89	92	67	75	81

Figure 4.1 Images taken from a field investigation showing the adjunct impervious areas in the catchments in Tshwane (Loots, 2020)

In Catchment U2H057, the lack of stormwater drainage information to estimate *ACRU's* ADJIMP parameter required conducting additional field investigations. The 2018 SANLC map identified impervious areas in Catchment U2H057 to be mostly disconnected from streams and drainage infrastructure, and therefore draining onto the surrounding pervious areas of the catchment before discharging into the stream. Figure 4.2 shows a sample of typical settlements that were surveyed in the catchment and which have large unpaved pervious areas surrounding the impervious settlement structures.

Figure 4.2 Typical settlement structures with disjunct impervious areas in the Slangspruit catchment

Most of the house plots were unpaved with short grass that had patches of bare land cover, as seen in Figure 4.2. The small areas of ADJIMP areas were made up of paved roads, walkways

and building roofs that were connected to drainage paths. The images in Figure 4.3 show the areas of the catchment that had portions of ADJIMP and DISJIMP fractions.

Figure 4.3 ADJIMP and DISJIMP area portions from ground investigation in Catchment U2H057

During the field visit, 7 sample plots covered by urban land use classes represented in the 2018 SANLC map were visited in Catchment U2H057 and the adjunct and disjunct impervious area portions of the land use classes were measured using a measuring tape, as shown in Figure 4.3, and the averaged into percentages (Table 4.2). The areas recorded as ADJIMP were impervious surfaces adjacent to a drainage path, and DISJIMP were measured as impervious areas surrounded by pervious surfaces that are most likely to drain their runoff onto the pervious areas. The measurements of the observed total impervious areas and the ADJIMP and DISJIMP estimates are recorded in Table 4.2.

Table 4.2 Field measurements taken in the sample plots in Catchment U2H057

Sample plots	**Total sample area (m^2)**	**Pervious area (m^2)**	**TIA (m^2)**	**Percentage impervious (%)**	**ADJIMP (%)**	**DISJIMP (%)**
Natural vegetation and natural rocks	72	56	16	**22**	15	85
Bare surfaces and mining	58	50	8	**14**	17	83
Urban residential	159	146	13	**8**	46	54
Urban recreational	178	169	9	**5**	15	85
Village and smallholdings	159	141	18	**11**	7	93
Commercial and transport	59	39	20	**34**	81	19
Industrial	59	28	31	**53**	68	32

There were a few functional stormwater drainage systems in the catchment shown inFigure 4.4. The stormwater is draining onto the surrounding pervious areas and running into the nearest stream(s) (i.e. ADJIMP and DISJIMP flows).

Figure 4.4 Drainage in Catchment U2H057

To gain confidence in the pixel-based classification results, and therefore use it to parameterise the *ACRU* model, further verification of the land cover classification results for Catchment U2H057 were required, particularly in the lower less developed parts of the catchment.

However, due to the subsequent inaccessibility of the catchment as a result of prevailing safety issues, additional land cover classification verification was conducted using Google satellite images. This was done by selecting random sample areas within the catchment which included impervious features. The classification method was verified by measuring the area of the impervious features that the pixel-based method correctly classified as impervious. This area was compared to the impervious area estimated from the impervious features on the satellite image (measured using the area calculation tools in QGIS) that served as the "observed". The under-estimation or over-estimation of the area of impervious features from each sample area was then used to calculate the percentage error.

The first sample area is shown in Figure 4.5, where an industrial building with impervious features surrounded by vegetation was selected. From Sample Area 1 in Figure 4.5, the total area of the impervious features from the Google satellite image was estimated to be 20 991 m^2 and the pixel-based method classified 16 946 m^2 as impervious. Therefore, a 19.3% error was produced by the pixel-based LC classification. As seen from Figure 4.5, a section of the roof of the building detected in a brown colour was mis-classified as bare land cover.

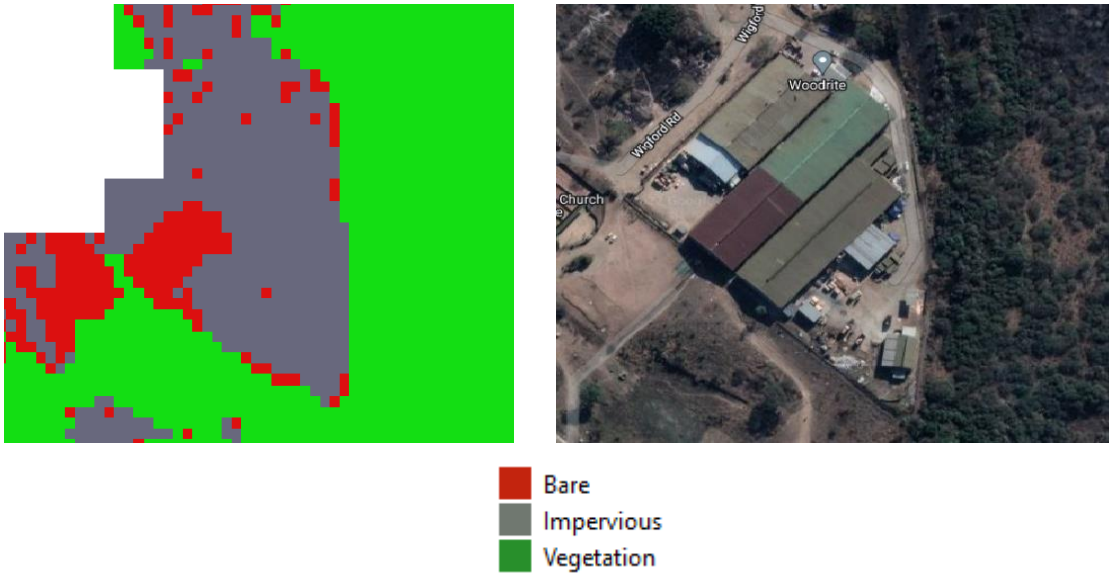

Figure 4.5 Impervious features selected as Sample Area 1 (showing classified image vs Google satellite image).

Sample Area 2, shown in Figure 4.6, illustrates school buildings as the selected impervious features, with a total impervious area of 3 099 m^2 calculated for the sample area. The pixel-based classification method over-estimated the total impervious area in this sample plot by

estimating a total impervious area of 3 958 m^2, indicating an over-estimation of imperviousness of 27.7%.

Figure 4.6 Impervious features selected as Sample Area 2 (showing classified image and Google satellite image).

Figure 4.7 shows Sample Area 3, with a small section of a residential area with houses and tarred roads. A total impervious area of 17 483 m^2 was estimated from the satellite image and 11 136 m^2 of imperviousness was classified in this sample plot. This indicates an under-estimation of 36% of impervious surfaces, as some of the impervious surfaces appear to have been misclassified as bare land cover (indicated by red in the classified image).

Figure 4.7 Impervious features selected as Sample Area 3 (showing classified image and Google satellite image).

Figure 4.8 (Sample Area 4) shows a small section of the catchment, illustrating a better representation of what is on the ground. A total impervious area of 13 215 m^2 was calculated, and a total impervious area of 13420 m^2 was estimated by the pixel-based classification. A minor over-estimation of 2% was noted from this sample plot.

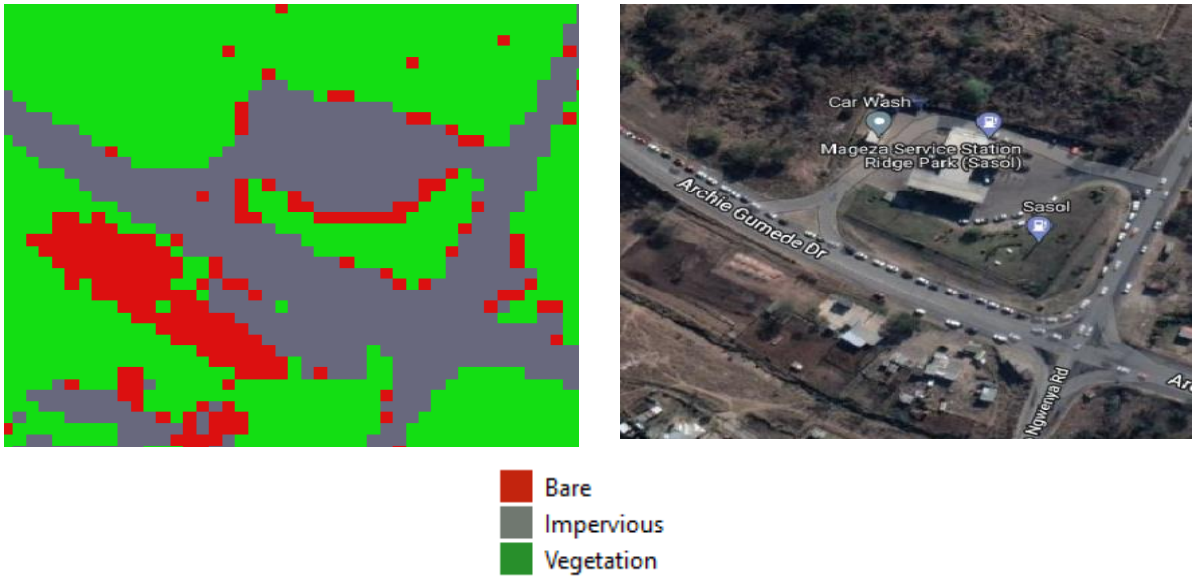

Figure 4.8 Impervious features selected as Sample Area 4 (showing classified image and Google satellite image)

A larger sample area consisting of residential buildings with paved roads and parking lots was selected as Sample Area 5, shown in . The total impervious area calculated from the satellite image for this sample plot was 100 745 m^2 and the classified imperviousness was calculated as 100 695 m^2, therefore less than 1% of the impervious area was under-estimated.

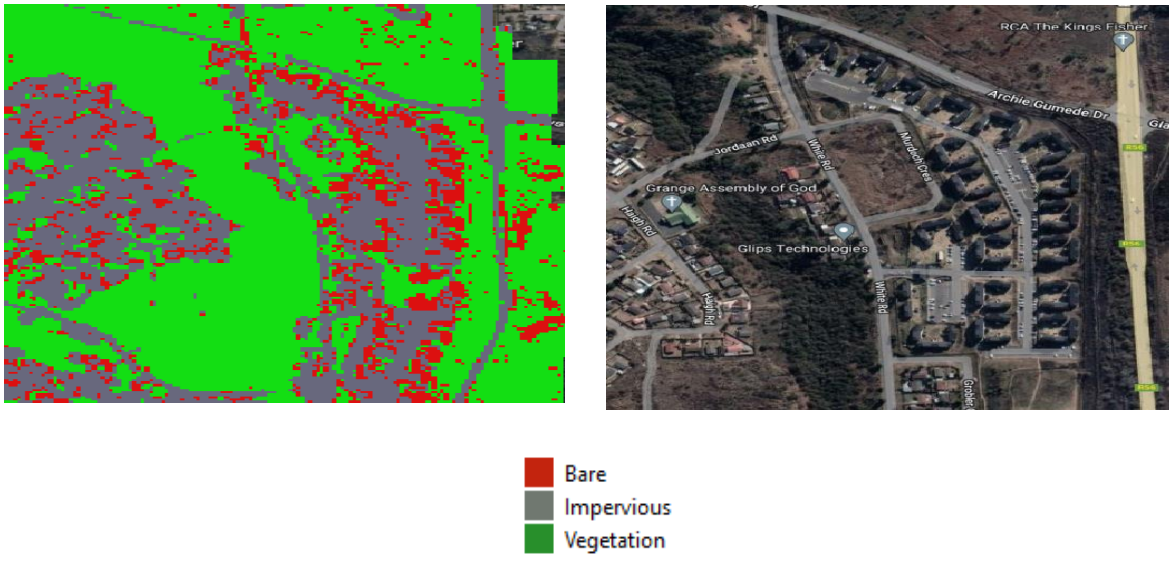

Figure 4.9 Impervious features selected as Sample Area 5 (showing classified image and Google satellite image).

Figure 4.10 illustrates Sample Area 6, where a school building together with a few residential houses were selected as impervious features. A total impervious area of 14 204 m^2 was estimated from the satellite image and 19 930 m^2 was classified as impervious areas, producing an over-estimation of 40.3% of impervious surfaces mapped out in Sample Area 6.

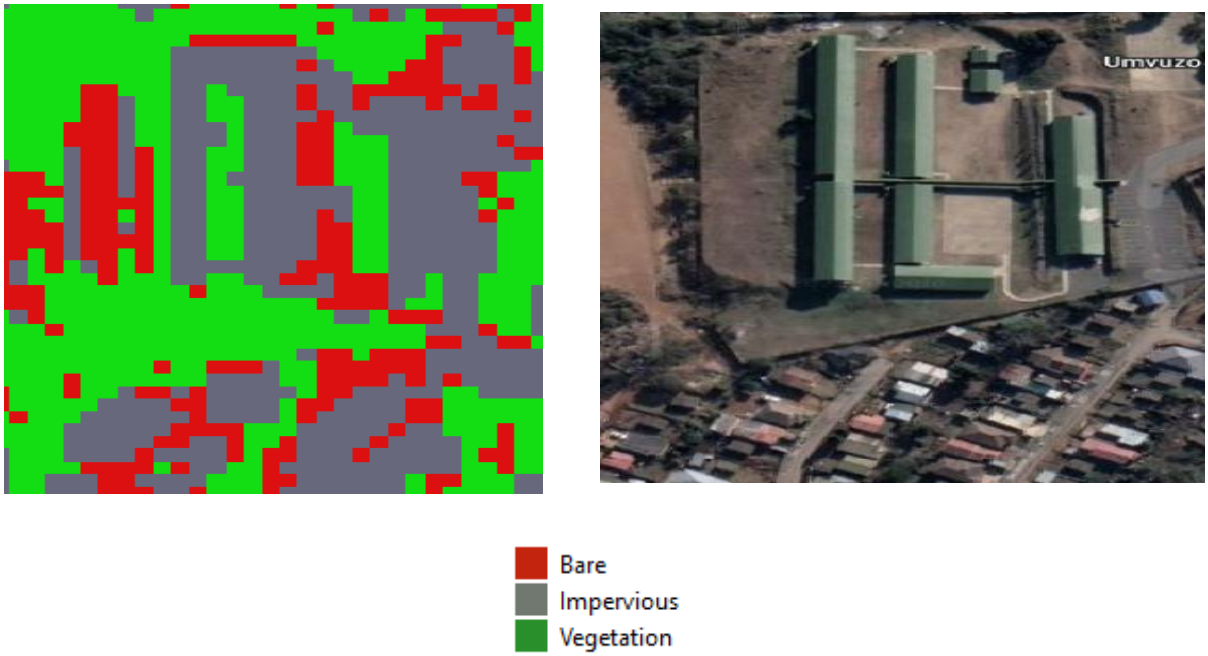

Figure 4.10 Impervious features selected as Sample Area 6 (showing classified image and Google satellite image).

Table 4.3 provides a summary and assessment of the average absolute values for land cover classification verification of the pixel-based, GMIAS and GAIA impervious mapping methods when compared against the "observed" (estimated imperviousness from Google satellite images). The pixel-based and GMIS methods relatively represented the "ground" observations better, with overall absolute indices of performance of 7 % and 11%. The GAIA method over-estimated impervious land cover (15%).

Table 4.3 Summary of the impervious mapping verification conducted for Catchment U2H057

No.	Pixel-based	GMIS	GAIA
1	-1%	-19%	36%
2	-3%	28%	15%
3	5%	-36%	5%
4	10%	2%	-5%
5	0%	0%	0%
6	4%	40%	-2%
7	-14%	10%	-24%
8	9%	3%	-11%
9	8%	-5%	14%
10	-5%	0%	9%
11	10%	4%	14%
12	-6%	15%	-36%
13	11%	23%	15%
14	-2%	3%	10%
15	17%	2%	-5%
16	0%	-2%	-7%
17	-16%	7%	16%
18	12%	8%	25%
19	5%	-2%	44%
20	-9%	8%	8%
Average ABS values	7%	11%	15%

4.2 An Assessment of the Accuracy of LC Classification and Impervious Mapping

Land cover classification using the supervised pixel-based method was carried out and completed for the three study catchments. Additional total impervious percentage areas were extracted from the readily available datasets, i.e. the Global Man-made Impervious Surface (GMIS) and the Global Artificial Impervious Areas (GAIA), as mentioned earlier.

Table 4.4 provides the total impervious and pervious areas mapped for each of the study catchments using the three different methods. These results are compared to the “observed” percentage of the estimated areas (impervious cover from the entire catchment roughly estimated from satellite images using Google Earth pro polygon tools supported by brief field

investigations). The land cover mapping methods produced similar land cover classification results compared to what was observed on the ground.

For example, from the results representing ground data, 66% of Catchment A2H054 was estimated to be pervious and 34% was estimated to be impervious. The land cover classification methods slightly over-estimated total impervious cover and under-estimated total pervious area mapped, with the GMIS and GAIA methods deviating the most from the observed results. Overall, the pixel-based method mapped pervious and impervious land lover classification that agree better with the "observed" for all the study catchments.

Table 4.4 Comparison between the 'observed' percentage areas and the classifed percentage area.

Catchment	**Estimates from Google Satellite images paired with field investigations ("observed")** **(km^2)**		**Impervious Area** **(km^2)**			**Pervious Area** **(km^2)**		
	Pervious	**Impervious**	**Pixel-based**	**GMIS**	**GAIA**	**Pixel-based**	**GMIS**	**GAIA**
A2H054	66%	34%	31%	37%	37%	69%	63%	63%
A2H063	64%	36%	40%	31%	42%	60%	69%	58%
U2H057	72%	28%	22%	24%	-	78%	76%	-

Table 4.5 shows the kappa coefficients illustrating the overall accuracy produced by the pixel-based and GAIA methods. The pixel-based method produced an average classification accuracy of 72% for all the study catchments and the GAIA estimated global impervious areas with an 89% accuracy.

Table 4.5 Accuracy report illustrating the kappa coeffiecients for the pixel-based and GAIA land cover classification methods

Catchment	**Pixel-based**	**GAIA**
A2H054	0.75	0.89
A2H063	0.62	0.89
U2H057	0.78	0.89

Figure 4.11 illustrates the standard error of impervious surface percentages estimated for the GMIS dataset. The standard error in the South African region where the study catchments are located ranges between 0-10%, indicating a plausible representation/classification of actual impervious cover.

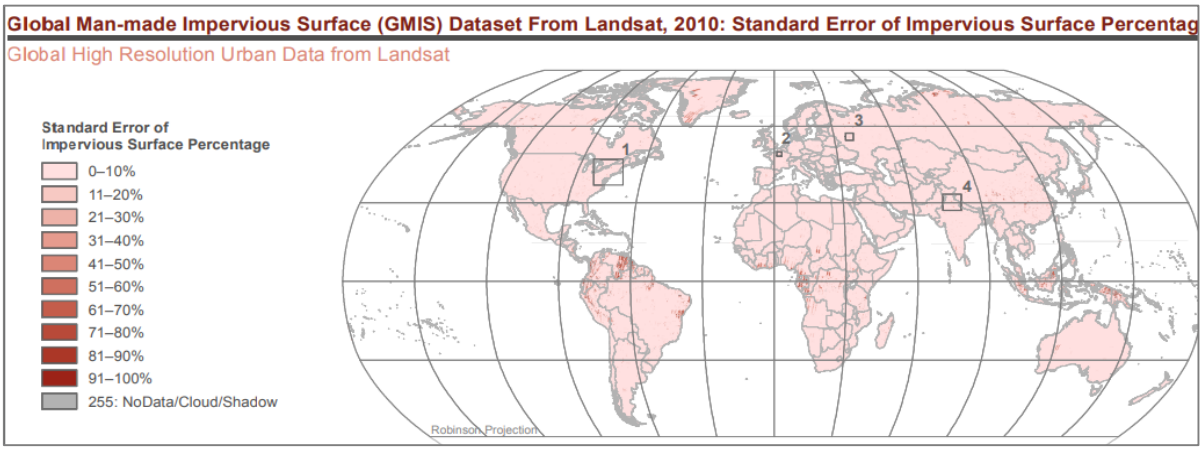

Figure 4.11 Standard Error of Impervious Surface Percentage for the Global Man-made Impervious Surface (GMIS) Dataset

4.3 *ACRU* Model Results

4.3.1 Analysis of *ACRU* volume simulations

The impervious components of the *ACRU* model (ADJIMP and DISJIMP variables) were parameterised using the impervious data from the classifications and impervious land cover extractions. The impervious data were used to calculate the ADJIMP and DISJIMP fractions for each of the urban HRU components and these results are included in the Appendix C. The streamflow simulations achieved from the impervious configurations from each impervious method (i.e. Pixel-based, GMIS and GAIA) are compared for each catchment. The model was also parameterised with the *ACRU* default values derived by Tarboton and Schulze (1992) for all three study catchments and values estimated by Loots (2020) for Catchments A2H054 and A2H063. *ACRU* Simulations computed from all the above impervious estimations are compared to each other and verified against the observed values. It is important to note that static land cover/impervious area estimations for the simulation periods of 1985-2018 (Catchments A2H054 and A2H063) and 1995-2018 (Catchment U2H057) were assumed and used in the results presented.

4.3.2 Simulations of initial volumes

Catchment U2H057 was initially modelled with a coarse land cover grouping, whereby the catchment was divided into only 5 HRUs, and the urban land use classes were lumped into one HRU grouped as 'built-up residential'. All the impervious mapping methods resulted in exacerbated over-simulations in streamflow volumes and the simulations were not responsive to realistic adjustments made to land cover, soils variables and stormflow response parameters which were altered in an attempt to improve the simulation. This section illustrates the poor initial results simulated and the subsequent section (section 4.3.3) shows the steps taken to improve the observed data and the *ACRU* model configuration.

Initially the PMB Rainfall Station no. 02396985 raingauge was selected to represent the rainfall in the catchment, based on the station's proximity to the catchment and the reliability and consistency of rainfall data. The missing data were infilled using median monthly rainfall data to adjust rainfall data from surrounding stations. Based on the initial streamflow simulation results represented by the cumulative and frequency analysis plots in Figure 4.12, it can be seen that the model was grossly over-estimating observed streamflow and there was no seasonality in either the simulated or observed graphs. At first, it was assumed that the poor simulation

could have been as a result of the complexity of the catchment type (combination of formal and informal land use). However, previous studies done on this catchment produced reasonable streamflow simulation results. Therefore, thorough investigations and further checks were done on the observed data, the input parameters and the model configuration to improve model performance and refine the results. Section 4.3.3 includes a detailed methodology that was followed in order to improve the runoff simulations from the initial run and obtain results that better represents the hydrology of the catchment using all impervious classification methods.

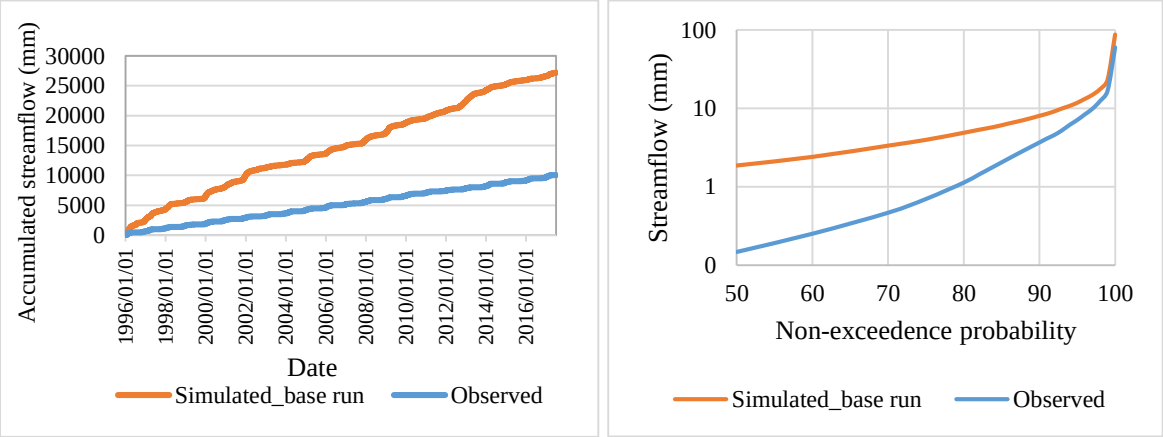

Figure 4.12 Initial accumulated daily streamflow (left) and frequency analysis results (right) for Catchment U2H057

4.3.3 **Evaluation of observed data**

Thorough data investigations and checks were conducted with the intention to improve the over- simulation results produced by the *ACRU* model for Catchment U2H057. This was done subsequent to the initial configuration and a range of changes were applied to the input data to rerun the *ACRU* model. After effecting the changes for Catchment U2H057, the same changes were applied to Catchments A2H054 and A2H063, however the procedure is only described for Catchment U2H057. The following investigations and checks were carried out:

- The reliability of observed rainfall and runoff was further investigated, i.e. checks whether the observed runoff (Q) values are consistent with the rainfall (P) and if the Q/P ratio was reasonable and consistent with other studies in the area. The flags for the observed data were further investigated.

- The high Q/P ratio of 23 % calculated from the observed data was investigated.

- A more suitable P station was re-selected for the catchment which was consistent with the observed Q values, the simulations were to be re-run with the new rainfall data.

- The simulated runoff depths, volumes and total runoff for each day were further investigated for any inconsistencies or anomalies.

- As an alternative to further reduce the over-simulation, the disjunct impervious areas were rerouted to flow onto larger pervious HRUs which are likely to be between the impervious area and the stream and the results were investigated. This was done as a result of the large impervious volume of HRU running onto much smaller pervious part of the HRU with little re-infiltration occurring. The intention of this change was to investigate if the problem was the volume of runoff from the impervious area running onto a small pervious section.

- The land use group representing the 'built-up residential' HRU was further divided into five HRUs, i.e. urban residential, urban recreational, village and smallholdings, commercial and transport and industrial HRUs. This was done to accommodate for a wider, courser range of land use classes, particularly when modelling a complex environment such as an urban catchment.

- The possible influence of the discrepancy between daily rainfall being measured from 08:00 to 08:00 while runoff being conventionally recorded from midnight to midnight and the influence it could have on runoff simulations was noted. Data recorded at different time intervals would result in different amounts of runoff production and, after the routing, different hydrographs. However, due to the tedious and additional calculations required to aggregate or disaggregate either dataset, this factor was not fully investigated for this study.

4.3.4 **Refined *ACRU* volume simulations**

The streamflow simulations discussed below were achieved using the refined configuration (i.e. newly selected rain gauge, re-configuration and re-routing of HRU). The *ACRU* model was parameterised using the different impervious mapping methods (i.e. default values, pixel-based, GMIS, GAIA and Loots (2021) impervious estimates) to derive flow simulations for the study catchments. Catchment U2H057 was not studied in Loots (2020) and the GAIA

impervious dataset boundary did not cover Catchment U2H057, hence these methods could not be applied for this catchment.

4.3.4.1 Catchment U2H057

Figure 4.13 shows the accumulated daily observed and simulated flows at Catchment U2H057 for the three impervious area estimation methods. The *ACRU* model produced improved simulations, with the pixel-based classification method providing the best simulations followed by the default values. The GMIS and default values over-simulated the high flows for the latter part of the simulation period. The pixel-based method did, however, slightly over-simulate low flows in the early stages of the simulation period and later under-simulated streamflow from the catchment. The circled part of the graph illustrates that the model simulated very low flows (below 1 mm) during the initial stages of the simulation period.

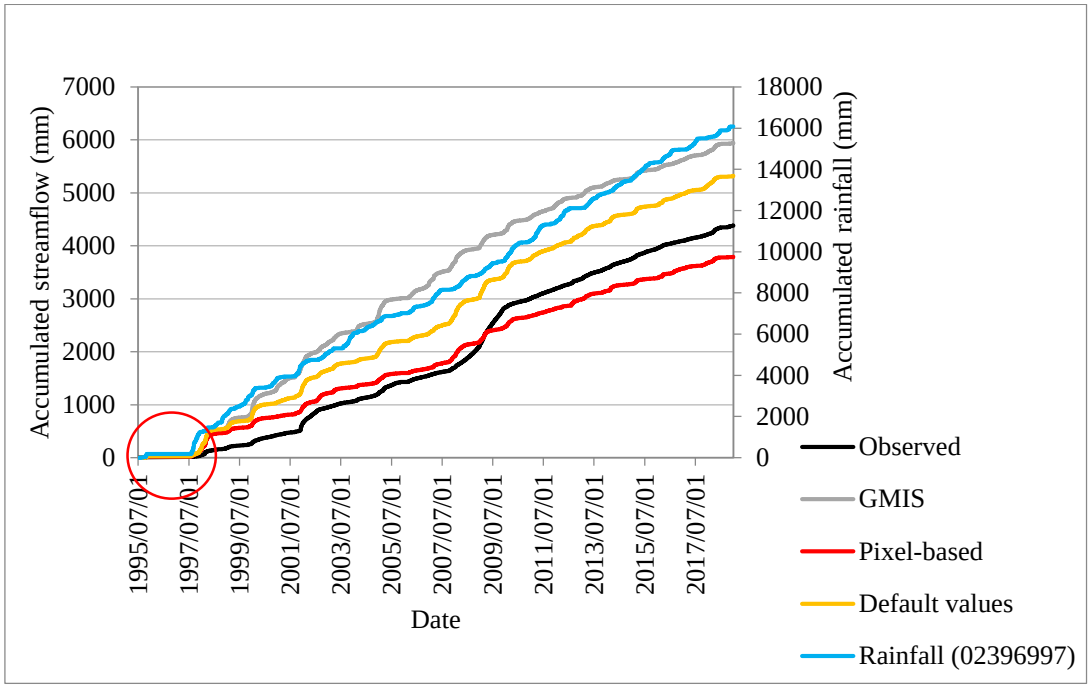

Figure 4.13 Accumulated daily observed and simulated flows at Catchment U2H057

The increase in the slope of the observed runoff graph after 2009 could be as a result of the increase in the accumulated rainfall graph shown in Figure 4.13. An increase in impervious cover as a result of an increase in urbanisation between 2007 and 2009 could also result in the increase in the observed streamflow noted during this period. The dynamic range of land uses represented in the catchment as a whole, and within the individual HRUs, made it difficult to

achieve representative streamflow simulations. This challenge is reflected in model simulations throughout the results chapter.

Figure 4.14 illustrates a section of the time series plot of the simulated streamflow graph from the different impervious classification methods, and it is evident from the graph that the default values and GMIS dataset are over-simulating the high flows and low flows. The observed streamflow is well simulated in terms of timing and flow magnitudes by the pixel-based method. The high daily flows are simulated moderately, with a few instances of over-simulation. The pixel-based method appears to have also over-simulated some of the high flows. With reference to the frequency analysis plot in Figure 4.15, the over-simulation from the GMIS and default values graphs is further emphasised, more so in the lower percentiles. Figure 4.14 and Figure 4.15 both indicate an under-simulation of the baseflows and an over-simulation of surface flows by the GMIS and default values. The GMIS and default values produced better simulations of low flows and high flows for Catchment A2H054.

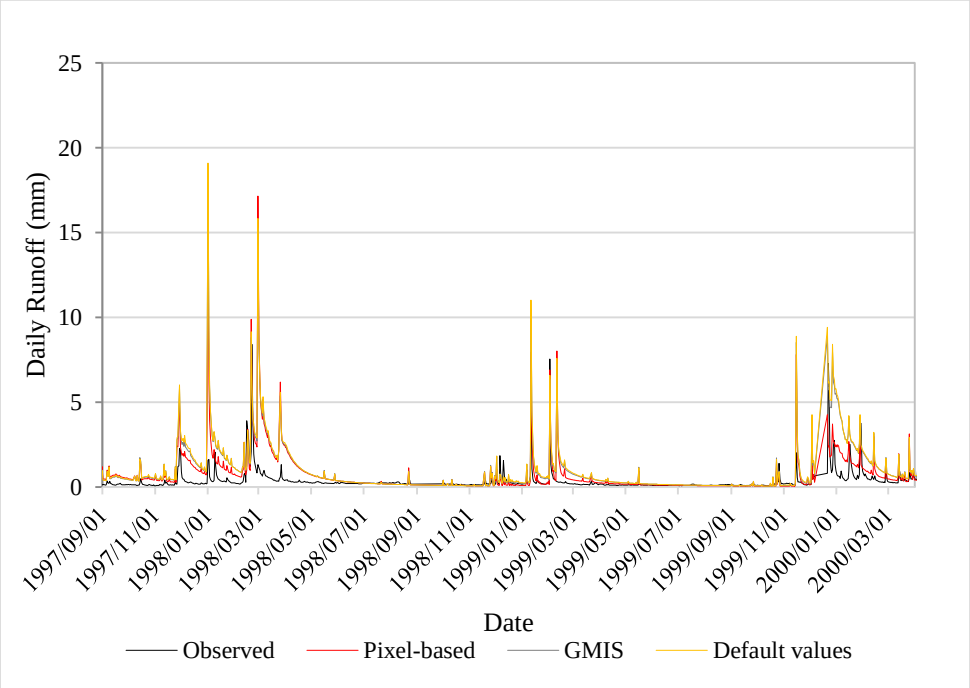

Figure 4.14 Time series illustration of the simulated streamflow from each method against the observed streamflow at Catchment U2H057

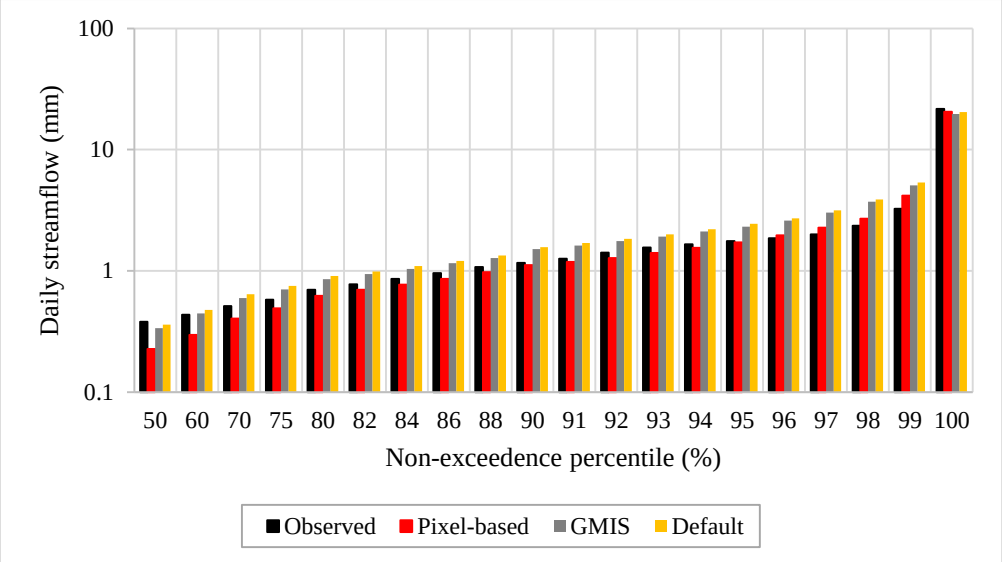

Figure 4.15 Frequency analysis of simulated and observed daily streamflow depth at Catchment U2H057

4.3.4.2 Catchment A2H054

The daily accumulated streamflow as simulated by the *ACRU* model is shown in Figure 4.16 for each impervious area classification method and is compared against the daily accumulated observed streamflow recorded at weir A2H054 for the period of available observed flow data (1984-2018). As a result of the pixel-based and GMIS method of mapping similar impervious cover for Catchment A2H054, the methods produced a similar streamflow simulation as seen by the graphs overlapping in Figure 4.16. The two methods also simulated the observed graph better compared to the other methods, showing that these methods provided a better representation of the impervious cover in the catchment. The default values and the GAIA method largely over-simulated streamflow. This could be as a result of the impervious area over-estimation extracted from the GAIA method. The default ADJIMP and DISJIMP fractions were probably not applicable for this particular catchment, which is why using these fractions resulted in an over-simulation of streamflow (depending on the characteristics of the catchments calibrated for deriving the default values). The impervious estimations by Loots (2020) produced streamflow that slightly over-simulated the GMIS and pixel-based methods, however; the simulation was not as exaggerated as the default values and GAIA. The simulated graphs take on a curved increased between 1996 and 2005 and thereafter they steadily increase. This curve could be as a result of simulations being run on static land cover and not accounting

for dynamic land cover, with relevant parameters changing with time(dynamically with relevant parameters changing with time).

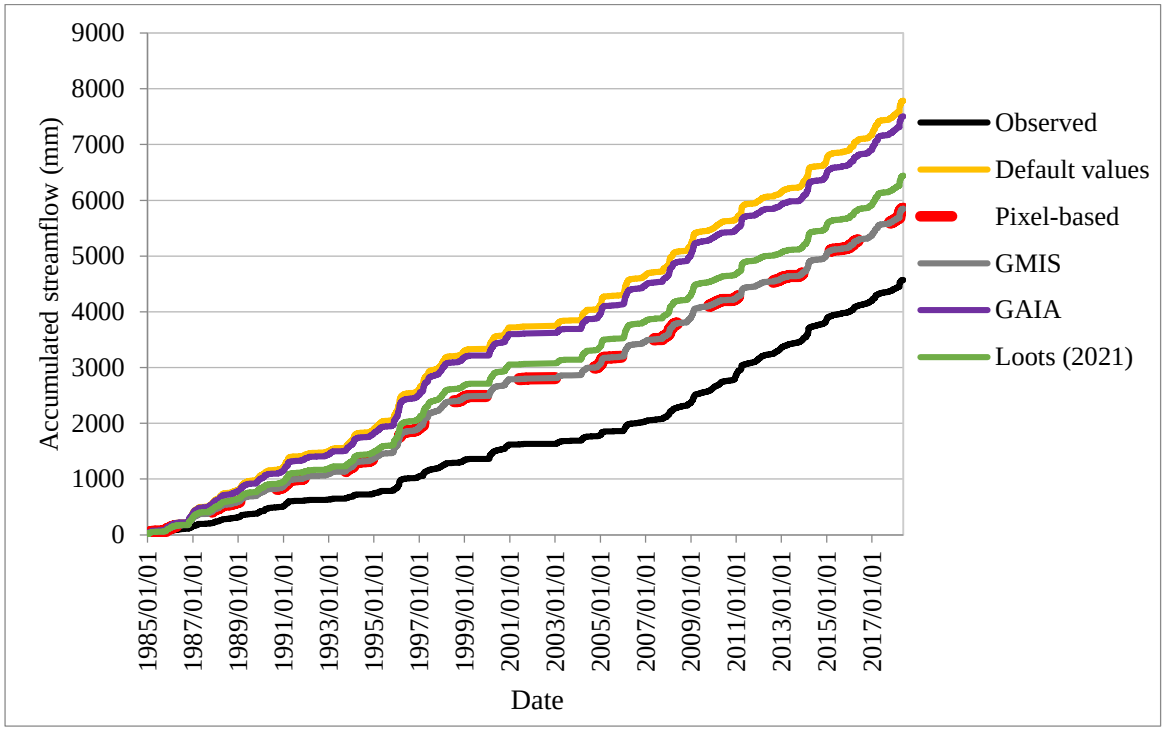

Figure 4.16 Accumulated daily observed and simulated flows at Catchment A2H054

A section of the time series plot was extracted to assess the variability or seasonality of streamflow simulated by the different methods and comparing it against the observed flow in Catchment A2H054 (Figure 4.17). This plot emphasises the over-simulation achieved by all the methods, i.e. the simulated streamflow does not closely mimic the observed in terms of timing and the rising and receding limb of the hydrograph. A general over-simulation of the peaks is evident. Loots (2020) approach and the default values appear to have simulated the low flows reasonably. The GAIA method significantly over-simulated the high flows.

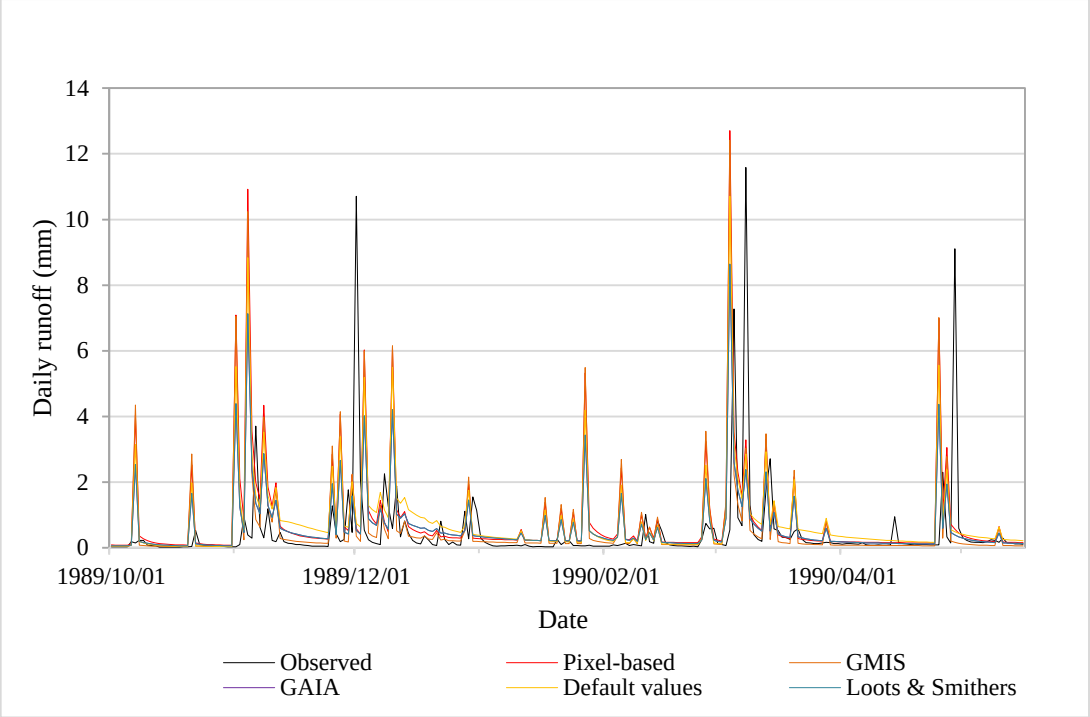

Figure 4.17 Time series plot of the simulated streamflow from each method against the observed streamflow at Catchment A2H054

Figure 4.18 illustrates a frequency analysis of the daily simulated and observed streamflows. This figure emphasises that the GAIA method over-simulated the low flows and the high flows. The frequency analysis curves indicate that the variability of streamflow was adequately simulated by most of the methods (indicated by the shape of the curves and their convergence for higher percentiles).

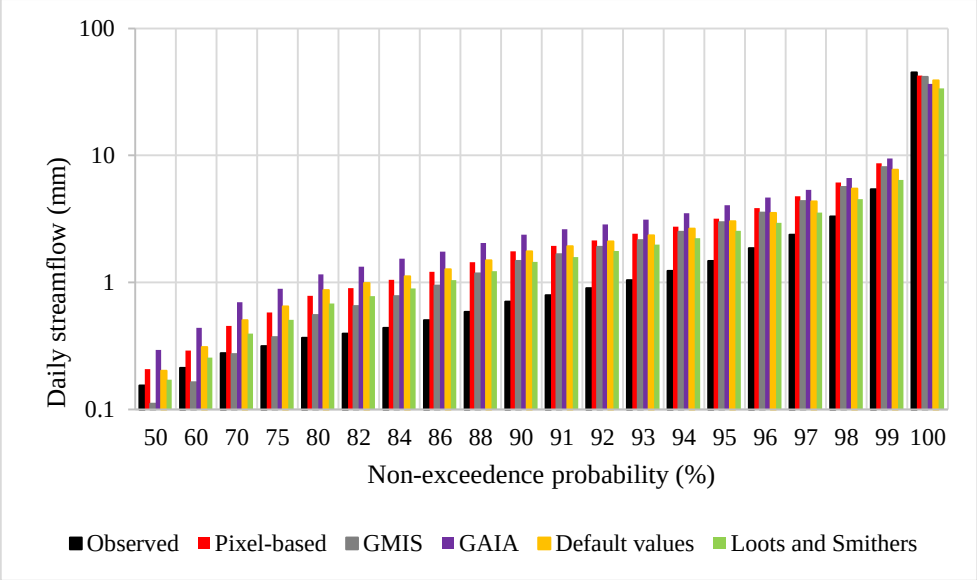

Figure 4.18 Frequency analysis of simulated and observed daily streamflow depth at Catchment A2H504

4.3.4.3 Catchment A2H063

Figure 4.19 illustrates a cumulative plot of daily simulated streamflow against observed streamflow for Catchment A2H063. The observed data after 1999 are questionable as there is a constant increase in streamflow with minimal to no seasonality. This continuous streamflow may have been caused by Type-X mechanical recorder cable system entanglements in the recorder well or mistakes in the electronic data-logger readings. Daily streamflow was over-simulated in this catchment for both low and high flows. Seasonality in streamflow is evident in all the simulated graphs in the early stages of the simulation period up to 1996, where the graphs take a dip and then steadily increase from there. All the impervious parameterising methods resulted in an over-simulation of streamflow. The GMIS and GAIA both produced similar streamflow simulations and the default values derived by Tarboton and Schulze (1992) produced the largest over-simulation (Figure 4.19). Loots (2020) values also resulted in an over-simulation of streamflow, simulating similar values to the GMIS and GAIA methods. The pixel-based classification produced the lowest and closest simulated values to the observed graph of streamflow;, however, the simulation was still over-estimated.

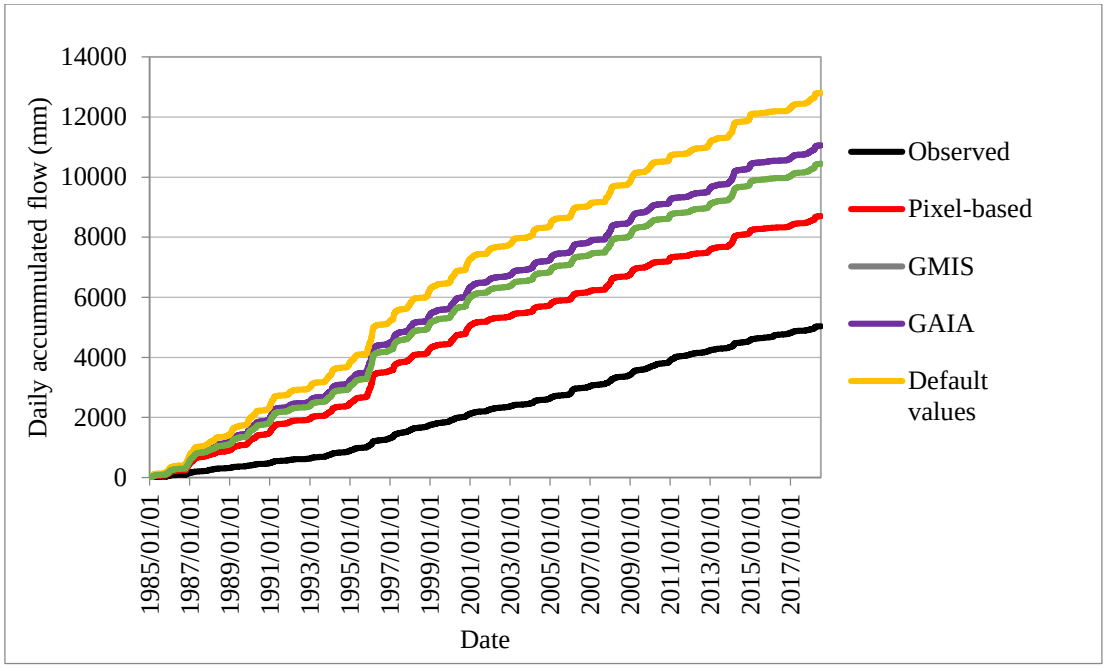

Figure 4.19 Accumulated daily observed and simulated flows at Catchment A2H063

Figure 4.20 shows a section of the time series plot, illustrating the performance of the impervious classification methods from daily streamflow simulations. From Figure 4.20 it can be seen that Loots (2020) and default values produced an over-simulation of high flows. The low flows were correctly simulated throughout the simulation period, except after the year 2018. The overall oversimulation of streamflow produced by the impervious mapping methods could be attributed to the fact that the available precipitation data's areal distribution was not representative and did not reasonably account for the spatial variation in precipitation and stormflow distributions. The graphs have some correlation with the observed graph, however, not to a great extent.

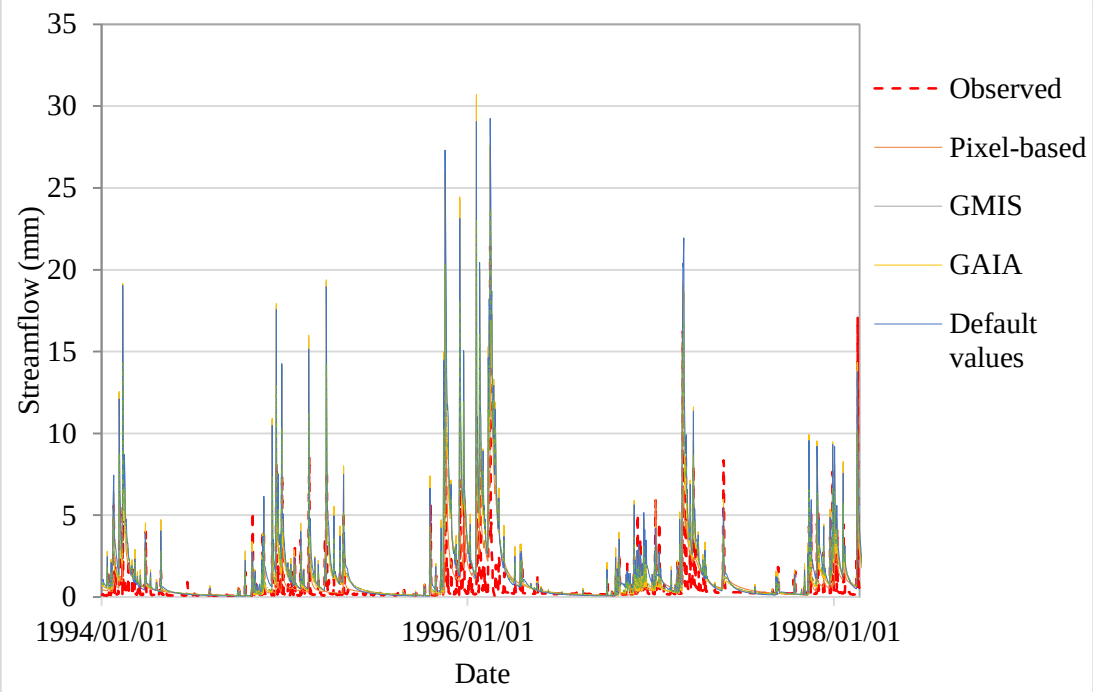

Figure 4.20 Time series illustration of the simulated streamflow from each method against the observed streamflow at Catchment A2H063

Figure 4.21 shows a frequency analysis of streamflow simulations achieved from the different methods. The frequency analysis curves show that the variability of streamflow was inadequately simulated by all of the methods, except for the pixel-based classification method which shows an improvement in the higher percentiles (97th percentile). Overall, it appears that the pixel-based method followed by Loots (2020) provided better simulations compared to the other methods for Catchment A2H063.

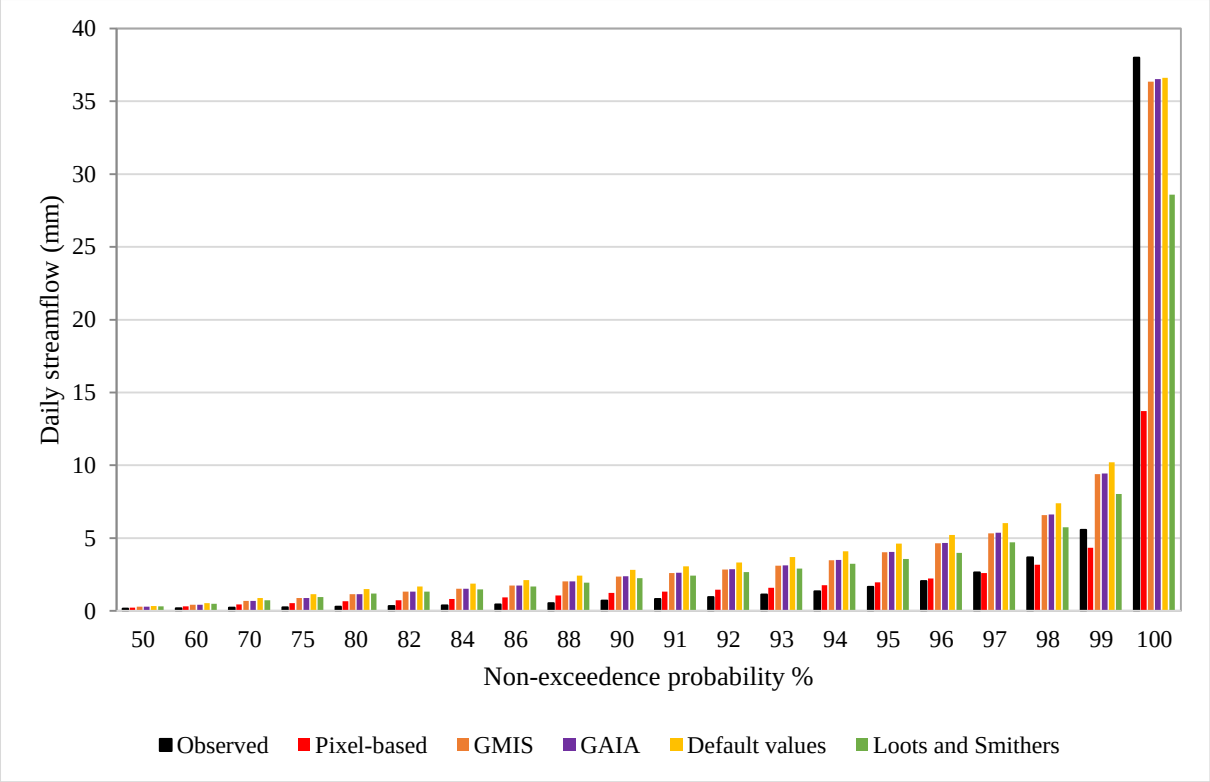

Figure 4.21 Frequency analysis of simulated and observed daily streamflow depth at Catchment A2H063

The extremely small observed and simulated values shown as less than 0.1 mm for the lower percentiles (i.e. 50th -92nd)could be as a result of seasonality changes where very little rainfall and therefore very little streamflow was recorded, or inaccuracies in the observed streamflow, where very little to zero streamflow was recorded at the weir under low flow conditions.

4.3.5 **Discussion and conclusions: *ACRU* Simulations**

The results obtained in the above sections emphasises the importance of obtaining accurate, reliable and consistent model input data as such data, impacts significantly on the quality and representativeness of the output results and simulations. From the above sections, considerable time was spent sorting and refining input data to eliminate errors and anomalies. However the results still did not match closely what was observed from the ground stations as a result of mainly rainfall and land use variability as well as model structure assumptions and parameter settings . The *ACRU* default values which have been used widely in research when modelling urban areas, did not produce good runoff simulations for this study. As seen from the model statistical evaluation in Table 4.6, the low NSE values and very high MARE (>10 %) values emphasise the poor performance of the model not only for the default values, but for all of the

impervious parameterisation methods. The *ACRU* model performed better when parameterised with impervious data from the pixel-based and GMIS method in Catchment A2H054, where the simulation produced a good NSE coefficient of 0.79, indicating good model predictive ability. The low MRE values indicate an acceptable goodness of fit between the simulated and observed (value closer to zero indicates good performance).

Overall, given the low quality of the input data fed into the models, the *ACRU* and SCS-SA models performed reasonably well in simulating runoff volumes from the complex urban catchments.

Table 4.6 Verification statistics of *ACRU* runoff volumes for the different impervious methods

A2H054	**Default values**	**Pixel-based**	**GMIS**	**GAIA**	**Loots (2020)**
MARE	>10%	>10%	>10%	>10%	>10%
MRE	0.013	0.007	0.007	0.012	0.008
NSE	0.11	0.79	0.79	0.24	0.63
A2H063					
MARE	>10%	>10%	>10%	>10%	>10%
MRE	0.03	0.016	0.024	0.024	0.22
NSE	-2.47	0.08	-1.18	-1.18	-0.8
U2H057					
MARE	>10%	>10%	>10%		
MRE	0.01	0.007	0.013		
NSE	0.1	0.13	0		

5. SCS-SA MODEL RESULTS

The SCS-SA model was run for the three study catchments. As discussed in the methodology section, the catchments were discretised into 9 HRUs that represent the catchment land cover. The SCS-SA model was run using parameters derived from the same input data used for the *ACRU* model, such as soils, slope, elevation, rainfall stations, MAP and land cover.. To assess the performance of the SCS-SA model, the design runoff and peak discharge are compared against design values computed from the observed data. The Log-Pearson Type 3 (LP3) probability distribution recommended by Griffis and Stedinger (2007) was fitted to the AMS using the Method of Moments to compute design values.

The study catchments were simulated in three scenarios, one where the catchment was divided and modelled with 9 HRUs compared to the use of a single, lumped representation of the catchment as done widely in practice. The HRUs varied in sizes and were assigned individual curve numbers based on the type of land cover and hydrological soil groups. The resulting graphs for this scenario are represented as "distributed". In the second scenario, the catchments were modelled in a "lumped" manner and assigned an area-weighted CN representing the dominant land cover. The first and second simulation scenarios (i.e. the distributed and lumped) were computed using curve numbers derived by Loots (2020). The third simulation scenario shows runoff and peak discharge computed using the tabular CN from the SCS-SA manual, represented as "CN_SCS". The design runoff and peak discharge for the different configurations are compared and discussed.

5.1 Catchment A2H054

With reference to Figure 5.1 and Figure 5.2 it can be seen that even though both design graphs are over-estimating design floods for the high return periods, the lumped scenario produces larger design floods compared to the distributed graph. This indicates that the best method for this catchment when running the SCS-SA model is to discretise the catchment into multiple HRUs based on the catchment size and land cover variability.

The design runoff achieved using the CNs from the SCS-SA manual (CN_SCS) over-simulated the "distributed" graph computed from curve numbers derived by Loots (2020), indicating that the most representative runoff scenario for this catchment was achieved by the distributed graph using Loots (2020) CNs. The "distributed" and "SCS_CN" graphs slightly under-simulated runoff for the smaller return periods and over-simulated runoff for the higher return periods. The lumped scenario produced an over simulation of runoff and peak discharge.

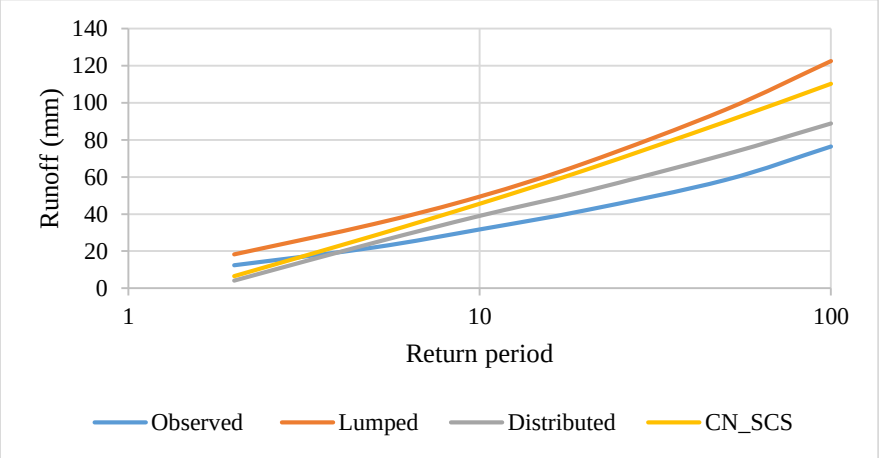

Figure 5.1 Design runoff depth for the simulated scenarios and observed data at Catchment A2H054

For peak discharge simulation in Figure 5.2, the "CN_SCS" graph estimated peak discharge better compared to the other simulated scenarios. However, overall the SCS-SA model in distributed mode simulated the observed peaks for Catchment A2H054 reasonably well, particularly for the smaller return periods.

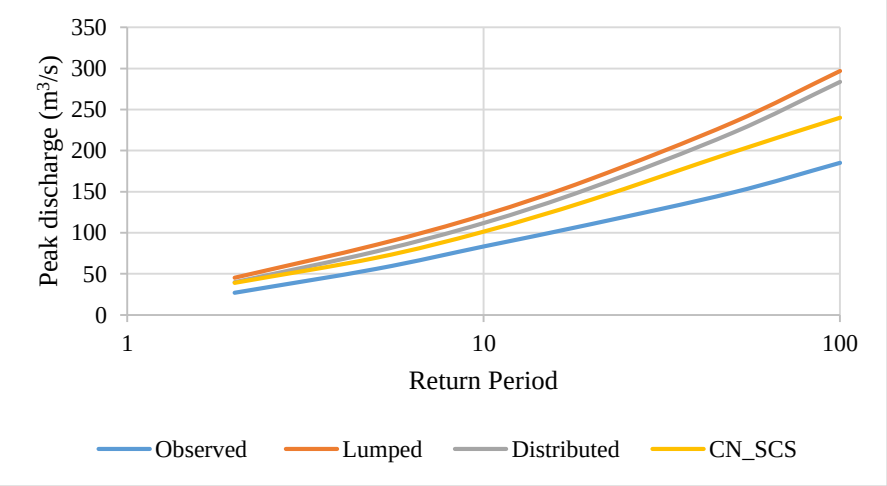

Figure 5.2 LP3 design peak discharge for the simulated scenarios and observed values at Catchment A2H054Catchment A2H063

Figure 5.3 and Figure 5.4 shows runoff and peak discharge simulations run for the different scenarios compared against the observed runoff and peak discharge for Catchment A2H063. Similar to Catchment A2H054, when Catchment A2H063 is modelled in a lumped manner and is represented by a single area-weighted CN, the model simulates higher runoff depths and peak discharges. On the

other hand, when the catchment is discretised into multiple sub-catchments representing different land use characteristics, lower design runoff depths are simulated which correlate better with the observed graph (Figure 5.3 and Figure 5.4). Therefore, based on the design floods results, it makes more hydrological sense to discretise a catchment when using the SCS-SA model, especially when modelling urban catchments that have a range of land uses.

The "CN_SCS" graph over-simulated the "distributed" values between the 5 year and 90 year return periods and slightly under-simulated runoff for the smaller return periods. Generally, the SCS-SA model simulated the design runoff from Catchment A2H063 reasonably well, with the best representative graph being the "distributed" graph using Loots (2020)'s CNs.

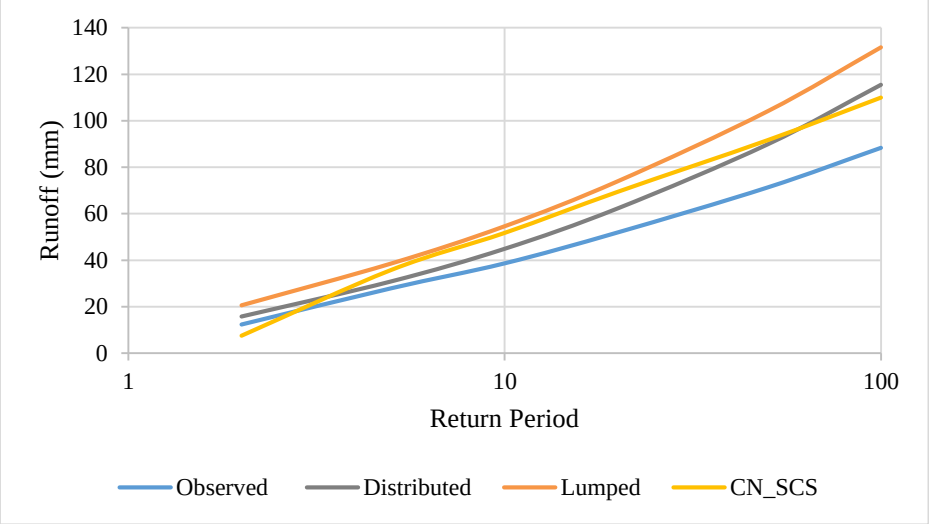

Figure 5.3 LP3 design runoff for the simulated scenarios and observed values at Catchment A2H063

In the case of peak discharge simulations for Catchment A2H063, the "CN_SCS" graph simulated the observed peaks better than the other scenarios; however, the design graphs produced an overall over-simulation of observed peak discharges.

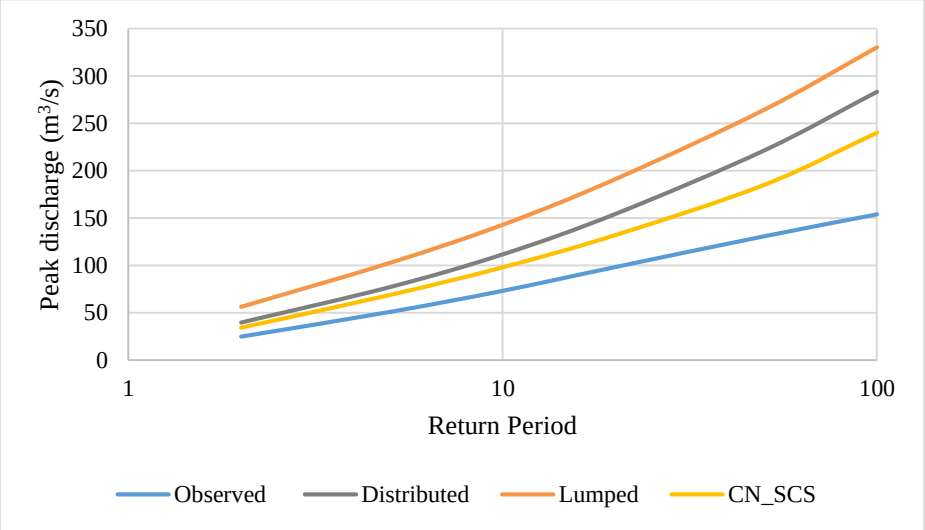

Figure 5.4 LP3 design peak discharge for the simulated scenarios and observed values at Catchment A2H063

5.2 Catchment U2H057

Figure 5.5 and Figure 5.6 illustrate the design runoff and peak discharge simulations for Catchment U2H057. The SCS-SA model over-simulated design runoff depths at this weir, particularly for the higher return periods. The large over-simulation can be attributed to the high curve numbers assigned to each HRU that represented the land cover properties within Catchment U2H057. Based on field observations, it was noted that the study area had excess surface flow due to the steep topography of the catchment and possibly inefficient drainage, and therefore high flows were over-simulated. The observed runoff data consisted of long periods of missing data, which affected the AMS values. This probably also added to the over-simulation of design runoff depths.

The “lumped” scenario graph over-simulated runoff and peak discharge. The “distributed” and “CN_SCS” graphs produced a similar simulation (over-simulated) of runoff and peak discharge, indicating that for this catchment, using the CNs from the SCS-SA manual produced a better simulation of both runoff and peak discharge as seen from the graphs (“distributed” and “CN_SCS”) agreeing better with each other. As noted from the previous catchments, the “lumped” scenario over-simulates both runoff and peak discharge compared to the distributed method of modelling.

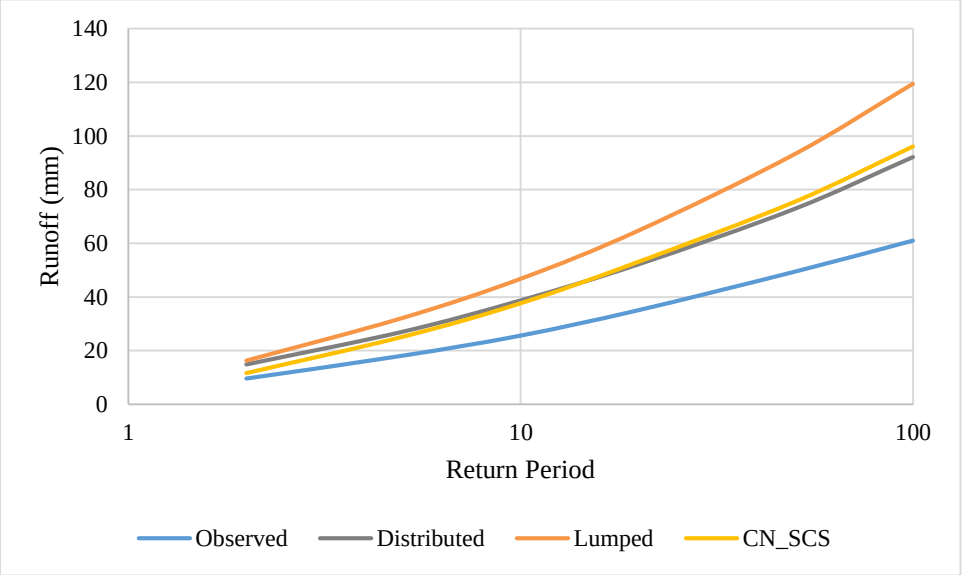

Figure 5.5 LP3 design runoff for the simulated scenarios and observed values at Catchment U2H057

The peak discharge (Figure 5.6) from the catchment is better simulated by the SCS-SA model compared to the runoff depths (by both the "distributed" and "CN_SCS" graphs). The "CN_SCS" graph mimics the observed peaks better than the "distributed" graph. A slight under-simulation of peaks is produced by the "distributed" graph in the smaller return periods, but it slightly over-simulates peaks towards the higher return periods.

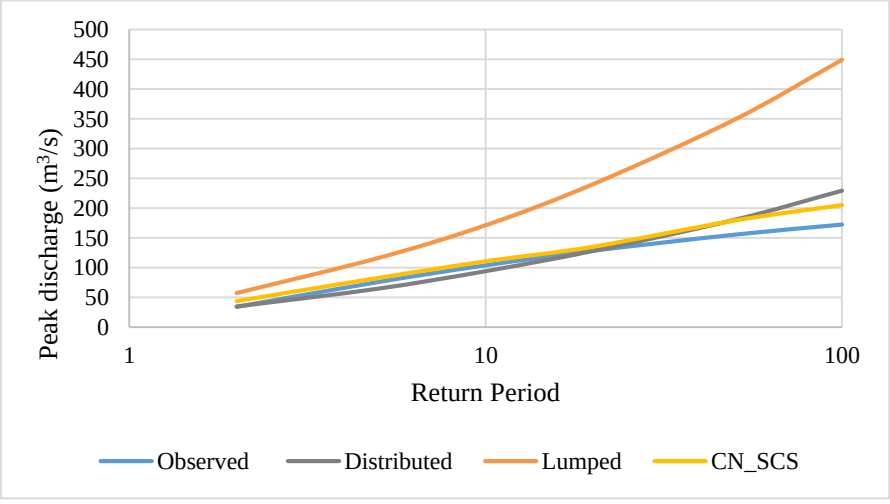

Figure 5.6 LP3 design peak discharge for the simulated scenarios and observed values at Catchment U2H057

5.3 Discussion and Conclusions

Overall, the SCS-SA model simulated observed runoff well. The results in this chapter show that the distributed scenario configured with CNs gives the best simulation. This is evident from the model statistical evaluation shown in Table 5.1, with low values of MARE. MRE values were low for the distributed and CN_SCS scenarios and slightly higher for the lumped scenario. This trend was noted for all catchments indicating a good model performance with the NSE ratios also being very close to 1, further emphasising the goodness-of-fit achieved by the "distributed" scenario. Lumping the catchment into one HRU and assigning an area-weighted CN did not prove to be the best method to model an urban catchment using the SCS-SA model, and this can be seen by the relatively higher MARE values and lower NSE ratios.

Using tabular CN from the SCS-SA manual is usually a default when running the SCS-SA model, and usually these CNs produce satisfactory simulations. However, for this study, the CNs derived by Loots (2020) and used for the Distributed and Lumped configurations, provided better runoff simulations. However, it is important to note that in order to be fully confident in the Loots (2020) derived CNs, it is recommended for future research to evaluate these CNs on a separate model configuration, where all model variables are kept constant and only the CNs are altered.

Table 5.1 Statisical evaluation of runoff simulations from the different SCS-SA scenarios configured for the study areas

A2H054	**Lumped**	**Distributed**	**CN_SCS**
MARE	0.096	0.046	0.075
MRE	0.645	0.267	0.302
NSE	0.612	0.951	0.762
A2H063			
MARE	0.036	0.079	0.052
MRE	0.566	0.301	0.291
NSE	0.932	0.783	0.924
U2H057			
MARE	0.139	0.084	0.074
MRE	0.894	0.586	0.455
NSE	0.151	0.742	0.734

6. COMPARISON OF PEAK DISCHARGES FROM *ACRU* AND SCS-SA MODELS

In this section, the design runoffs and peak discharge from the *ACRU* and SCS-SA models achieved from the best configuration scenarios (i.e. the pixel-based impervious parametrisation for the *ACRU* model and the distributed scenario assigned with Loots (2020) CNs for the SCS-SA model) are compared against the observed runoff and peaks discharge. Design runoff volumes and peak discharges are analysed for the catchments as well as from individual land use class HRUs to assess hydrological responses to land use change from a catchment and HRU scale. The Fortran distribution tool was used to fit the distributions to obtain design values. The LP3 probability distribution has been used for design flood estimation in this study. Alexander (1990) recommended the use of the LP3 probability distribution for design flood estimation in South Africa as it was found to be very applicable and it produced good design flood estimations. The LP3 distribution is fitted by L-moments and was used by Smithers *et al.* (2015) to estimate the design floods based on the statistics of the AMS at each selected gauge.

6.1 Catchment A2H054

Design runoff from the *ACRU* and SCS-SA models is compared against the observed runoff in Figure 6.1. The SCS-SA model over-simulated runoff depth particularly for the lower return periods and under-simulated flows for the higher return periods. The *ACRU* slightly under-simulated flows for the lower return periods and over-simulated for the higher return periods, however for this catchment, the *ACRU* model simulated runoff depth better than the SCS-SA model. The improved simulation achieved by the *ACRU* model could be attributed to the model being process-based and able to model runoff in a more complex manner from a range of land uses. The sum of the *ACRU* design runoff depths for each HRU are also assessed, in order to investigate the variability of simulated runoff from the different land use classes, shown in Figure 6.2. The urbanised HRUs produced more runoff than expected, due to the large areas of impervious cover, with bare surfaces and mining producing the highest runoff depths, followed by commercial and transport land uses.

It was noted that HRUs with a smaller area produced higher runoff depths and vice-versa. This can be seen with urban residential areas with the largest area of 14 539 km^2 but simulating a relatively lower runoff depth. Generally, catchment size is the most important catchment characteristic in determining the amount and timing of surface runoff at the outlet. The larger the catchment size, the greater the potential amount of rainfall that can be captured and routed to the catchment outlet.

Catchment size primarily controls the volume of runoff past the outlet. Catchment shape and topography are also key catchment characteristics controlling the routing of runoff to the basin outlet, and they primarily control the timing of the peak, and to a lesser extent, the magnitude of the peak flow. Soil properties to a large degree determine the infiltration rate, storage, and release of the rainfall from the overburden. Soils affect the amount and type of vegetation, which also influence the infiltration rate. Land use and modifications to the natural surface have a significant effect on the runoff from a catchment as reiterated in the literature review section.

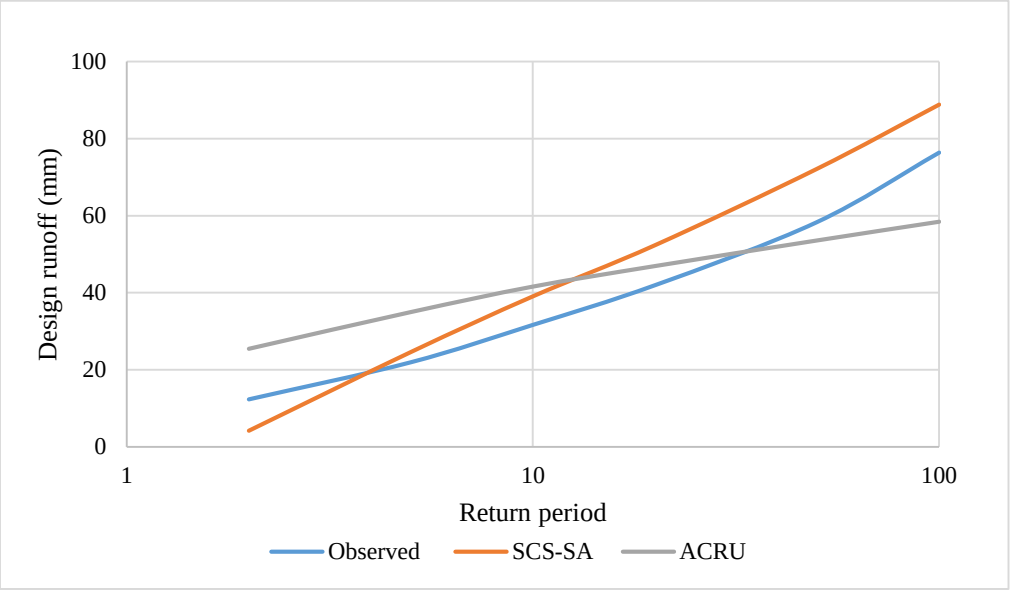

Figure 6.1 Design floods computed from the observed and simulated runoff depths in Catchment A2H054

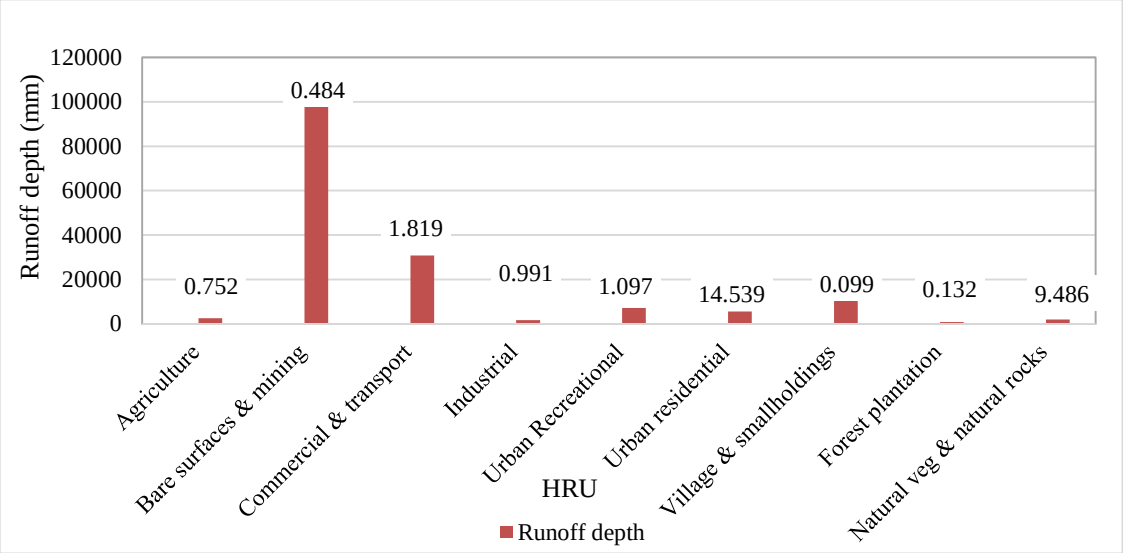

Figure 6.2 Runoff depths simulated for each HRU by the *ACRU* model

A high runoff depth value for Bare Surface and Mining was simulated. This could have been caused by either faulty observed data or a result of the volume from a large area running onto a smaller area and hence the large depths, or both reasons. Peak discharge is another essential parameter in urban design flood estimation as it determines the actual flood event. Peak discharge estimation is an important process of the *ACRU* modelling system and estimations of the magnitude of design floods are normally centred on the application of methods that represent the major processes that influence the runoff response of a catchment to rainfall. Peak discharge from small catchments relates closely to stormflow volume and the accurate estimation of antecedent soil water status. Stormflow volume is therefore of primarily importance in estimating peak discharge.

The design peaks simulated by the *ACRU* and SCS-SA models are compared to the observed values measured at Catchment A2H054 in Figure 6.3. The *ACRU* model simulated the catchment's peak discharge better. However, the model did slightly under-simulate the peaks for a few return periods. For example, for the 100 year return period the observed peaks were under-simulated by 58 m^3/s. The SCS-SA model over-simulated the observed peak discharge by almost 100 m^3/s for the 100 year return period.

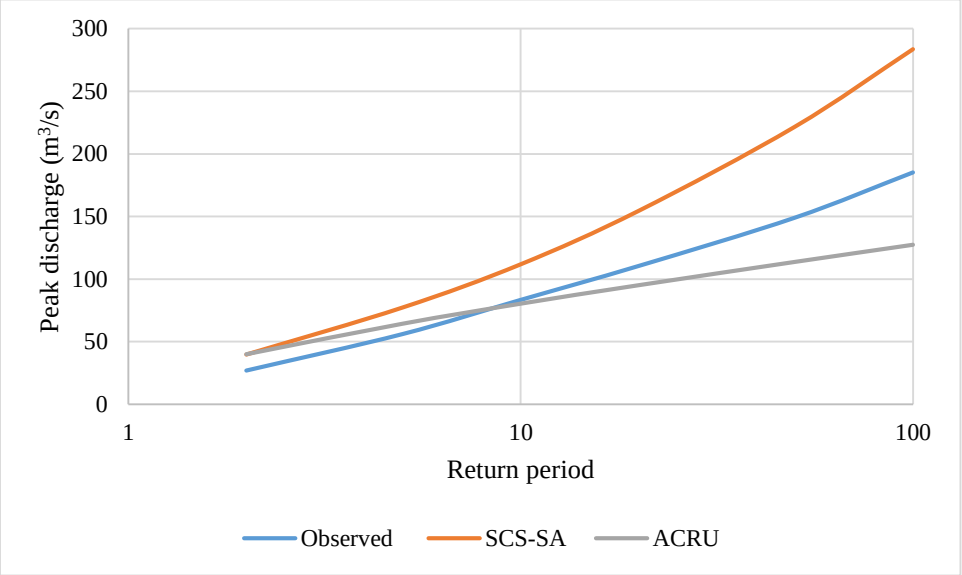

Figure 6.3 Design floods computed from the observed and simulated data at Catchment A2H054

6.2 Catchment A2H063

In Catchment A2H063 both the models over-simulated runoff depths, with the SCS-SA model over-simulating more. However, the flows are generally well simulated with reference to the gradient of the graphs in Figure 6.4.

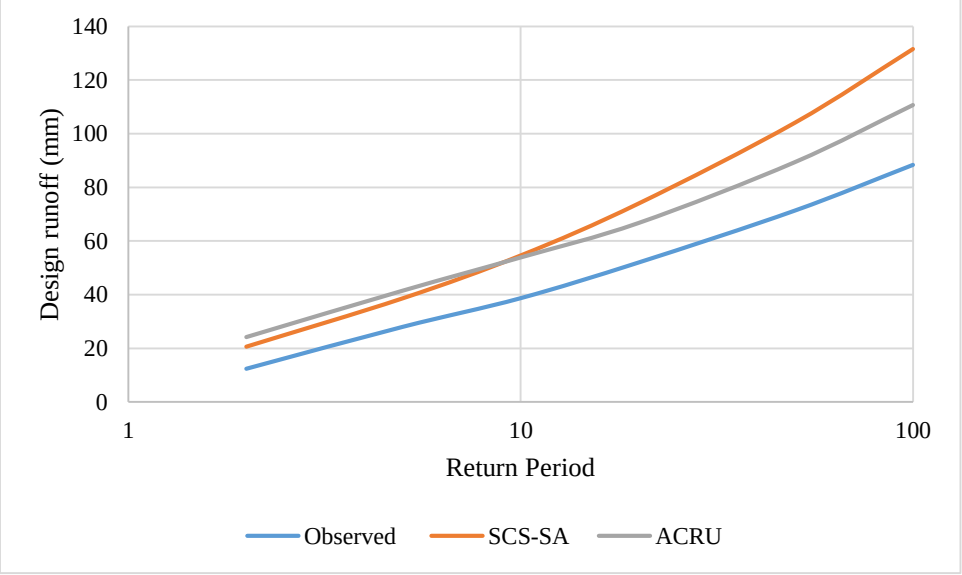

Figure 6.4 Design runoff computed from the observed and simulated data at Catchment A2H063

Runoff depth totals for each HRU in Catchment A2H063 are graphed in Figure 6.5, with individual areas labelled. A similar area-runoff depth relationship to Catchment A2H054 is noted for A2H063. Industrial areas simulated the highest runoff depth for the duration of the simulation period (taking into consideration land cover change over the years). Forest plantations produced the lowest runoff depths due to the presences of deep rooted and dense vegetation cover that capture rainfall and stormflow.

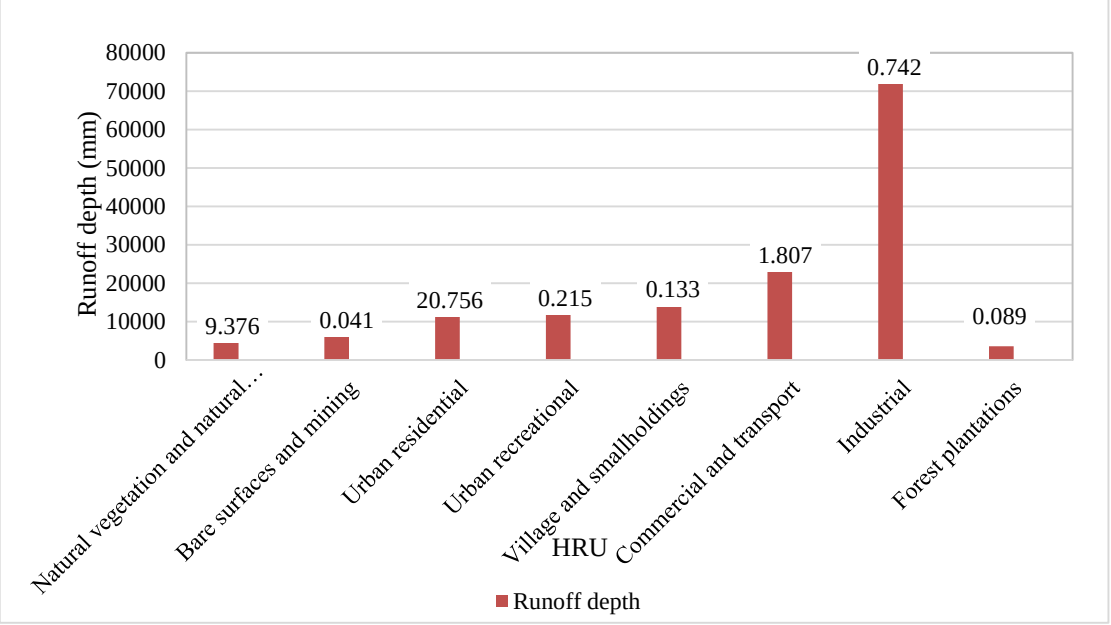

Figure 6.5 Runoff depths totals plotted for each HRU modelled in Catchment A2H063

Figure 6.6 shows the peak discharge simulations for Catchment A2H063. The *ACRU* model simulated observed peak discharge reasonably well, however it over-simulated peaks by 15 m^3/s for the 2 year return period, and under-simulated peaks for the 100 year return period by 27 m^3/s. The SCS-SA model grossly over-simulated peak discharge, particularly for the higher return periods. This could be explained by the model simulating high runoff depths from the industrialised and commercial HRUs.

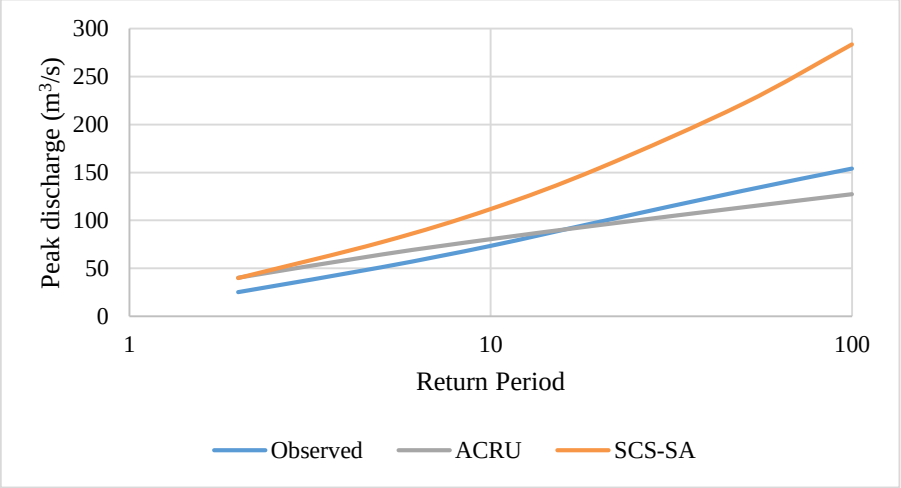

Figure 6.6 Design floods computed for the observed and simulated values at Catchment A2H063

6.3 Catchment U2H057

Both the models performed poorly on Catchment U2H057, more so for the higher return periods (i.e. beyond the 10 year return period mark) as seen in Figure 6.7. The *ACRU* model under-simulated runoff depths and the SCS-SA model over-simulated runoff. The observed and simulated runoff depths from this catchment are relatively lower compared to Catchment A2H063 due to the vast difference is land use (Catchment U2H057 is largely pervious and vegetated).

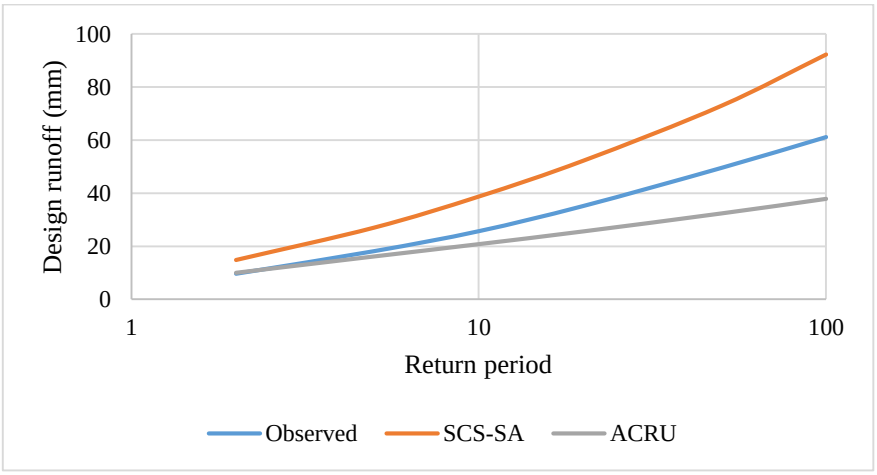

Figure 6.7 Design runoff computed for the observed and simulated values at Catchment U2H057

Runoff depth totals for individual HRUs and their respective areas are plotted in Figure 6.8. Industrial areas with the smallest area of 0.043 km^2 simulated the highest runoff depth. The HRUs that were

modelled with the ADJIMP and DISJIMP components simulated the highest runoff depths compared to the vegetated HRUs, which is expected based on literature findings.

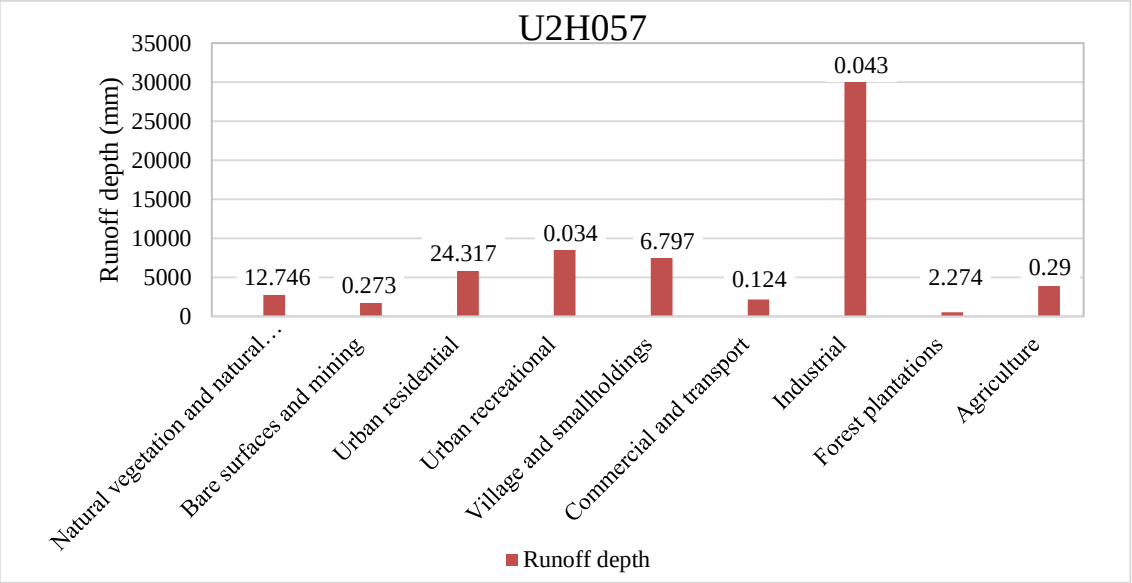

Figure 6.8 Runoff totals for individuals HRUs modelled in Catchment U2H057

Simulated vs observed peaks are shown for Catchment U2H057 in Figure 6.9. Both models seem to have simulated peak discharge reasonably well. The *ACRU* model under-simulated peaks for the most part and then over-simulated for low to medium return periods while the SCS-SA model matched the observed peaks to medium return periods and overestimated for high return periods. In most cases, the models perform poorly for higher return periods, and this needs to be further investigated in future research. Based on this study, the 10 to 50 year return periods are generally simulated well. An average flood event of 120 m^3/s is simulated by the models for Catchment U2H057.

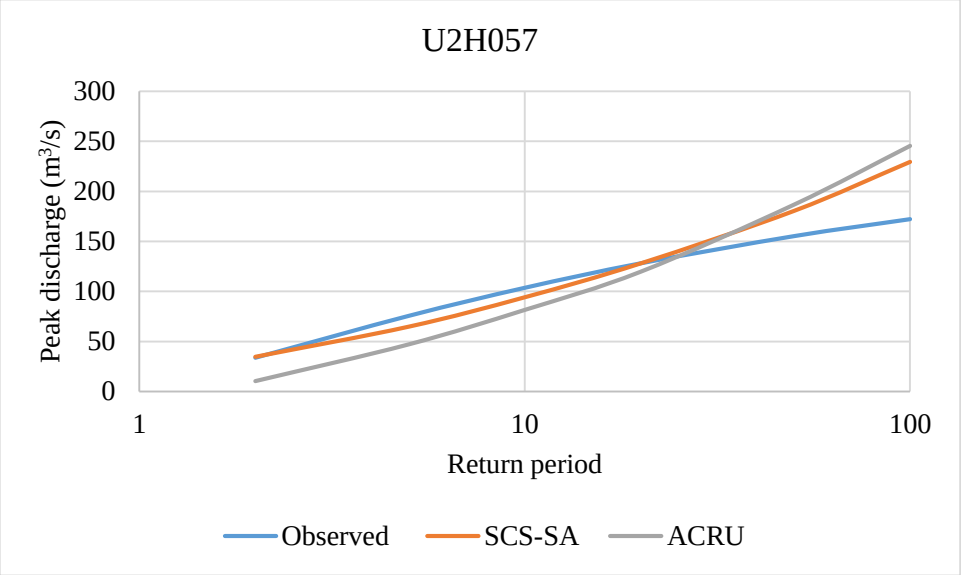

Figure 6.9 Design floods computed for observed and simulated datasets at Catchment U2H057

6.4 Discussions and Conclusions

Peak discharge simulations were used to assess the overall performance of the *ACRU* and SCS-SA models against the observed data and against each other. Based on the peak discharge results in Section 6, the *ACRU* model appears to have outperformed the SCS-SA model. The statistics in Table 6.1 agree with the above results. The very low MARE and MREs values, indicate a good model performance and a fair goodness-of-fit between observed and simulated values. The high NSE ratios for all the catchments indicate a reasonable predictive ability of the *ACRU* model. The SCS-SA model produced acceptable peak discharge simulations as well, with an average NSE ratio of 0.74 for all catchments.

However, the poor translation of runoff simulations to peak discharge needs to be assessed in future studies, as it was noted that the *ACRU* model produced poor simulations of runoff, and produced good simulations for peak discharge. This could be as a result of faulty observed streamflow data or undetected errors in the data.

Table 6.1 Statistical evaluation of model performance using design values for peak discharge for the study areas

A2H054	***ACRU***	**SCS-SA**
MARE	0.038	0.072
MRE	0.313	0.769
NSE	0.941	0.774
A2H063		
MARE	0.036	0.103
MRE	0.100	0.844
NSE	0.972	0.485
U2H057		
MARE	0.055	0.021
MRE	0.500	0.043
NSE	0.912	0.953

7. THE EFFECT OF CHANGE IN URBAN AREA ON PEAK RUNOFF

The literature review of this study emphasised the issue of rapid urbanisation over time and the effects that it has on urban hydrology. Urbanisation is reported to have a significant impact on the overall runoff volumes, the reduction of runoff lag time, increases flood return periods, and elevation of peak discharges during storm events. A flashiness of streamflow has been a frequently detected "symptom" of urban development and impervious surfaces. All of these factors, including a higher population of people living in urban areas as opposed to rural areas, emphasise the need for design flood estimation and improvement of design flood estimation methods to be focused particularly in growing urban areas. Therefore, this section integrates the theoretical understanding of urbanisation and the associated surface runoff simulated by the *ACRU* model from the urban catchments.

A dataset of global land cover classification of urban areas (in this case regarding modelling the equivalent to impervious areas) dataset as estimated by Gong *et al.* (2020) for the years, 1990, 1995, 2000, 2005, 2010, 2015 and 2018 was clipped for the urban study catchments and the results are analysed and discussed in this section. An automatic delineation framework to generate a multi-temporal dataset of Global Urban Boundaries (GUB) using 30 m global artificial impervious area (GAIA) data was used to estimate the extent urban areas. Accumulated streamflows from simulation results with urban areas, and with the urban areas replaced by natural vegetation, is also included to provide a picture of the effects of urban areas on generated streamflow on each of the study catchments.

Figure 7.1 illustrates the area covered with urban land uses from 1990 until 2018 for the three study catchments. It is evident from this graph that urban area increases with an increase in years. The catchment area covered with urban land is estimated to be 2.33 km^2 and 2.46 km^2 in 1990 for Catchments A2H054 which A2H063 and increases to almost double the area in 2018. This is quite drastic, bearing in mind the small sizes of the total catchment area (i.e. 29.6 km^2, 33.2 km^2). There is a sharp increase in urban area from 1990 to 1995 and then afterwards it increases more gradually as the years progress.

The same trend in urbanisation is true for Catchment U2H057 (48 km^2). The area covered with 'urban area' as indicated in Figure 7.1 for this catchment is not necessarily related to the level of development, as Catchment U2H057 is less developed then Catchments A2H054 and A2H063. Dense informal settlements can at times be classified as urban impervious features (possibly due to their pixel properties resulting from building material), and this may add to the total urban area classified

for this catchment. Therefore, it is important to note that in some cases, higher impervious cover does not necessarily mean a higher level development of an area. There is also an abrupt increase in urbanisation noted between the beginning of the simulation period in 1990 and 2000. Thereafter, urbanisation remains constant for about 15 years, probably without significant development taking place as this catchment is characterised as an informal settlement. There is a slight expansion in the urban area of about 0.5 km^2 from 2015 to 2018.

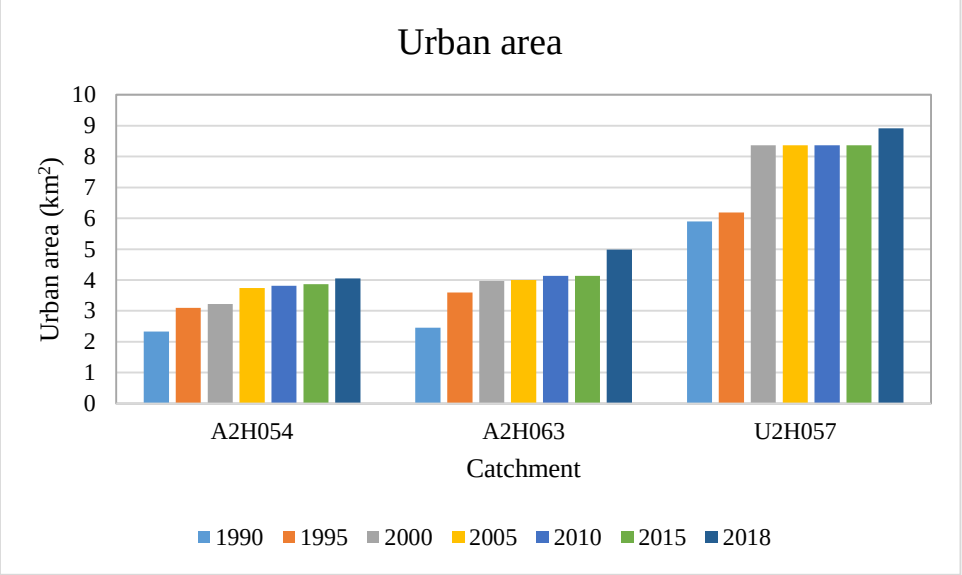

Figure 7.1 Urban areas estimated over time for the three study catchments for the years 1990-2018

Figure 7.2 illustrates accumulated streamflows simulated from Study Catchments A2H054, A2H063 and U2H057 where the catchments were modelled with urban areas and then without urban areas (replaced with natural vegetation) within a fixed period of time. The streamflow simulated from the urban area scenario produced an over-simulation of streamflow in Catchments A2H054 and A2H063, with the over-simulation being emphasised in Catchment A2H054, possibly as a result of additional factors encouraging streamflow generation (drainage, slope, vegetation, soil etc.). The streamflow graph where the urban areas were replaced by natural vegetation under-simulated flows in Catchment A2H054 and U2H057 and over-simulated streamflow in Catchment A2H063. The higher flows are mostly over-simulated.

In Catchment U2H057, the urban area scenario over-simulated low flows in the beginning of the simulation period and then under-simulated high flows towards the end of the simulation period. Owing to the nature of Catchment U2H057 (highly pervious and with rural features), the graph with

urban areas did not significantly over-simulate streamflow for the most part. On the other hand, the simulation without urban areas produced very low flows, therefore indicating the influence on impervious/urban area on streamflow simulations.

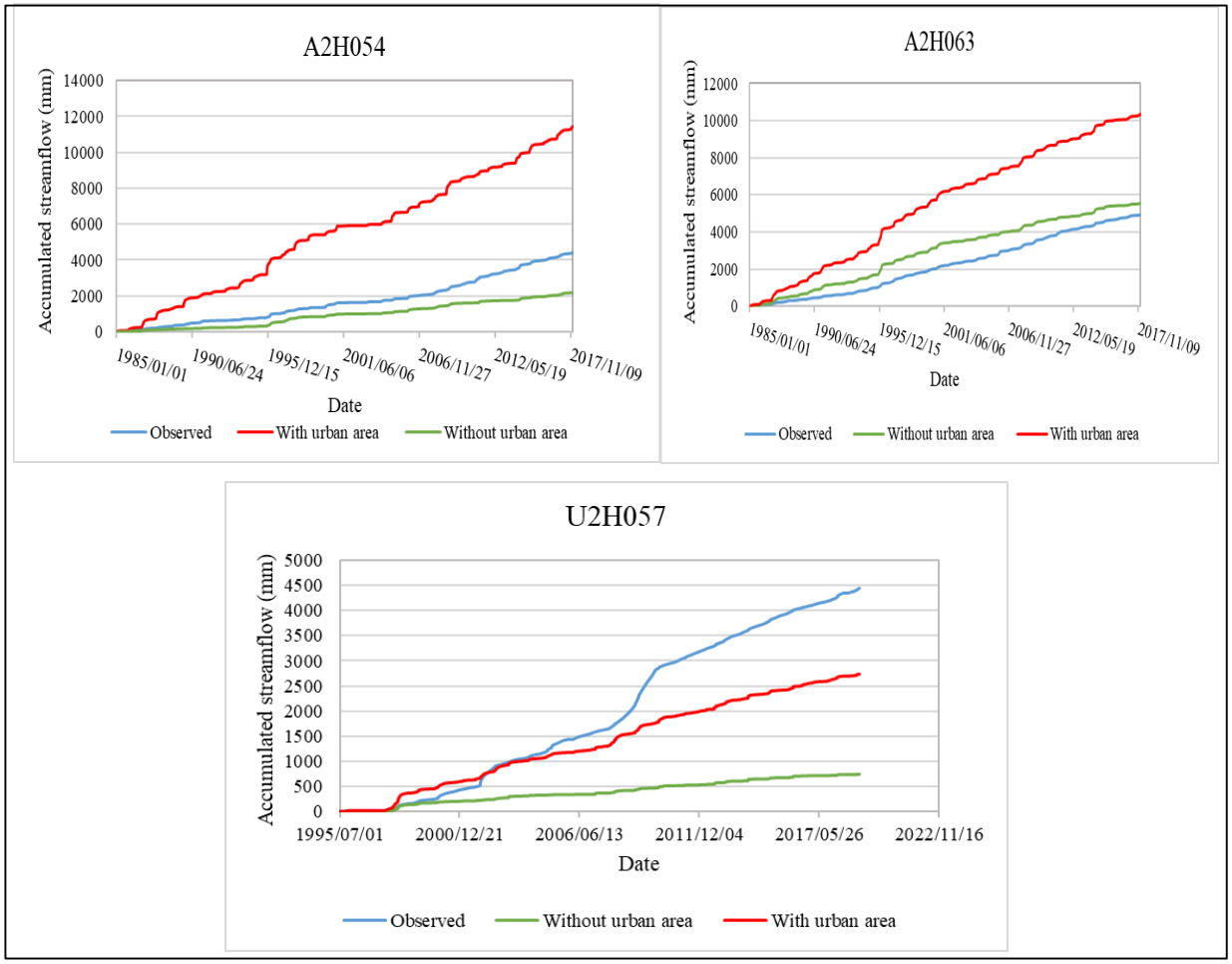

Figure 7.3 Simulation results of accumulated flows with urban areas and with the urban areas replaced by natural vegetation, plotted for each study catchment

8. DISCUSSION, CONCLUSIONS AND RECOMMENDATIONS

This chapter contains concluding remarks and recommendations based on the objectives of this study. A summary is included on how each objective was achieved and the challenges that were encountered. Recommendations based on the findings of the study and the results obtained are made for future research purposes.

Research Aims and Objectives

The overall aim for this study was to assess and to evaluate the performance of runoff simulation and design flood estimation in urban areas using the *ACRU* and SCS-SA models.

The objectives were to:

a) Reviewing relevant literature based on international and local urbanisation trends and their effects on the hydrology of urban areas, application of the *ACRU* and SCS-SA models in urban areas and researching existing mapping methods of Impervious Surface Areas (ISA) that could be integrated with design flood estimation models.
b) Identify suitable study catchments and obtain reliable and consistent climate and land cover data to be used to derive model input data and parameters.
c) Use GIS and Remote Sensing to obtain more accurate input parameters and developing guidelines to estimate the impervious model parameters in urban areas.
d) Configure the *ACRU* and SCS-SA models using different impervious parameterisation methods and scenarios to detect the best configuration.
e) Assess and improve simulations from the models where necessary.
f) Study urban land cover change over time and the effect of impervious cover on streamflow.

The key results from the set objectives are summarised and discussed in following sections.

Literature pertaining to urban hydrology and design flood estimation methods

a) Hydrology of urban areas

Several factors that influence the hydrology of urban areas were discussed. These included drainage paths. Development alters the natural drainage pathways and increases the urban flood hazards. The influence of catchment slopes on runoff flow velocity was reviewed, as steep concreted catchment slopes promote high volumes of turbulent runoff flow. This reduces the levels of baseflow and increases peak flows. And lastly, the main point highlighted from the urban hydrology literature was the connection between urbanisation/development, imperviousness and the increase in flood risk. Resulting flood hydrographs plotted following urban development appeared to have high volumes of runoff and high peak discharges. A sub-category of total imperviousness, ADJIMP is used in the *ACRU* model as an indicator of the level of urbanisation. The literature findings were proven true by the model simulations, whereby there were significant over-simulations noted with impervious cover.

b) Application of the *ACRU* and SCS-SA models in urban areas

A vast amount of work has been put into further developing and refining existing design flood estimation methods and models. The *ACRU* and SCS-SA models have been applied extensively in catchments across a range of land uses, and more particularly rural catchments. Only a few studies have applied these models in urban catchments with typical South African urban characteristics. From the late 1990s, work has continued to be done on the *ACRU* model to improve its performance in urban areas. According to the literature, continuous simulation models produce more in-depth analysis of hydrological processes compared to design event modelling. The *ACRU* model was data-intensive, less user-friendly than the simpler SCS-SA model. The configuration of the ADJIMP and DISJIMP fractions in the *ACRU* model and streamflow relationship needs to be refined to fit the context of different catchments with different land cover dynamics. Besides the tendency of underestimating peaks flows, the *ACRU* model provided better simulated design values compared to the SCS-SA model when compared to observed values. The addition of the ADJIMP and DISJIMP components when modelling urban areas affected the sensitivity of catchment characteristics to streamflow response, and therefore this made running a sensitivity test very challenging, as the catchment was less responsive to parameter adjustments. Both the models have been reported to have produced good simulations in all types of catchments, provided they are provided with reliable consistent data.

c) Researching existing ISA mapping methods that could be integrated with design flood estimation models

The integration of hydrological modelling and remote sensing has previously been studied and applied by multiple authors. A wide range of methods are available for mapping ISA, with the common ones making use of remote sensing and GIS. For this study, different land cover/impervious mapping methods were studied to assess the best suited RS method that will be compatible with the selected hydrological models and provide the best results. A combination of coding, running GIS software and desktop sampling went into finding the best method for running land cover classification to map ISA. The process of impervious mapping proved to be tedious and challenging, and over-estimated impervious land cover. Historical land cover classification was extracted from existing datasets for the simulation period to detect changes in land cover over the years, particularly a change in urban area cover. There is a lack of readily available impervious datasets with a good spatial resolution. The global datasets provided reasonable results. However, the large scale resolution affected the accuracy of the impervious estimations at catchment level, and some of the datasets did not cover the Slangspruit catchment (U2H057). From using information from the literature review, a connection between the expansion of impervious surfaces with runoff generation was analysed to draw up conclusions and assist in flood forecasting for urban areas based on the impervious surface cover trends assessed in this study. It was also deduced from literature that incorporating RS and GIS into hydrological models enhances the efficiency and practicability of hydrological models. However, the procedures to getting the best results may be time consuming.

Identifying suitable urban study areas and obtaining reliable and consistent climate and land cover observed data to serve as model parameters

Suitable catchments that fitted the context and objectives of the study (i.e. catchments with urban areas) were selected. The availability of reliable rainfall and flow data was a major challenge during the configuration of the *ACRU* model. The rainfall data required patching, using data from surrounding rainfall stations (that also had long periods of missing data). The runoff gauge stations had long periods of missing data. Data collected and analysed for this study confirm the non-uniformity of precipitation in time and space, and are evidence for the validity of the assumption that unsteady runoff conditions are generated from varied precipitation, overland flow, and subsurface stormflow. These gaps and inconsistencies affected the simulations. The unavailability of flow data for Catchment U2H057 prior to 1995 affected the consistency of drawing comparisons across the urban catchments. The lack of good resolution satellite imagery to conduct land cover classification

confidently proved to be a disadvantage in running and obtaining reliable land cover classification results/mapping TIA and therefore accurately parameterising the models.

Using GIS and Remote Sensing to obtain more accurate input parameters and developing guidelines to estimate the model parameters in urban area.

Research was undertaken on remote sensing and GIS methods that are used to conduct land cover classification, more particularly to map impervious surfaces. This was done with the purpose of estimating *ACRU*'s ADJIMP and DSIJIMP areas more accurately for improved urban modelling. Additional data such as the stream network, stormwater information, altitude, soils, and slope were also computed using GIS tools. Executing land cover classifications for South African catchments can at times be exceedingly challenging because global data sources do not cover the region, therefore causing further stumbling blocks in accessing reliable data and limiting the range of data sources. There are not many studies whereby the available impervious land cover datasets were employed and verified. However, thorough field work was done with the attempt to verify the results achieved from the RS land cover classification methods that were used to parameterise the *ACRU* model.

Configuring the ACRU and SCS-SA models using different impervious parameterisation methods and scenarios to detect the best configuration

The simulations from the *ACRU* and SCS-SA models were extracted and analysed. The *ACRU* model's design values were over-simulated in most cases. The poor performance of the *ACRU* model in the daily streamflow simulations could be as a result of the unreliable, poor quality, and patched rainfall. The SCS-SA model over-simulated design runoff and peak discharge, and this could have been caused by the mis-representation of land cover classes.

Assessing and improving simulations from the models where necessary

The *ACRU* results were put through a sensitivity analysis test where several variables from the *ACRU* model such as from different rainfall stations, soil depth, SMDDEP, COFRU and the CAY coefficients were chosen as sensitive variables. These *ACRU* variables were changed by mostly increasing the sensitive parameters to a plausible (realistic to the *ACRU* model) value with these changing the resulting simulations. Most of the variables reduced the over-simulation of both high and low flows by an insignificant percentage, and hence those results were not included.

Studying urban land cover change over time and the effect of impervious cover on streamflow

Achieving this objective fully was challenging as a result of the lack of historical satellite imagery, land cover classification maps and mapped imperviousness. Therefore, changes and trends in urban area could only be studied for a shorter period. The inability of the *ACRU* 4 version of the model to simulate dynamic land cover change also hindered studying the influence of land cover and land use change on streamflow volumes optimally. The conclusions from this chapter are that there is definitely a constant increase in urban area with time from the studied catchments, and this is directly proportional to an increase in impervious cover which in turn significantly affects urban flows.

The graph illustration in Figure 7.2 (Catchment A2H054) shows an over-estimation of accumulated streamflow relative to the observed streamflow with added *ACRU* impervious components whereas in previous runoff simulations (Figure 6.1), *ACRU* is shown to have under-estimated runoff relative to the observed and SCS-SA design values. This discrepancy in design values from these illustrations could suggest that *ACRU* overestimated the lower flows while underestimating the peak/high flows.

Recommendations for Future Research

The main challenge experienced during the course of the study was data collection and obtaining reliable input data for the *ACRU* and SCS-SA models. Finding primary daily rainfall data where the stations were actually within the catchments, that is free of errors and continuous for most of the record was a challenging task since the focus of the study was assessing the performance of rainfall-runoff models in urban areas. Therefore, a bias against the models was introduced by feeding the models with unreliable and often patched input data. It is recommended, therefore, to improve the quality of observed rainfall and runoff data collected from ground stations. The ground stations should be frequently monitored and maintained to reduce errors and failure of the gauge to record rainfall on days where it rained. It was also observed that another possible cause of the relatively poor simulations is the fact that daily rainfall is measured from 08:00 to 08:00 while runoff is conventionally recorded from midnight to midnight. Recommendation for future research to look into eliminating all possible scenarios that may lead to poor simulations when testing the performance of a model, as this introduces a bias. Another challenge that was experienced was obtaining stormwater drainage information from the local municipality for Catchment U2H057. From all the three study catchments, data was most scarce for Catchment U2H057.

Another challenge was accessing historical satellite images that have a fine resolution for land cover classification purposes. Running land cover classifications with satellite imagery that has a coarse resolution and incomplete band combination reduces the accuracy of the land cover classification. Therefore, for future research, there should be an imagery hub that is easily accessible, with a range of satellite imagery including that from as far back as the 1960's and 1980's covering all regions. Historical data are important for identifying trends and predicting future projections on a specific topic, such as imperviousness, urbanisation, surface temperature, rainfall trends etc.

Further research should be focused on investigating land cover classification methods that are able to easily distinguish and map bare surfaces from tinned roof surfaces that have a shining appeal, as in the case for informal urban areas. The mis-classification usually occurs when working with gray-scale imagery. The two features appear to have the same pixel information and, therefore, in many classification cases the two surfaces are usually mis-classified. More research needs to be focused on refining remote sensing land cover classification methods, to reduce bare land mis-classification and impervious cover over-estimation. The mis-classification introduces a number of errors when the classification results are to be used for further decision making. More research should be undertaken on merging and creating a constructive integration platform between GIS and remote sensing and hydrological modelling. There is room for considerable possibilities and mutual advancement if the two disciplines were integrated.

Recommendation for future research into refining the methodology to calculate *ACRU* 's impervious components (i.e. ADJIMP and DISJIMP) to avoid the possibility of introducing flow over-estimations. Running a sensitivity test on the various assumptions made will improve the robustness and validity of the methodology.

Recommendation for future research to look into the likely impact of rainfall intensity on flow simulation in urban areas. In order to further understand the influences of urbanization on rainfall intensity, case studies would be extremely beneficial. Analysis of case studies would provide insight into which parameters are altered by urbanisation of which of these parameters influence the precipitation intensity. The inability of the design stormflow peak discharge equation used in *ACRU* to account for the actual distribution of daily rainfall, i.e. the rainfall intensity, on a given day is a model limitation. If a methodology to account for rainfall intensity on a day-to-day basis is developed and included within the *ACRU* model, the relationship between catchment lag time and rainfall intensity can be useful to adjust estimated lag times based on the rainfall intensity. This is important

since this relationship influences the simulation of the stormflow contribution to peak discharge. The consistent over-simulation in runoff noted for this study can be attributed to variations in daily stormflow responses, catchment lag time and rainfall intensity, all of which are approximated with estimates of average or typical conditions. Further room for improvement, particularly with the *ACRU* model, has been reported by previous CSM studies.

Several of the plots of design runoff and peak discharge in Chapter 6 suggest that *ACRU* has a tendency of underestimating peak design flows at high return periods. This implies that caution needs to be taken in using this method in practice as factors or margins of safety are applied to allow for the inevitable uncertainties of modelling real-life systems.

Lastly, from this study, it is recommended that more research and development be focused on updating and enhancing design flood estimation methods and models so as to better represent the hydrological cycle of the more complex catchments which contain informal and peri-urban areas. This will enable better design of urban hydraulic infrastructure and help in decision making related to floods.

9. REFERENCES

Abustan, I, Sulaiman, AH, Wahid, NA and Baharudin, F. 2008. Determination of rainfall-runoff characteristics in an urban area: Sungai Kerayong Catchment, Kuala Lumpur. *11th International Conference on Urban Drainage, Edinburgh, Scotland, UK*, 1-10.

Aduah, MS, Jewitt, GP and Toucher, MLW. 2017. Assessing suitability of the ACRU hydrological model in a rainforest catchment in Ghana, West Africa. *Water Science* 31 (2): 198-214.

Ahn, J, Cho, W, Kim, T, Shin, H and Heo, J-H. 2014. Flood frequency analysis for the annual peak flows simulated by an event-based rainfall-runoff model in an urban drainage basin. *Water* 6 (12): 3841-3863.

Alexander, W. 2002. The standard design flood. *Journal of the South African Institution of Civil Engineering= Joernaal van die Suid-Afrikaanse Instituut van Siviele Ingenieurswese* 44 (1): 26-30.

Alexander, WJR. 1990. *Flood Hydrology for Southern Africa*. South African National Committee on Large Dams,

Alley, WM and Veenhuis, JE. 1983. Effective impervious area in urban runoff modeling. *Journal of Hydraulic Engineering* 109 (2): 313-319.

Anderson, JR. 1976. *A land use and land cover classification system for use with remote sensor data*. US Government Printing Office,

Arnold, CL and Gibbons, CJ. 1996. Impervious surface coverage: The emergence of a key environmental indicator. *Journal of the American planning Association* 62 (2): 243-258.

Aron, G. 1982. Rainfall abstractions. *Urban stormwater hydrology*, Amercican Geophysical Union, Washington, D.C., United States.

Bell, CD, McMillan, SK, Clinton, SM and Jefferson, AJ. 2016a. Hydrologic response to stormwater control measures in urban watersheds. *Journal of Hydrology* 541: 1488-1500.

Bell, JM, Simonson, AE and Fisher, IJ. 2016b. *Urban hydrology—Science capabilities of the US Geological Survey*. 2327-6932. USGS Northeast Region Urban Landscapes Capability, US Geological Survey, United States.

Bezuidenhout, CN. 2005. Development and evaluation of model-based operational yield forecasts in the South African sugar industry. Unpublished thesis,

Bickford-Smith, V. 1995. South African urban history, racial segregation and the unique case of Cape Town? *Journal of Southern African Studies* 21 (1): 63-78.

Brabec, E, Schulte, S and Richards, PL. 2002. Impervious surfaces and water quality: a review of current literature and its implications for watershed planning. *Journal of planning literature* 16 (4): 499-514.

Bui, DH and Mucsi, L. 2021. From Land Cover Map to Land Use Map: A Combined Pixel-Based and Object-Based Approach Using Multi-Temporal Landsat Data, a Random Forest Classifier, and Decision Rules. *Remote Sensing* 13 (9): 1700.

Calver, A and Lamb, R. 1995. Flood frequency estimation using continuous rainfall-runoff modelling. *Physics and Chemistry of the Earth* 20 (5-6): 479-483.

Calver, A. 1996. Development and experience of the TATE rainfall runoff model. *Proceedings of the Institution of Civil Engineers-Water Maritime and Energy* 118 (3): 168-176.

Cameron, D, Beven, KJ, Tawn, J, Blazkova, S and Naden, P. 1999. Flood frequency estimation by continuous simulation for a gauged upland catchment (with uncertainty). *Journal of Hydrology* 219 (3-4): 169-187.

Chen, M, Zhang, H, Liu, W and Zhang, W. 2014. The global pattern of urbanization and economic growth: evidence from the last three decades. *PloS one* 9 (8), *p.e 103799*

Chen, Y, Zhou, H, Zhang, H, Du, G and Zhou, J. 2015. Urban flood risk warning under rapid urbanization. *Environmental Research* 139 3-10.

Chetty, K and Smithers, J. 2005. Continuous simulation modelling for design flood estimation in South Africa: Preliminary investigations in the Thukela catchment. *Physics and Chemistry of the Earth, Parts A/B/C* 30 (11-16): 634-638.

Choi, W, Nauth, K, Choi, J and Becker, S. 2016. Urbanization and rainfall–runoff relationships in the Milwaukee River basin. *The Professional Geographer* 68 (1): 14-25.

Corburn, J and Sverdlik, A. 2017. Slum upgrading and health equity. *International Journal of Environmental Research and Public Health* 14 (4): 342.

Cronshey, R. 1986. *Urban hydrology for small watersheds*. US Dept. of Agriculture, Soil Conservation Service, Engineering Division.

Cu, PT and Ball, JE. 2017. The influence of the calibration metric on design flood estimation using continuous simulation. *International Journal of River Basin Management* 15 (1): 9-20.

Daniell, KA, Rinaudo, J-D, Chan, NWW, Nauges, C and Grafton, Q. 2015. Understanding and managing urban water in transition. In: *Understanding and Managing Urban Water in Transition*. Springer.

De Colstoun, EB, Huang, C, Wang, P, Tilton, JC, Tan, B, Phillips, J, Niemczura, S, Ling, P-Y and Wolfe, R. 2017. Documentation for the global man-made impervious surface (GMIS) dataset from landsat. *NASA Socioeconomic Data and Applications Center (SEDAC): Palisades, NY, USA*.

Delgado, C. 1969. Three proposals regarding accelerated urbanization problems in metropolitan areas: The Lima case. *American Behavioral Scientist* 12 (5): 34-45.

Diacon, D. 1997. *Slum Networking: An innovative approach to urban development*. Building and Social Housing Foundation Coalville, Leicestershire,, UK.

Dunsmore, SJ, Schulze, RE and Schmidt, EJ. 1986. *Antecedent Soil Moisture in Design Runoff Volume Estimation: Interim Report to the Water Research Commission on the Project" Design Stormflow and Peak Discharge Rates for Small Catchments in Southern Africa"*. Water Research Commission, Pretoria, South Africa.

Falkenmark, M, Andersson, L, Castansson, R, Sundbland, K, Batchelor, C, Gardiner, J, Lyle, C, Peters, N, Pettersen, B and Quinn, P. 1999. *Water a Reflection of Land Use: Options for Counteracting Land and Water Mismanagement*. Swedish Natural Science Council NFR, Stockolm,(Sweden).

Fan, F, Deng, Y, Hu, X and Weng, Q. 2013. Estimating composite curve number using an improved SCS-CN method with remotely sensed variables in Guangzhou, China. *Remote Sensing* 5 (3): 1425-1438.

Geneletti, D and Gorte, B. 2003. A method for object-oriented land cover classification combining Landsat TM data and aerial photographs. *International Journal of Remote Sensing* 24 (6): 1273-1286.

Goel, N, Kurothe, R, Mathur, B and Vogel, R. 2000. A derived flood frequency distribution for correlated rainfall intensity and duration. *Journal of Hydrology* 228 (1-2): 56-67.

Goetz, SJ, Wright, RK, Smith, AJ, Zinecker, E and Schaub, E. 2003. IKONOS imagery for resource management: Tree cover, impervious surfaces, and riparian buffer analyses in the mid-Atlantic region. *Remote Sensing of Environment* 88 (1-2): 195-208.

Gong, P, Li, X, Wang, J, Bai, Y, Chen, B, Hu, T, Liu, X, Xu, B, Yang, J and Zhang, W. 2020. Annual maps of global artificial impervious area (GAIA) between 1985 and 2018. *Remote Sensing of Environment* 236: 111510.

Graser, A, Mearns, B, Mandel, A, Ferrero, VO and Bruy, A. 2017. *QGIS: Becoming a GIS power user*. Packt Publishing Ltd, Birmingham, UK.

Griffis, V and Stedinger, J. 2007. Log-Pearson type 3 distribution and its application in flood frequency analysis. II: Parameter estimation methods. *Journal of Hydrologic Engineering* 12 (5): 492-500.

Grinfelde, I and Bakute, A. 2017. Urban hydrological response unit parameter calibration and verification for conceptual hydrological model METQ. *Engineering for Rural Development* 16 1117-1122.

Haghighi, S, Jasemi, M, Hessabi, S and Zolanvari, A. 2018. PyCM: Multiclass confusion matrix library in Python. *Journal of Open Source Software* 3 (25): 729.

Hameed, HM. 2017. Estimating the effect of urban growth on annual runoff volume using GIS in the Erbil sub-basin of the Kurdistan Region of Iraq. *Hydrology* 4 (1): 12.

Hargreaves, GH and Samani, ZA. 1985. Reference crop evapotranspiration from temperature. *Applied Engineering in Agriculture* 1 (2): 96-99.

Hoes, O and Nelen, F. 2005. Continuous simulation or event-based modelling to estimate flood probabilities? *WIT Transactions on Ecology and the Environment* 80

Hossain, S, Hewa, GA and Wella-Hewage, S. 2019. A Comparison of Continuous and Event-Based Rainfall–Runoff (RR) Modelling Using EPA-SWMM. *Water* 11 (3): 611.

Hu, X and Weng, Q. 2009. Estimating impervious surfaces from medium spatial resolution imagery using the self-organizing map and multi-layer perceptron neural networks. *Remote Sensing of Environment* 113 (10): 2089-2102.

Hu, X and Weng, Q. 2011. Impervious surface area extraction from IKONOS imagery using an object-based fuzzy method. *Geocarto International* 26 (1): 3-20.

Soil Conservation Service. 1956. National engineering handbook, supplement a, section 4, chapter 10, soil conservation service. *USDA, Washington, DC.*

Jacobson, CR. 2011. Identification and quantification of the hydrological impacts of imperviousness in urban catchments: A review. *Journal of Environmental Management* 92 (6): 1438-1448.

Jadkowski, MA, Howard, RR and Brostuen, DE. 1990. Application of SPOT data for regional growth analysis and local planning. *Photogrammetric Engineering and Remote Sensing* 56 (2): 175-180.

Ji, M and Jensen, JR. 1999. Effectiveness of subpixel analysis in detecting and quantifying urban imperviousness from Landsat Thematic Mapper imagery. *Geocarto International* 14 (4): 33-41.

Kao, SE, Fogel, MM and Resnick, SD.1973. Effect of Urbanization on Runoff from Small Watersheds. Arizona-Nevada Academy of Science, Water Resources Research Centre, The University of Arizona. Tucson, Arizona, United States.

Kienzle, SW. 1993. Application of a GIS for simulating hydrological responses in developing regions. *IAHS PUBLICATION* No.309-309.

Kiker, G, Clark, D, Martinez, C and Schulze, R. 2006. A Java-based, object-oriented modeling system for southern African hydrology. *Transactions of the ASABE* 49 (5): 1419-1433.

Kjeldsen, TR. 2015. How reliable are design flood estimates in the UK? *Journal of Flood Risk Management* 8 (3): 237-246.

Kolsky, P. 1998. *Storm drainage*. Intermediate Technology Publications, London,

Kusangaya, S, Warburton, M and Archer van Garderen, E. 2017. Use of ACRU, a distributed hydrological model, to evaluate how errors from downscaled rainfall are propagated in simulated runoff in uMngeni catchment, South Africa. *Hydrological Sciences Journal* 62 (12): 1995-2011.

Lamb, R. 1999. Calibration of a conceptual rainfall-runoff model for flood frequency estimation by continuous simulation. *Water Resources Research* 35 (10): 3103-3114.

Lee, CA, Gasster, SD, Plaza, A, Chang, C-I and Huang, B. 2011. Recent developments in high performance computing for remote sensing: A review. *IEEE Journal of Selected Topics in Applied Earth Observations and Remote Sensing* 4 (3): 508-527.

Lee, JG and Heaney, JP. 2003. Estimation of urban imperviousness and its impacts on storm water systems. *Journal of Water Resources Planning and Management* 129 (5): 419-426.

Lennon, M, Scott, M and O'Neill, E. 2014. Urban design and adapting to flood risk: the role of green infrastructure. *Journal of Urban Design* 19 (5): 745-758.

Loots, I. 2020. *Design Flood Estimation in Urban Areas in South Africa: Preliminary Results from Tshwane Case Studies*. University of KwaZulu-Natal, Pietermaritzburg, KZN, South Africa. .

Lu, D, Li, G, Kuang, W and Moran, E. 2014. Methods to extract impervious surface areas from satellite images. *International Journal of Digital Earth* 7 (2): 93-112.

Lu, D, Moran, E and Hetrick, S. 2011. Detection of impervious surface change with multitemporal Landsat images in an urban–rural frontier. *ISPRS Journal of Photogrammetry and Remote Sensing* 66 (3): 298-306.

Lu, D and Weng, Q. 2006. Use of impervious surface in urban land-use classification. *Remote Sensing of Environment* 102 (1-2): 146-160.

Lucci, P, Bhatkal, T, Khan, A and Berliner, T. 2015. What works in improving the living conditions of slum dwellers. A review of the evidence across four programmes. *ODI Dimenstion Paper* 4. London, UK.

Lumbroso, D, Boyce, S, Bast, H and Walmsley, N. 2011. The challenges of developing rainfall intensity–duration–frequency curves and national flood hazard maps for the Caribbean. *Journal of Flood Risk Management* 4 (1): 42-52.

Lynch, S. 2003. Development of a Raster Database of Annual, Monthly and Daily Rainfall for Southern Africa. Unpublished thesis, School of Bioresources Engineering and Environmental Hydrology, University of Natal, Pietermaritzburg, South Africa.

Maharaj, B and Narsiah, S. 2002. From apartheid apologism to post-apartheid neo-liberalism: Paradigm shifts in South African urban geography. *South African Geographical Journal* 84 (1): 88-97.

Marceau, DJ, Howarth, PJ, Dubois, J-MM and Gratton, DJ. 1990. Evaluation of the grey-level co-occurrence matrix method for land-cover classification using SPOT imagery. *IEEE Transactions on Geoscience and Remote Sensing* 28 (4): 513-519.

Mauck, BA. 2012. The impacts of future urban growth on streamflow in the Mgeni catchment. Unpublished thesis, University of KwaZulu-Natal, Pietermaritzburg, South Africa.

McGrane, SJ. 2016. Impacts of urbanisation on hydrological and water quality dynamics, and urban water management: a review. *Hydrological Sciences Journal* 61 (13): 2295-2311.

Mejía, AI and Moglen, GE. 2010. Spatial distribution of imperviousness and the space-time variability of rainfall, runoff generation, and routing. *Water Resources Research pp*.46 (7):

Mitchell, A and Minami, M. 1999. *The ESRI Guide to GIS Analysis: Geographic Patterns & Relationships*. ESRI, Inc.California, US.

Muthanna, T, Sivertsen, E, Kliewer, D and Jotta, L. 2018. Coupling Field Observations and Geographical Information System (GIS)-Based Analysis for Improved Sustainable Urban Drainage Systems (SUDS) Performance. *Sustainability* 10 (12): 4683.

Myeza, NN. 2019. Improved modelling of the hydrological impacts of urban land use in the Limpopo North Water Management Area. Unpublished thesis, School of Agriculture, Earth and Environmental Sciences, University of KwaZulu-Natal, Pietermaritzburg, South Africa.

United Nations. 2019. World population prospects 2019: Data Booklet (ST/ESA/SER.A/424). Department of Economic and Social Affairs, Population Division (2019).

Packman, J. 1980. The effects of urbanisation on flood magnitude and frequency. Report No 63. Institute of Hydrology, Wallingford, UK.

Pafka, E and Dovey, K. 2017. Permeability and interface catchment: measuring and mapping walkable access. *Journal of Urbanism: International Research on Placemaking and Urban Sustainability* 10 (2): 150-162.

Parikh, H, Surkar, D and Zanders, M-O. 2002. Sustainable infrastructure development for slums and villages. Sustainable environmental sanitation and water services: Porceedings of the 28th WEDC International Conference 4p.p., Loughborough University, Kolkata (Calcutta), India.

Park, K and Lee, M-H. 2019. The development and application of the urban flood risk assessment model for reflecting upon urban planning elements. *Water* 11 (5): 920.

Parkinson, J, Tayler, K and Mark, O. 2007. Planning and design of urban drainage systems in informal settlements in developing countries. *Urban Water Journal* 4 (3): 137-149.

Patel, AM and Suthar, A. 2020. AdaBoosted Extra Trees Classifier for Object-Based Multispectral Image Classification of Urban Fringe Area. *International Journal of Image and Graphics* 2140006.

Pegram, G. 1997. Patching rainfall data using regression methods. 3. Grouping, patching and outlier detection. *Journal of hydrology* 198 (1-4): 319-334.

Phinn, S, Stanford, M, Scarth, P, Murray, A and Shyy, P. 2002. Monitoring the composition of urban environments based on the vegetation-impervious surface-soil (VIS) model by subpixel analysis techniques. *International Journal of Remote Sensing* 23 (20): 4131-4153.

Phiri, D, Simwanda, M, Salekin, S, Nyirenda, VR, Murayama, Y and Ranagalage, M. 2020. Sentinel-2 data for land cover/use mapping: A review. *Remote Sensing* 12 (14): 2291.

Pourali, SH, Arrowsmith, C, Mitchell, D and Matkan, A. 2014. Modelling An Overland Water Flow Path In An Urban Catchment Using GIS. *Geoinformatica: An International Journal* 4 (1): 1-19.

Powell, RL, Roberts, DA, Dennison, PE and Hess, LL. 2007. Sub-pixel mapping of urban land cover using multiple endmember spectral mixture analysis: Manaus, Brazil. *Remote Sensing of Environment* 106 (2): 253-267.

Rabe, A, Jakimow, B, Thiel, F, Hostert, P and van der Linden, S.2018. Enmap-box 3 a free and open source python plug-in for qgis. *IGARSS 2018-2018 IEEE International Geoscience and Remote Sensing Symposium*, 7764-7766. IEEE,

Rabori, AM and Ghazavi, R. 2018. Urban Flood Estimation and Evaluation of the Performance of an Urban Drainage System in a Semi-Arid Urban Area Using SWMM. *Water Environment Research* 90 (12): 2075-2082.

Rahman, A, Hoang, T, Weinmann, P and Laurenson, E. 1998. *Joint probability approaches to design flood estimation: A review*. Cooperative Research Centre for Catchment Hydrology,

Rahman, A, Weinmann, E and Mein, RG. 2002. The use of probability-distributed initial losses in design flood estimation. *Australasian Journal of Water Resources* 6 (1): 17-29. University of Canberra, Australia.

Rangari, VA, Patel, AK and Umamahesh, N.2015. Review of urban stormwater models. *HYDRO 2015, 20th International Conference on Hydraulics, IIT Roorkee, India*,

Rashed, T, Weeks, JR, Gadalla, MS and Hill, AG. 2001. Revealing the anatomy of cities through spectral mixture analysis of multispectral satellite imagery: A case study of the Greater Cairo region, Egypt. *Geocarto International* 16 (4): 7-18.

Rashed, T, Weeks, JR, Roberts, D, Rogan, J and Powell, R. 2003. Measuring the physical composition of urban morphology using multiple endmember spectral mixture models. *Photogrammetric Engineering & Remote Sensing* 69 (9): 1011-1020.

Rawls, WJ, Shalaby, A and McCuen, RH. 1981. Evaluation of methods for determining urban runoff curve numbers. *Transactions of the ASAE* 24 (6): 1562-1566.

Rowe, T and Smithers, J. 2018. Continuous simulation modelling for design flood estimation–A South African perspective and recommendations. *Water SA* 44 (4): 691-705. University of KwaZulu-Natal, Pietermaritzburg, South Africa.

Rowe, TJ. 2015. Development and assessment of rules to parameterise the ACRU model for design flood estimation. Unpublished thesis (Masters degree), University of KwaZulu-Natal, Pietermaritzburg, South Africa.

Rowe, TJ. 2019. Development and assessment of an improved continuous simulation modelling system for design flood estimation in South Africa using the ACRU model. Unpublished thesis,

Roy, AH and Shuster, WD. 2009. Assessing impervious surface connectivity and applications for watershed management 1. *JAWRA Journal of the American Water Resources Association* 45 (1): 198-209.

Ruiz Hernandez, IE and Shi, W. 2018. A Random Forests classification method for urban land-use mapping integrating spatial metrics and texture analysis. *International Journal of Remote Sensing* 39 (4): 1175-1198.

Schmidt, EJ and Schulze, R. 1984. *Improved estimates of peak flow rates using modified SCS lag equations*. University of Natal, Department of Agricultural Engineering, University of Natal, Pietermaritzburg, South Africa.

Schmidt, EJ, Schulze, RE and Dent, MC. 1987. *Flood volume and peak discharge from small catchments in Southern Africa, based on the SCS technique: Appendices*. Water Research Commission,

Schmitz, P and De Villiers, GdT. 1997. *The Development of an Urban Component of the ACRU Model*. WRC, Pretoria, South Africa.

Schulze, R. 1982. *Adapting the SCS Stormflow Equation for Application to Specific Events by Soil Moisture Budgeting*. Department of Agricultural Engineering, University of Natal, Pietermaritzburg, South Africa.

Schulze, R.1989. Non-stationary catchment responses and other problems in determining flood series: A case for a simulation modelling approach. *Proc. 4th SANCIAHS National Hydrological Symposium*, 20-22.

Schulze, R. 2021. *A National Assessment of Potential Climate Change Impacts on the Hydrological Yield of Different Hydro-Climatic Zones of South Africa: South African and International Verification Studies of the ACRU Daily Time-Step Model across a Range of Processes, Applications and Spatial Scales.*WRC Report No. K5/2833/1&2. Water Research Commission, Pretoria, South Africa.

Schulze, R, Angus, G, Lynch, S and Smithers, J. 1994. ACRU: Concepts and Structure. ACRU Theory Manual. Department of Agricultural Engineering, University of Natal, Pietermaritzburg, South Africa.

Schulze, R, Arnold, H. 1979. *Estimation of volume and rate of runoff in small catchments in South Africa based on the SCS technique*. Department of Agricultural Engineering, University of Natal, Pietermaritzburg, South Africa.

Schulze, R and Davis, N. 2018. *Practitioners' Handbook for Undertaking Current and Projected Future Climate Related Risk and Vulnerability Assessments. GIZ Contract Number 83259369 on "Development of a Framework and Methodology for Undertaking a Risk and Vulnerability Assessment in all Nine Water Management Areas of South Africa".* Schulze and Associates, Pietermaritzburg, South Africa.

Schulze, R and Horan, M. 2008. Section 4.2: Soils Hydrological Attributes. *ed. Schulze, RE, South African Atlas of Climatology and Agrohydrology. WRC Report* 1489 (1): 06. Water Research Commission, Pretoria, South Africa.

Schulze, R and Pike, A. 2004. Development and evaluation of an installed hydrological modelling system. *Water Research Commision Report* 1155 1. Water Research Commission, Pretoria, South Africa.

Schulze, R, Schmidt, E and Smithers, J. 1992a. *PC Based SCS Design Flood Estimates for Small Catchments in Southern Africa, SCSSA User Manual:* Pietermaritzburg, South Africa, University of Kwa-Zulu-Natal, Department of Agricultural Engineering.

Schulze, R, Schmidt, E and Smithers, J. 1992b. *SCS-SA User Manual. PC-Based SCS Design Flood Estimates for Small Catchments in Southern Africa*. University of Natal, Pietermaritzburg, South Africa.

Schulze, R, Schmidt, E and Smithers, J. 2004a. *Visual SCS-SA User Manual (Version 1.0)*. ACRUcons Report. University of Natal, Pietermaritzburg, South Africa.

Schulze, R, Schmidt, E and Smithers, J. 2004b. *Visual SCS–SA User Manual Version 1.0: PC based SCS design flood estimates for small catchments in Southern Africa*. ACRUcons Report.

Schulze, R and Schütte, S. 2018. *Mapping SCS Hydrological Soil Groups over South Africa at Terrain Unit Resolution*. University of KwaZulu-Natal, Pietermaritzburg, RSA.

Schulze, RaS, S. 2018. Mapping SCS Hydrological Soil Groups over South Africa at Terrain Unit Resolution. University of KwaZulu-Natal, Pietermaritzburg, South Africa.

Schulze, RE. 1995a. *Hydrology and agrohydrology: A text to accompany the ACRU 3.00 agrohydrological modelling system*. Water Research Commission, Pretoria, South Africa.

Schulze, REaT, K. C. 1995b. *Hydrological responses from urbanized areas, in: Hydrology and Agrohydrology: A Text to Accompany the ACRU 3.00 Agrohydrological Modelling System*. Water Research Commission, Pretoria, South Africa.

Schütte, S. 2014. Linkages between selected hydrological ecosystem services and land use changes, as indicated by hydrological responses: A case study on the Mpushini/Mkhondeni Catchments, South Africa. Unpublished thesis, University of KwaZulu-Natal, Pietermaritzburg, South Africa.

Schütte, S, Clark, DJ, Wolski, P, Kunz, RP and Smithers, JC, Schulze, R.E, Horan, M, Thornton-Dibb, S, and Stuart-Hill, S. 2020. *A National Assessment of Potential Climate Change Impacts on the Hydrological Yield of Different Hydro-Climatic Zones of South Africa*. University of KwaZulu-Natal, Pietermartzburg, South Africa.

Schütte, S and Schulze, R. 2017. Projected impacts of urbanisation on hydrological resource flows:A case study within the uMngeni Catchment, South Africa. *Journal of environmental management* 196 527-543. University of KwaZulu-Natal, Pietermaritzburg, South Africa.

SCS. 1972. *National Engineering Handbook*. Washington, DC, United States.

Shaw, R, Noguchi, Y and Ishiwatari, M. 2012. Green belts and coastal risk management.

Shu, Y, Li, H and Lei, Y. 2018. Modelling Groundwater Flow with MIKE SHE Using Conventional Climate Data and Satellite Data as Model Forcing in Haihe Plain, China. *Water* 10 (10): 1295.

Silva, EA and Clarke, KC. 2002. Calibration of the SLEUTH urban growth model for Lisbon and Porto, Portugal. *Computers, Environment and Urban systems* 26 (6): 525-552.

Slonecker, ET, Jennings, DB and Garofalo, D. 2001. Remote sensing of impervious surfaces: A review. *Remote Sensing Reviews* 20 (3): 227-255.

Smithers, J. 2011. *Methods for design flood estimation in South Africa*. School of Bioresources, Engineering and Environmental Hydrology, University of KwaZulu-Natal, Pietermaritzburg, South Africa.

Smithers, J. 2012. Methods for design flood estimation in South Africa. *Water SA* 38 (4): 633-646.

Smithers, J, Chetty, K, Frezghi, M, Knoesen, D and Tewolde, M. 2007. Development and assessment of a continuous simulation modelling system for design flood estimation. *Water Research Commission, South Africa, Rep* 1318 (1): 07.

Smithers, J, Chetty, K, Frezghi, M, Knoesen, D and Tewolde, M. 2013. Development and assessment of a daily time-step continuous simulation modelling approach for design flood estimation at ungauged locations: ACRU model and Thukela Catchment case study. *Water SA* 39 (4): 467-476.

Smithers, J, Schulze, R and Kienzle, S. 1997. Design flood estimation using a modelling approach: A case study using the ACRU model. *IAHS Publication* 240 365-376.

Smithers, J, Schulze, R, Pike, A and Jewitt, G. 2001. A hydrological perspective of the February 2000 floods: A case study in the Sabie River Catchment. *Water SA* 27 (3): 325-332.

Smithers, J, Streatfield, J, Gray, R and Oakes, E. 2015. Performance of regional flood frequency analysis methods in KwaZulu-Natal, South Africa. *Water SA* 41 (3): 390-397.

Strahler, AH, Woodcock, CE and Smith, JA. 1986. On the nature of models in Remote Sensing. *Remote Sensing of Environment* 20 (2): 121-139.

Sun, S, Barraud, S, Branger, F, Braud, I and Castebrunet, H. 2017. Urban hydrologic trend analysis based on rainfall and runoff data analysis and conceptual model calibration. *Hydrological Processes* 31 (6): 1349-1359.

Tarboton and Schulze, R. 1992. *Distributed Hydrological Modelling System for the Mgeni Catchment*. Water Research Commission, Pretoria, South Africa.

Tarboton, K. 1992. Interfacing GIS and hydrological modelling: Mgeni case study. *Water SA* 18 (4): 273-278.

Tarboton, K and Schulze, R. 1991. The ACRU modelling system for large catchment water resources management. *Hydrology for the Water Management of Large River Basins* 219-232.

Tarboton, KC, Lynch, SD and Schulze, R. 1992. *Distributed hydrological modelling system for the Mgeni catchment*. Water Research Commission, Pretoria, South Africa.

Terstriep, ML and Stall, JB. 1974. The Illinois urban drainage area simulator, ILLUDAS. *Bulletin (Illinois State Water Survey) no. 58*

Tikkanen, H. 2013. Hydrological modeling of a large urban catchment using a stormwater management model (SWMM) (Masters dissertation), Aalto University, Finland.

Van de Voorde, T, De Roeck, T and Canters, F. 2009. A comparison of two spectral mixture modelling approaches for impervious surface mapping in urban areas. *International Journal of Remote Sensing* 30 (18): 4785-4806.

Vazquez, M, Sorensen, B, Mark, O, Borgstrom, R, Juel-Berg, K and Tomicic, B. 2018. Applying Remote Sensing to Determine the Percent Imperviousness for Urban Drainage Modelling. *Research Journal of Environmental Sciences* 12 (3): 132-143.

Verma, RK, Kumari, KS and Tiwary, R.2009. Application of remote sensing and GIS technique for efficient urban planning in India. *Geomatrix Conference Proceedings*, National Institute of Industrial Engineering, Mumbai, India.

Voigtländer, S, Breckenkamp, J and Razum, O. 2008. *Urbanization in Developing Countries. Trends, health consequences and challenges*. Faculty of Health Sciences, Bielefeld University, Germany.

Walsh, CJ, Roy, AH, Feminella, JW, Cottingham, PD, Groffman, PM and Morgan, RP. 2005. The urban stream syndrome: current knowledge and the search for a cure. *Journal of the North American Benthological Society* 24 (3): 706-723.

Wang, B, Liu, D, Liu, S, Zhang, Y, Lu, D and Wang, L. 2012. Impacts of urbanization on stream habitats and macroinvertebrate communities in the tributaries of Qiangtang River, China. *Hydrobiologia* 680 (1): 39-51.

Wang, K and Dickinson, RE. 2012. A review of global terrestrial evapotranspiration: Observation, modeling, climatology, and climatic variability. *Reviews of Geophysics* 50 (2):

Warburton, ML. 2012. Challenges in modelling hydrological responses to impacts and interactions of land use and climate change. Unpublished thesis (Doctoral dissertation), University of KwaZulu-Natal, Pietermaritzburg, South Africa.

Warburton, ML, Schulze, RE and Jewitt, GP. 2010. Confirmation of ACRU model results for applications in land use and climate change studies. *Hydrology and Earth System Sciences* 14 (12): 2399.

Warsta, L, Niemi, TJ, Taka, M, Krebs, G, Haahti, K, Koivusalo, H and Kokkonen, T. 2017. Development and application of an automated subcatchment generator for SWMM using open data. *Urban Water Journal* 14 (9): 954-963.

Warwick, J and Tadepalli, P. 1991. Efficacy of SWMM application. *Journal of Water Resources Planning and Management* 117 (3): 352-366.

Weng, Q. 2012. Remote sensing of impervious surfaces in the urban areas: Requirements, methods, and trends. *Remote Sensing of Environment* 117 34-49.

Weng, Q and Hu, X. 2008. Medium spatial resolution satellite imagery for estimating and mapping urban impervious surfaces using LSMA and ANN. *IEEE Transactions on Geoscience and Remote Sensing* 46 (8): 2397-2406.

Weng, Q, Hu, X and Liu, H. 2009. Estimating impervious surfaces using linear spectral mixture analysis with multitemporal ASTER images. *International Journal of Remote Sensing* 30 (18): 4807-4830.

Weng, Q and Lu, D. 2009. Landscape as a continuum: An examination of the urban landscape structures and dynamics of Indianapolis City, 1991–2000, by using satellite images. *International Journal of Remote Sensing* 30 (10): 2547-2577.

Wheeler, D. 1986. Spectral characterization of urban land covers from Thematic Mapper data. *Remote Sensing for Resources Development and Environmental Management* Vol 893-898.

Wood, ML. 2012. Streamflow Analysis and a Comparison of Hydrologic Metrics in Urban Streams.

Wu, C. 2004. Normalized spectral mixture analysis for monitoring urban composition using ETM+ imagery. *Remote Sensing of Environment* 93 (4): 480-492.

Wu, C and Murray, AT. 2003. Estimating impervious surface distribution by spectral mixture analysis. *Remote sensing of Environment* 84 (4): 493-505.

Xu, H. 2010. Analysis of impervious surface and its impact on urban heat environment using the normalized difference impervious surface index (NDISI). *Photogrammetric Engineering & Remote Sensing* 76 (5): 557-565.

Xu, J, Zhao, Y, Zhong, K, Ruan, H and Liu, X. 2016. Coupling modified linear spectral mixture analysis and soil conservation service curve number (SCS-CN) models to simulate surface runoff: Application to the main urban area of Guangzhou, China. *Water* 8 (12): 550.

Yang, G, Bowling, LC, Cherkauer, KA, Pijanowski, BC and Niyogi, D. 2010. Hydroclimatic response of watersheds to urban intensity: An observational and modeling-based analysis for the White River Basin, Indiana. *Journal of Hydrometeorology* 11 (1): 122-138.

Yang, L, Huang, C, Homer, CG, Wylie, BK and Coan, MJ. 2003. An approach for mapping large-area impervious surfaces: synergistic use of Landsat-7 ETM+ and high spatial resolution imagery. *Canadian Journal of Remote Sensing* 29 (2): 230-240.

Zhou, Y and Wang, Y.2008. Remote Sensing of Impervious Surface Area for improved Hydrologic Modeling. *Proc. of ISPRS 2008 Congress*, pp.73-78. Department of Natural Resources Sciences, University of Rhode Island, Kingston, USA.

10. APPENDIX A: GROUPING OF LAND USE CLASSES

This section includes a spatial representation of the land use classes grouped into HRUs FOR Catchment A2H063 and U2H057.

Appendix A1 Land cover classes modolled as HRU1 for Catchment A2H063

Appendix A2 Land cover classes modelled as HRU 2 for Catchment A2H063

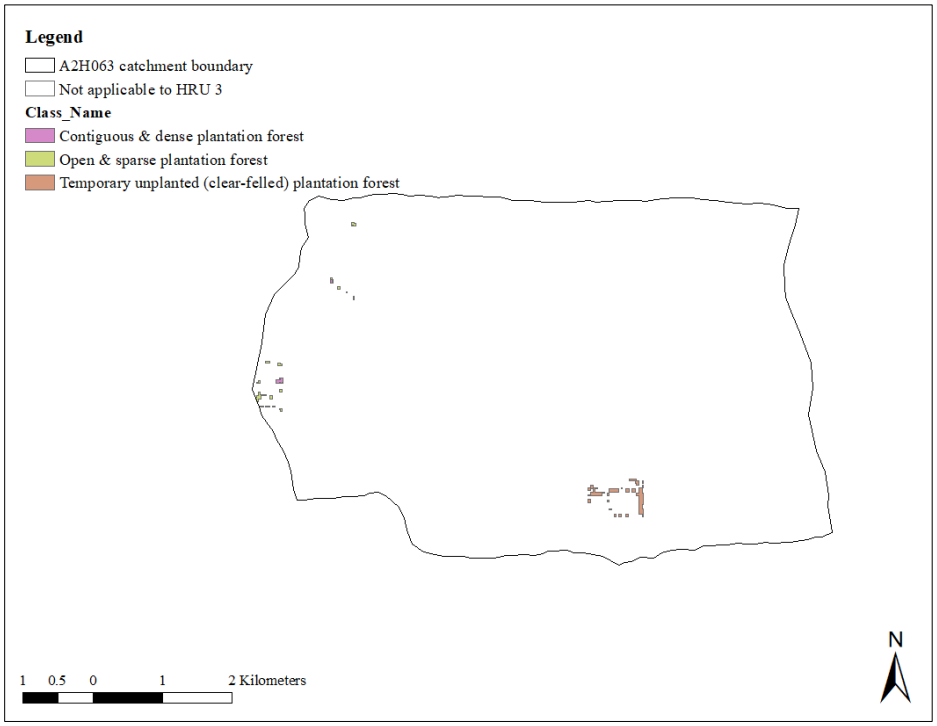

Appendix A3 Land cover classes modelled under HRU 3 for Catchment A2H063

Appendix A4 Land cover classes modelled as HRU 4 for Catchment A2H063

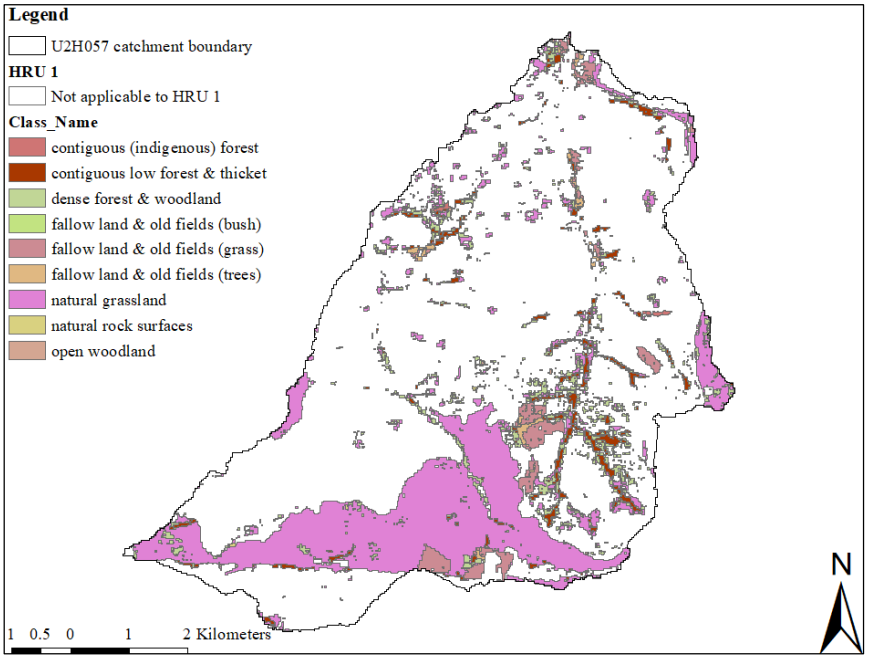

Appendix A5 Land cover classes modelled as HRU1 (Natural vegetation and natural rocks) for Catchment A2H054

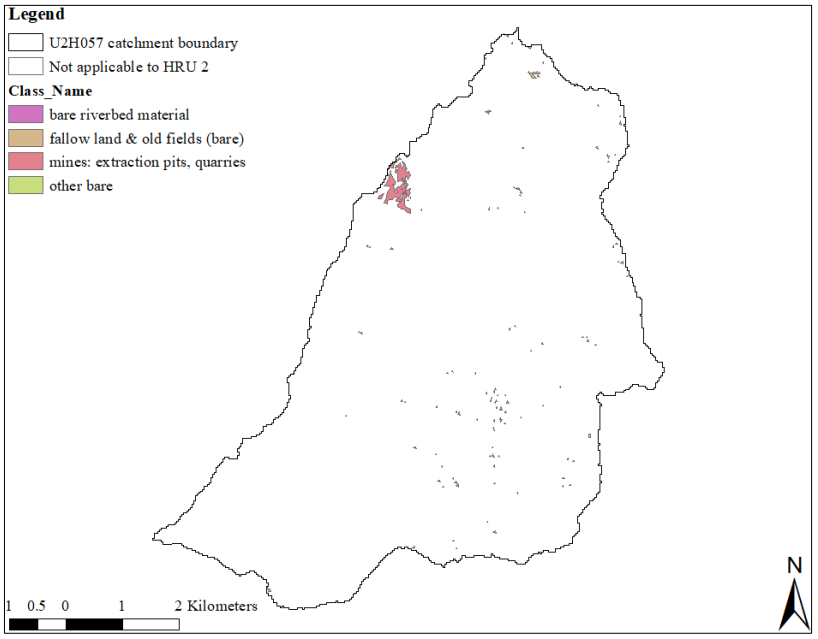

Appendix A6 Land cover classes that make up HRU 2 (bare surfaces and mining) for Catchment A2H054

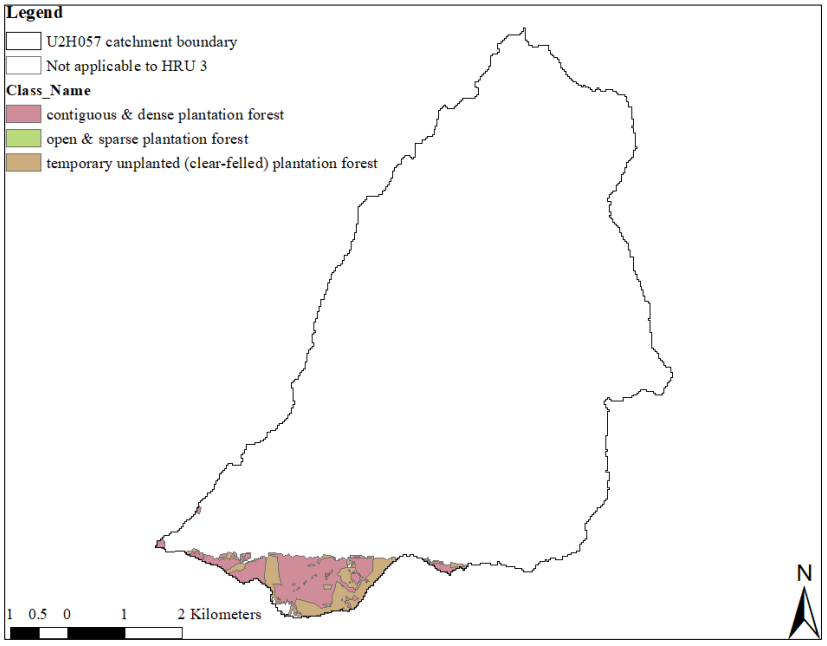

Appendix A7 Land cover classes under HRU 3 (planted forest) for Cathcmnent A2H054

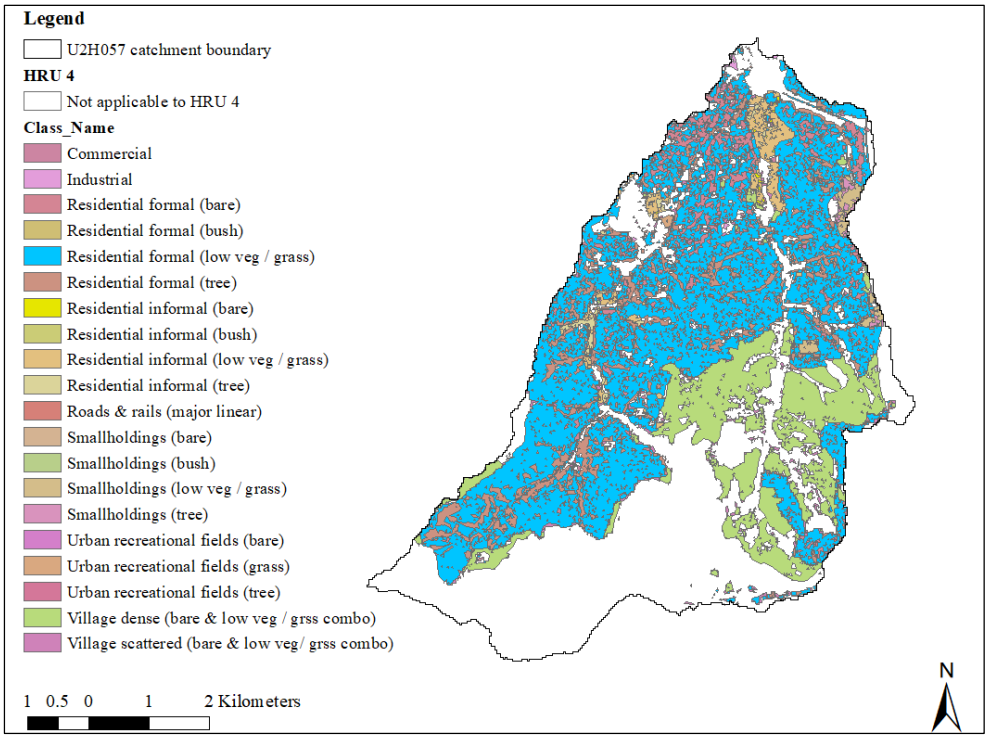

Appendix A8 Land cover classes modelled under HRU 4 (Built-up) for Cathcmnent A2H054

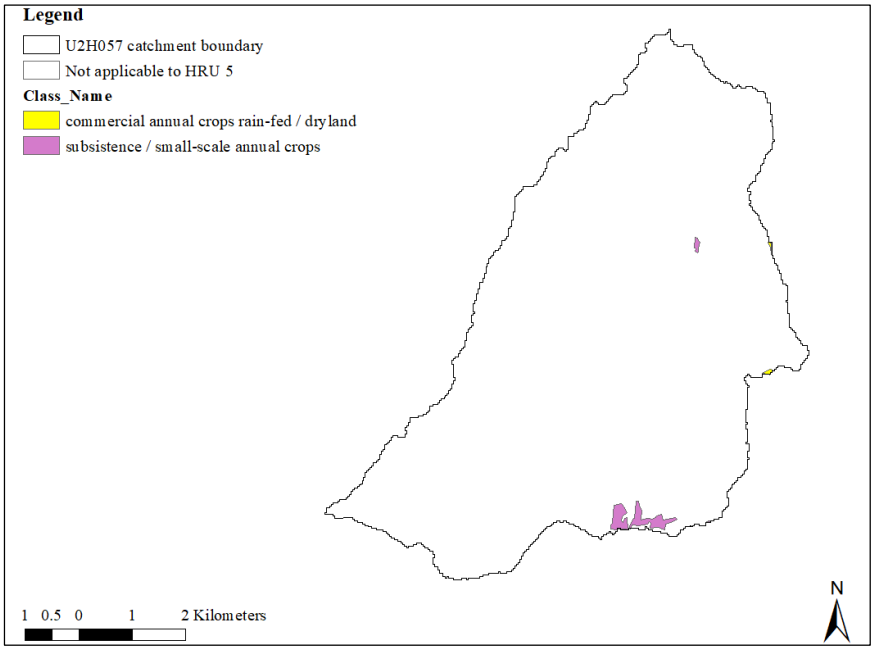

Appendix A9 Land cover classes modelled as HRU 5 (Agriculture) for Catchment A2H054

Appendix A10 Land cover classes modelled as sub-catchment 1 (built-up residential) for Catchment A2H063

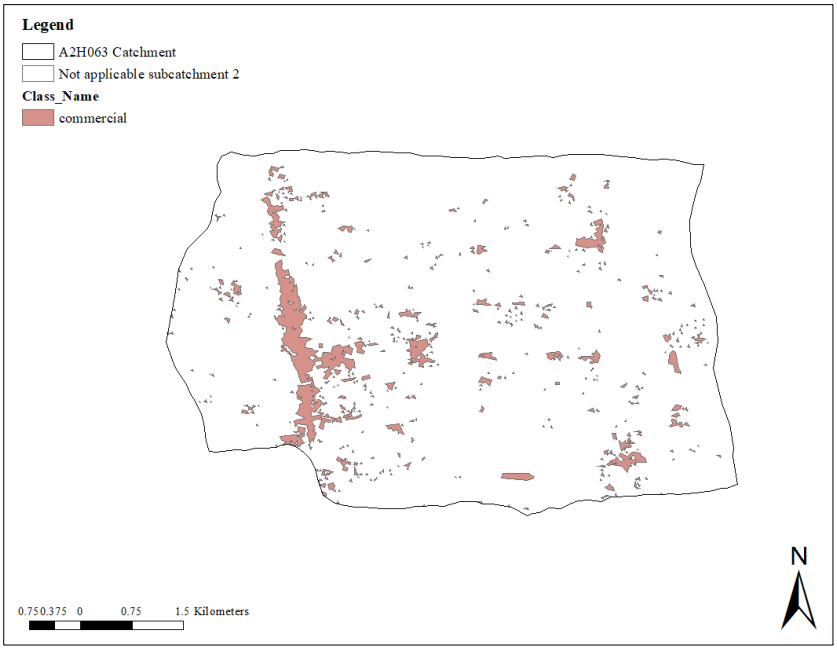

Appendix A11 Land cover classes modelled as sub-catchment 2 (Commercial) for Catchment A2H063

Appendix A12 Land cover classes modelled as sub-catchment 3 (Cultivated) for Catchment A2H063

Appendix A13 Land cover classes modelled as sub-catchment 4 (Forested land) for Catchment A2H063

Appendix A14 Land cover classes modelled as sub-catchment 5 (Industrial) for Catchment A2H063

Appendix A15 Land cover classes modelled as sub-catchment 6 (Barren surfaces and mines) for Catchment A2H063

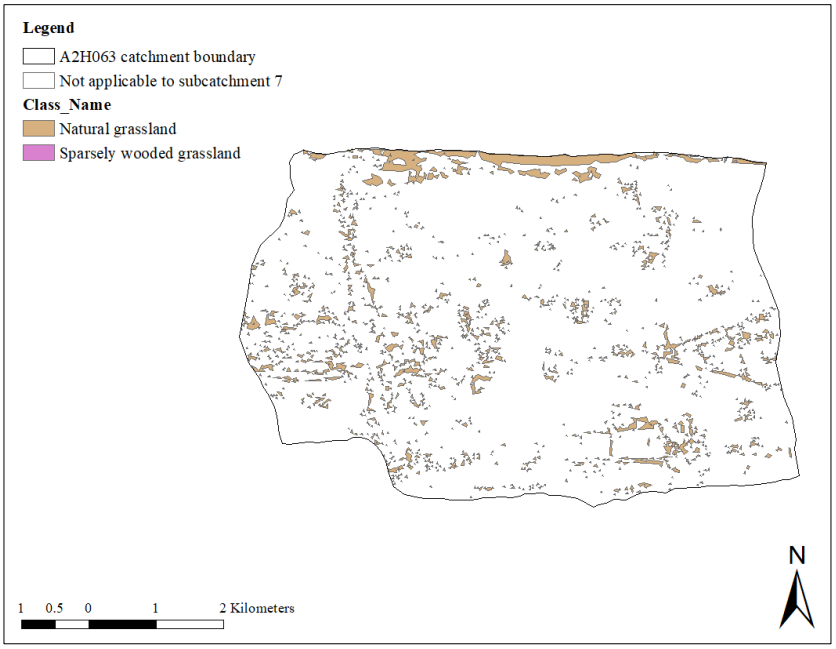

Appendix A16 Land cover classes modelled as sub-catchment 7 (Natural grassland) for Catchment A2H063

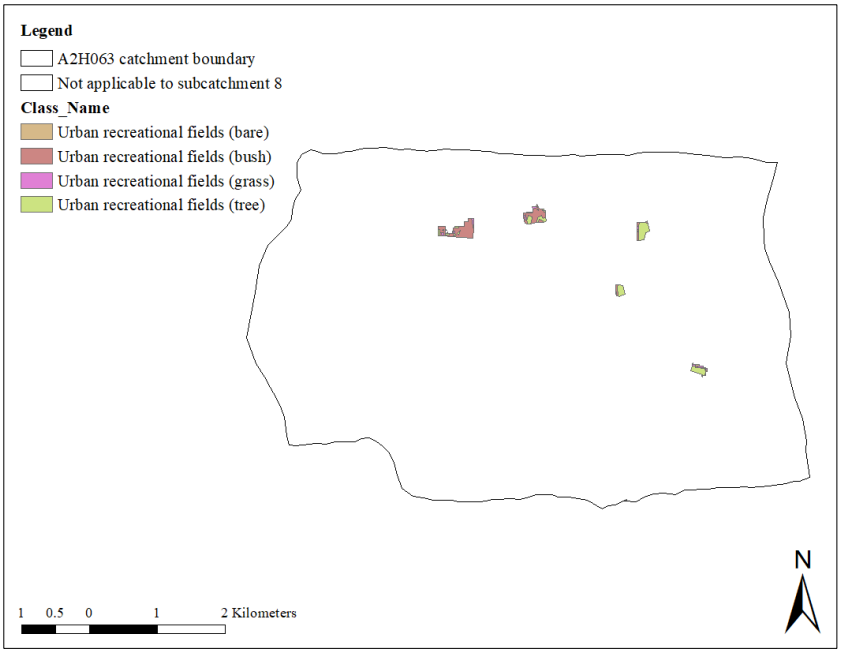

Appendix A17 Land cover classes modelled under sub-catchment 8 (Urban recreational) for Catchment A2H063

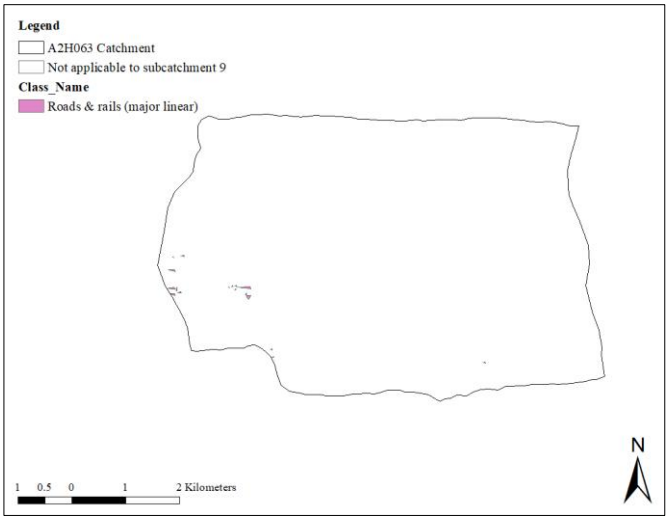

Appendix A18 Land cover classes modelled as sub-catchment 9 (roads and rail) for Catchment A2H063

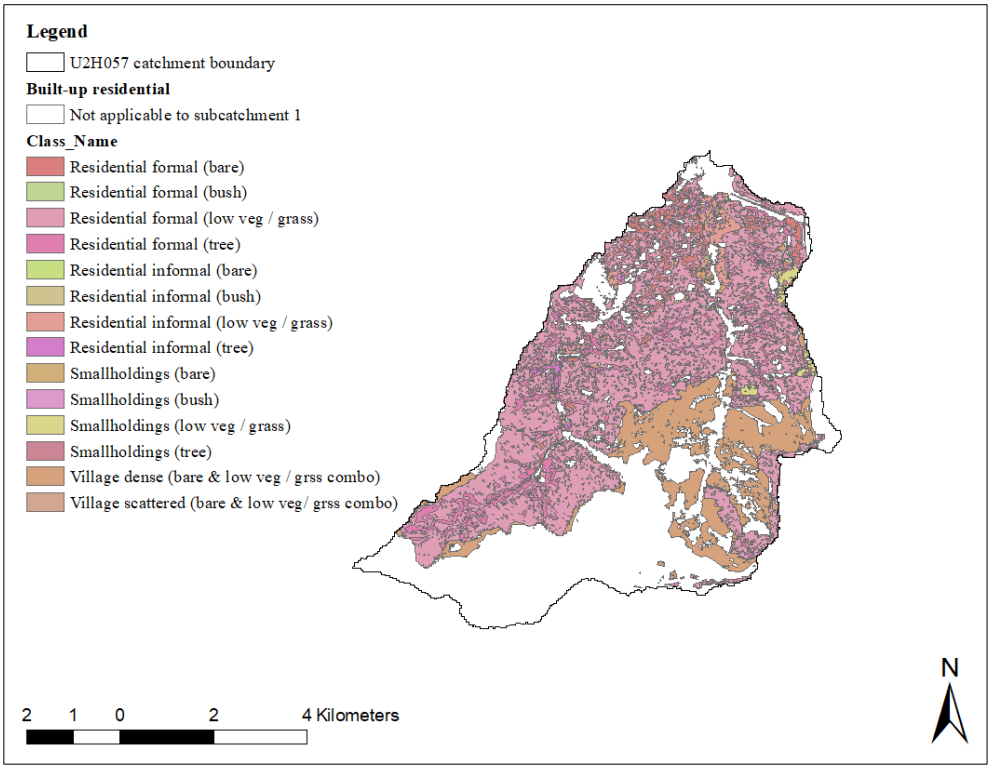

Appendix A19 Land cover classes under sub-catchment 1 (built-up residential) for Catchment U2H057

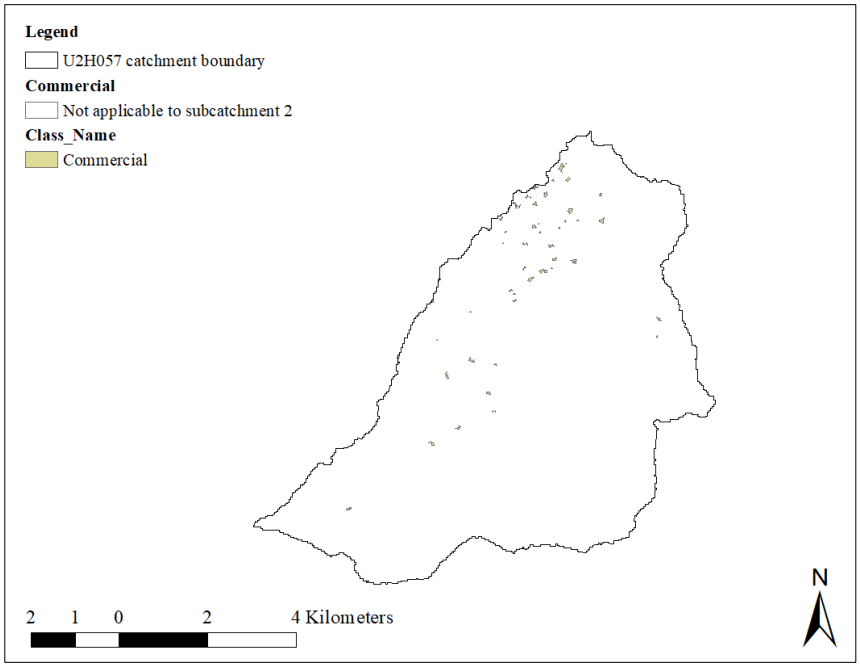

Appendix A20 Commercial land use modelled as sub-catchment 2 for Catchment U2H057

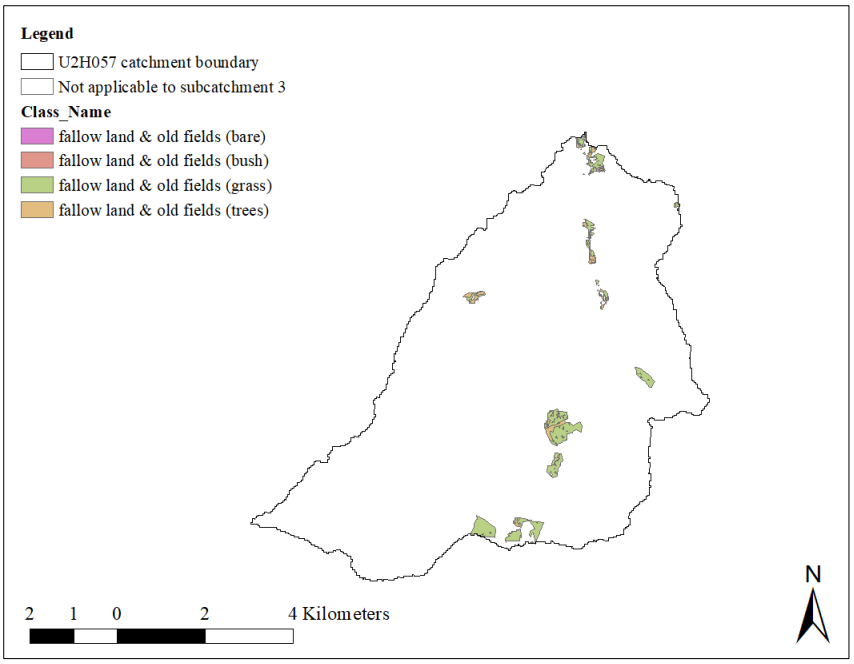

Appendix A21 Land cover classes modelled as sub-catchment 3 (Cultivated) for Catchment U2H057

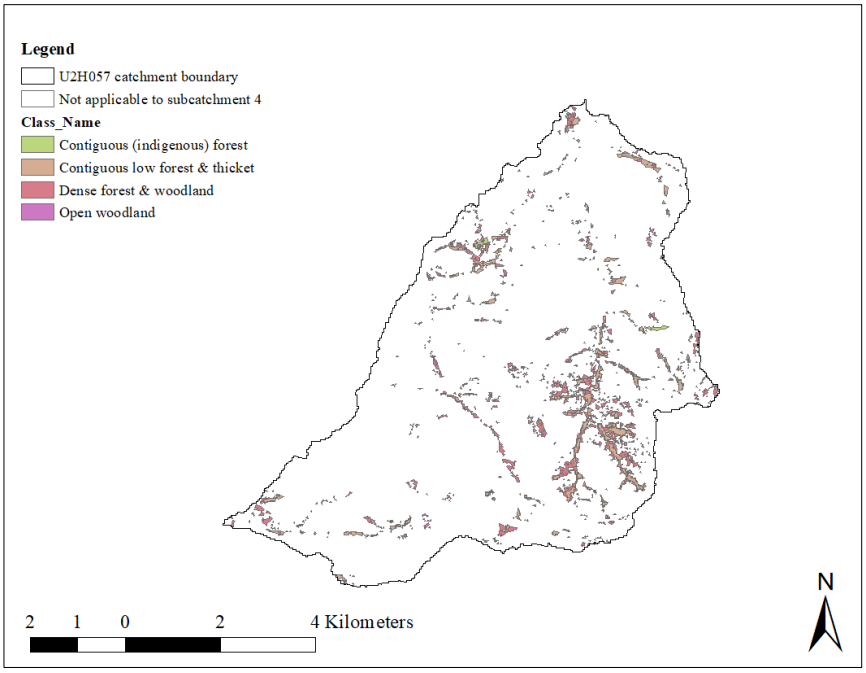

Appendix A22 Land cover classes modelled as sub-catchment 4 (Forested land) for Catchment U2H057

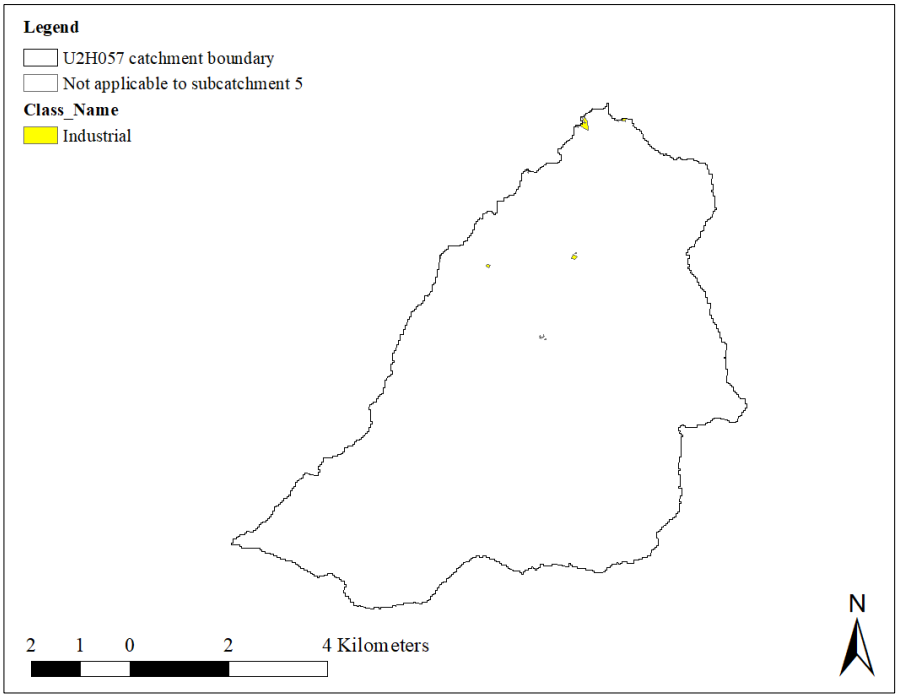

Appendix A23 Industrial land use modelled as sub-catchment 5 for Catchment U2H057

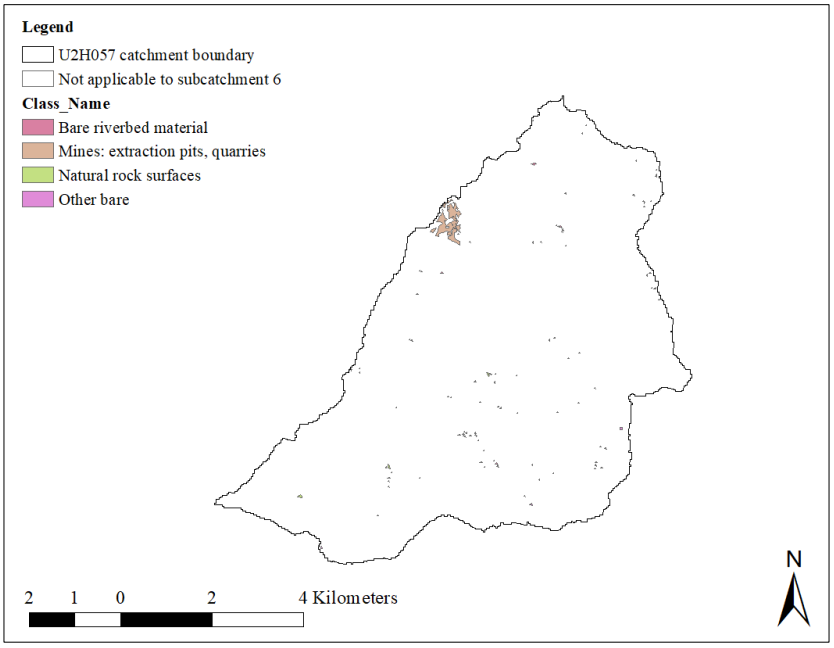

Appendix A24 Barren surfaces and mines modelled as sub-catchment 6 for Catchment U2H057

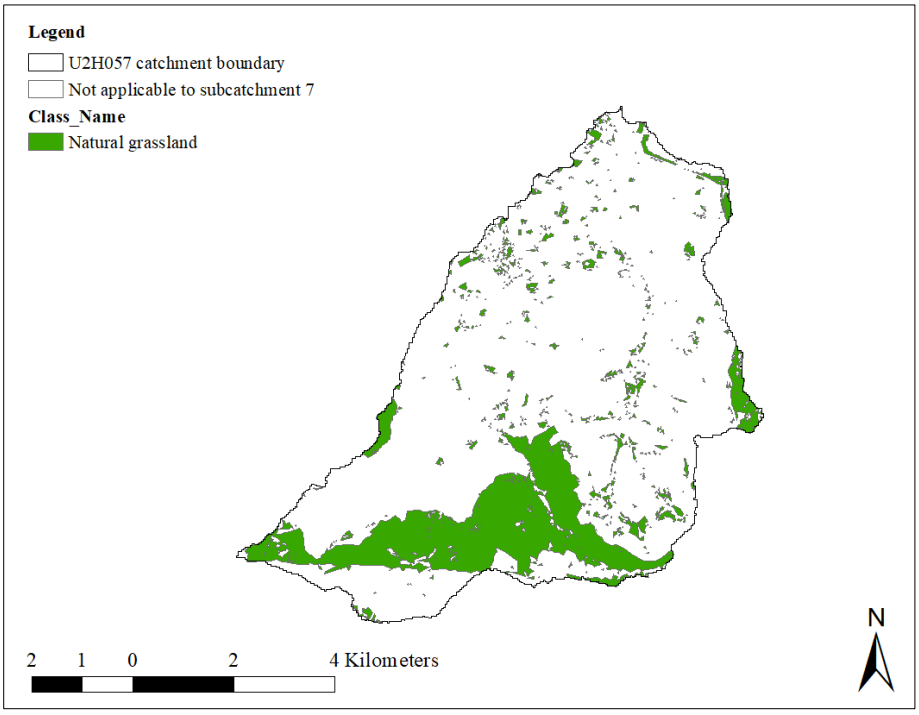

Appendix A25 Natural grassland modelled as sub-catchment 7 for Catchment U2H057

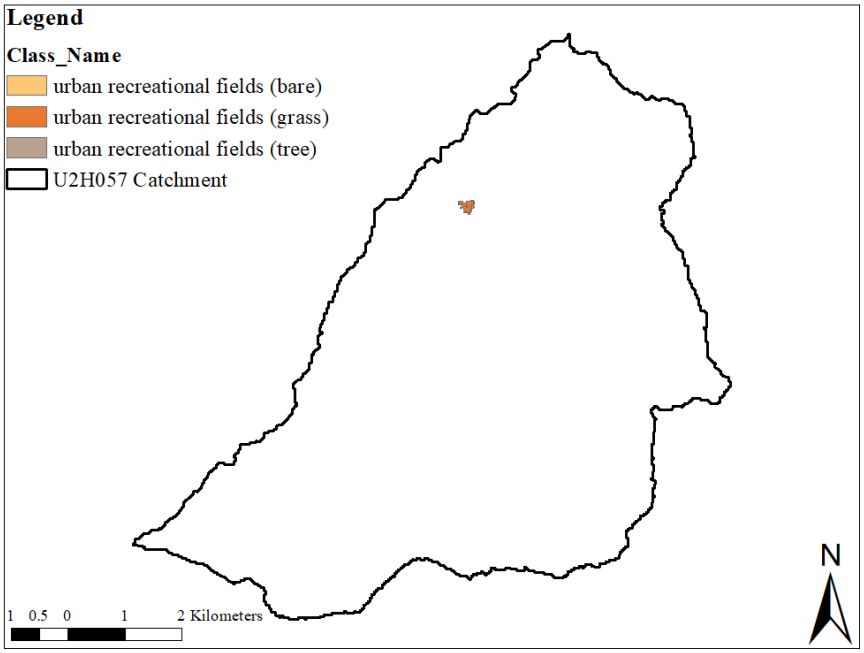

Appendix A26 Urban recreational fields modelled as sub-catchment 8 for Catchment U2H057

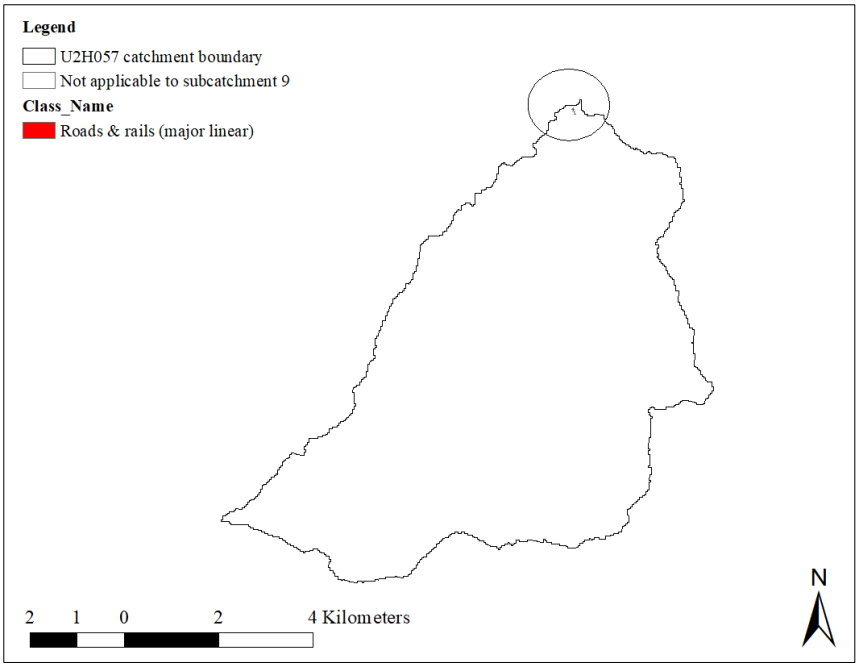

Appendix A27 Roads and rail modelled as sub-catchment 9, illustrated in the circled area in the catchment map for Catchment U2H057

11. APPENDIX B: LAND COVER CLASSIFICATION MAPS

This section includes land cover classification/impervious area classification maps completed using the pixel-based method, GMIS and GAIA impervious datasets.

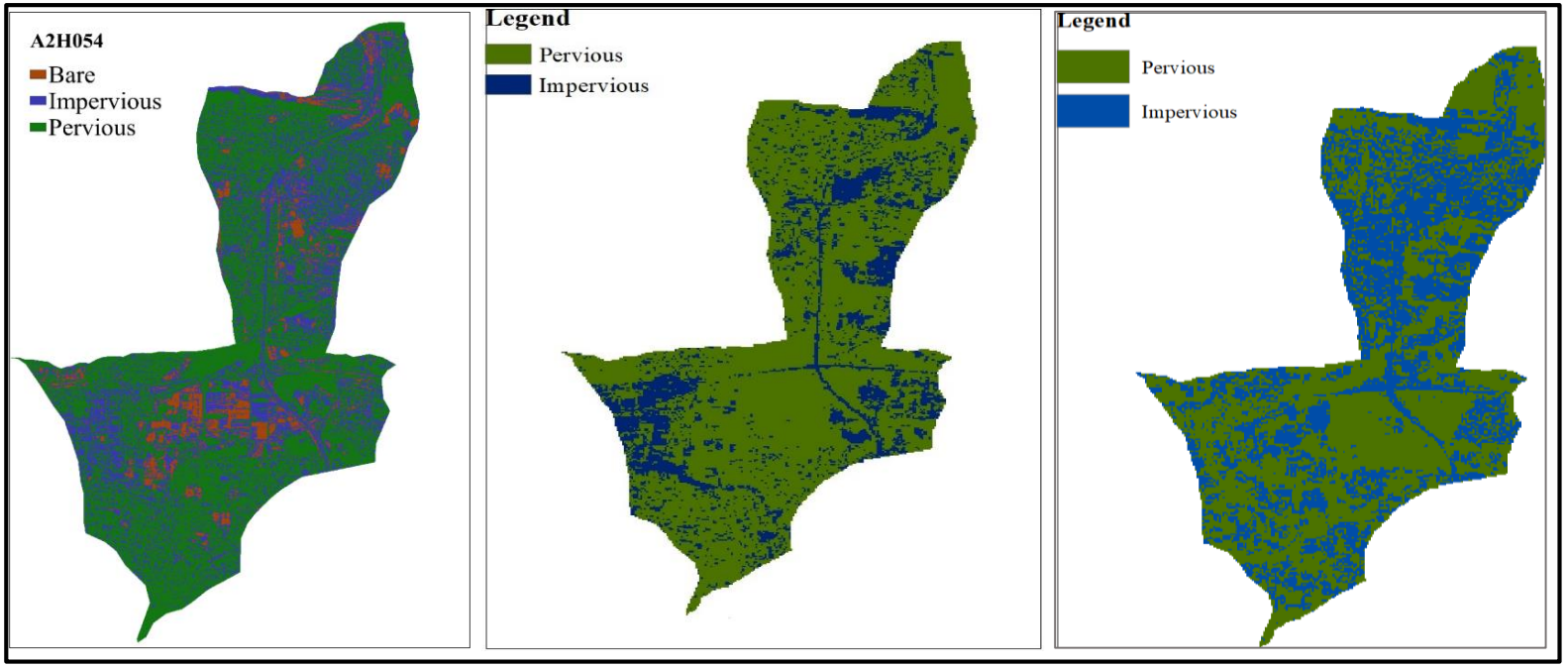

Appendix B1 Land cover classifcation maps derived from the Pixel-based, GMIS and GAIA impervious mapping methods for Catchment A2H054

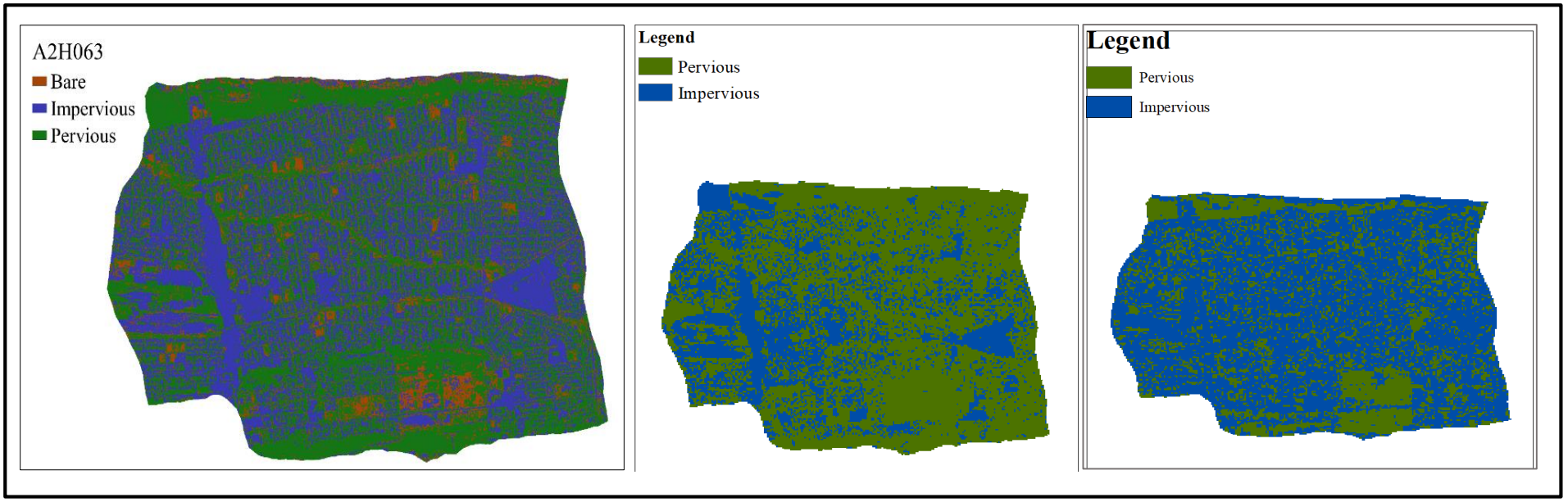

Appendix B2 Land cover classifcation maps derived from the Pixel-based, GMIS and GAIA impervious mapping methods for Catchment A2H063

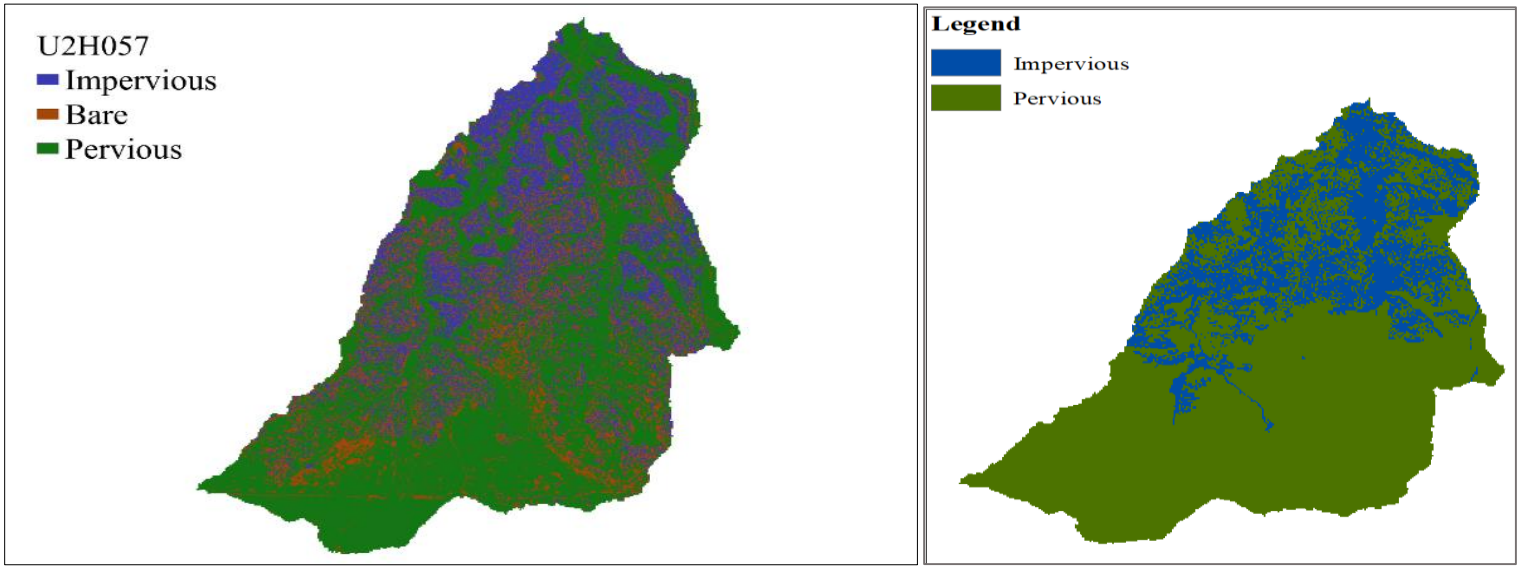

Appendix B3 Land cover classifcation maps derived from the Pixel-based and GAIA impervious mapping methods for Catchment U2H057

12. APPENDIX C: *ACRU* IMPERVIOUS PARAMETER CALCULATIONS

APPENDIX C1 ADJIMP and DISJIMP areas for Catchment A2H054 calculated from the pixel-based land cover classifcation

HRU	**AIA (%)**	**DIA (%)**	**Total area (km^2)**	**Pervious area (km^2)**	**Impervious area (km^2)**	**ADJIMP fraction**	**DISJIMP fraction**
Natural vegetation and natural rocks	15	85	9.486	9.41	0.076	0.011	0.065
Bare surfaces and mining	70	25	0.484	0.024	0.46	0.322	0.115
Urban residential	60	40	14.539	9.041	5.464	3.279	2.186
Urban recreational	35	65	1.097	0.927	0.179	0.063	0.116
Village and smallholdings	30	70	0.099	0.049	0.034	0.010	0.024
Commercial and transport	75	25	1.819	0.236	1.676	1.257	0.419
Industrial	80	20	0.991	0.041	0.499	0.399	0.100
Forest plantations	0	0	0.132	0.132	0	0	0
Agriculture	40	60	0.752	0.731	0.021	0.008	0.012

APPENDIX C2 ADJIMP and DISJIMP areas calculated for Catchment A2H063 from the pixel-based land cover classifcation

HRU	**AIA (%)**	**DIA (%)**	**Total area (km^2)**	**Pervious area (km^2)**	**Impervious area (km^2)**	**ADJIMP fraction**	***ACRU* DISJIMP fraction**
Natural vegetation and natural rocks	15	85	9.376	9.335	0.041	0.006	0.035
Bare surfaces and mining	0	0	0.041	0.041	0	0	0
Urban residential	60	40	20.756	15.000	5.756	3.454	2.302
Urban recreational	35	65	0.215	0.138	0.077	0.027	0.050
Village and smallholdings	30	70	0.133	0.096	0.037	0.011	0.026
Commercial and transport	80	20	1.807	0.263	1.545	1.236	0.309
Industrial	80	20	0.742	0.042	0.699	0.559	0.140
Forest plantations	0	0	0.089	0.089	0	0	0

APPENDIX C3 ADJIMP and DISJIMP areas calculated for Catchment U2H057 from the pixel-based land cover classification

HRU	**AIA (%)**	**DIA (%)**	**Total area (km^2)**	**Pervious area (km^2)**	**Impervious area (km^2)**	**ADJIMP fraction**	**DISJIMP fraction**
Natural vegetation and natural rocks	20	80	12.746	12.731	0.015	0.003	0.012
Bare surfaces and mining	15	85	0.273	0.072	0.201	0.030	0.171
Urban residential	30	70	24.317	16.654	7.663	2.299	5.364
Urban recreational	15	85	0.034	0.021	0.013	0.002	0.011
Village and smallholdings	10	90	6.797	4.466	2.331	0.233	2.098
Commercial and transport	75	25	0.124	0.003	0.121	0.091	0.030
Industrial	75	25	0.043	0.012	0.031	0.023	0.008
Forest plantations	0	0	2.274	2.274	0	0	0
Agriculture	0	0	0.290	0.290	0	0	0

APPENDIX C4 ADJIMP and DISJIMP areas calculated for each HRU in Catchment A2H054 based imperviousness extracted from the GMIS dataset

HRU	AIA (%)	DIA (%)	Total area ($km^{2`}$)	Pervious area (km^2)	Impervious area (km^2)	ADJIMP fraction	DISJIMP fraction
Natural vegetation and natural rocks	15	85	9.486	8.965	0.521	0.078	0.443
Bare surfaces and mining	70	25	0.484	0.026	0.458	0.321	0.115
Urban residential	60	40	14.539	8.111	6.428	3.857	2.571
Urban recreational	35	65	1.097	0.837	0.260	0.091	0.169
Village and smallholdings	30	70	0.099	0.049	0.050	0.015	0.035
Commercial and transport	75	25	1.819	0.236	1.583	1.187	0.396
Industrial	80	20	0.991	0.041	0.950	0.760	0.190
Forest plantations	0	0	0.132	0.132	0	0	0
Agriculture	40	60	0.752	0.731	0.021	0.008	0.013

APPENDIX C5 ADJIMP and DISJIMP areas calculated for each HRU in Catchment A2H063 based imperviousness extracted from the GMIS dataset

HRU	**AIA (%)**	**DIA (%)**	**Total area (km^2)**	**Pervious area (km^2)**	**Impervious area (km^2)**	**ADJIMP fraction**	**DISJIMP fraction**
Natural vegetation and natural rocks	15	85	9.376	8.313	1.063	0.159	0.904
Bare surfaces and mining	0	0	0.041	0.041	0	0	0
Urban residential	60	40	20.756	14.412	6.344	3.806	2.538
Urban recreational	35	65	0.215	0.148	0.067	0.023	0.044
Village and smallholdings	30	70	0.133	0.121	0.012	0.004	0.008
Commercial and transport	80	20	1.807	0.163	1.644	1.315	0.329
Industrial	80	20	0.742	0.043	0.699	0.559	0.140
Forest plantations	0	0	0.089	0.089	0	0	0

APPENDIX C6 ADJIMP and DISJIMP areas calculated for each HRU in Catchment U2H057 based imperviousness extracted from the GMIS dataset

HRU	**AIA (%)**	**DIA (%)**	**Total area (km^2)**	**Pervious area (km^2)**	**Impervious area (km^2)**	**ADJIMP fraction**	**DISJIMP fraction**
Natural vegetation and natural rocks	20	80	12.746	11.631	1.115	0.223	0.892
Bare surfaces and mining	15	85	0.273	0.082	0.191	0.029	0.162
Urban residential	30	70	24.317	17.344	6.973	2.092	4.881
Urban recreational	15	85	0.034	0.022	0.012	0.002	0.010
Village and smallholdings	10	90	6.797	4.766	2.031	0.203	1.828
Commercial and transport	75	25	0.124	0.003	0.121	0.091	0.030
Industrial	75	25	0.043	0.012	0.031	0.023	0.008
Forest plantations	0	0	2.274	2.274	0	0	0
Agriculture	0	0	0.29	0.29	0	0	0

APPENDIX C7 ADJIMP and DISJIMP calculation for Catchments A2H054 and A2H063 derived from the GAIA impervious mapping

HRU	AIA (%)	DIA (%)	Total area (km^2)	Pervious area (km^2)	Impervious area (km^2)	ADJIMP fraction	DISJIMP fraction
Natural vegetation and natural rocks	15	85	9.486	7.213	2.273	0.341	1.932
Bare surfaces and mining	70	25	0.484	0.026	0.458	0.321	0.115
Urban residential	60	40	14.539	7.515	7.024	4.214	2.810
Urban recreational	35	65	1.097	0.638	0.459	0.161	0.298
Village and smallholdings	30	70	0.099	0.049	0.050	0.015	0.035
Commercial and transport	75	25	1.819	0.189	1.630	1.223	0.408
Industrial	80	20	0.991	0.003	0.988	0.790	0.198
Forest plantations	0	0	0.132	0.132	0	0	0
Agriculture	40	60	0.752	0.731	0.021	0.008	0.013
HRU	**AIA (%)**	**DIA (%)**	**Total area (km^2)**	**Pervious area (km^2))**	**Impervious area (km^2)**	**ADJIMP fraction**	**DISJIMP fraction**
Natural vegetation and natural rocks	15	85	9.376	8.211	1.165	0.175	0.990
Bare surfaces and mining	0	0	0.041	0.041	0	0	0
Urban residential	60	40	20.756	14.400	6.356	3.814	2.542
Urban recreational	35	65	0.215	0.141	0.074	0.026	0.048
Village and smallholdings	30	70	0.133	0.121	0.012	0.004	0.008
Commercial and transport	80	20	1.807	0.155	1.652	1.322	0.330
Industrial	80	20	0.742	0.033	0.709	0.567	0.142
Forest plantations	0	0	0.089	0.089	0	0	0